Low Stress Creep of Copper and Some Aluminium and Magnesium Alloys at High and Intermediate Homologous Temperatures

Vivek Srivastava

Supervisors: Prof. H. Jones

Prof. G. W. Greenwood

Department of Engineering Materials

University of Sheffield

A thesis submitted in partial fulfilment of the requirements for the degree of

Doctor of Philosophy

August 2003

Summary

Creep behavior of high purity copper under low stress has been investigated in tension for bamboo grain-structured wires 25 –500 μm diameter and foils 0.4 and 0.6 mm thick and, in bending, for foils 100 and 250 μm thick. Additionally, creep behavior of polycrystalline 7075 aluminium and AZ61 magnesium alloy has been investigated under low applied tensile stress. The conditions explored feature diffusional creep and related mechanisms expected to be operative at the high temperatures and low stresses involved.

The creep and surface profile of copper (>99.99%) wires has been investigated close to their melting temperature (0.93 T_m) under stresses up to 0.35 MPa for which strain rate varied linearly with stress. For the thinnest wires (diameter 25-125 μm), the strain rate was about twice that expected from Nabarro–Herring diffusional creep theory and between one and two orders of magnitude larger than expected from Harper–Dorn creep. For 500 μm diameter wire, the measured rate was initially near to Harper–Dorn prediction but became constant only at longer durations at a level about five times lower than this. The lower rates were about 1.5 times that expected from diffusional creep. The surface profile observations indicated a small contribution of grain boundary sliding to the creep process when grain boundaries were not closely perpendicular to the stress. The observed effect of grain aspect ratio on the creep rate is shown to provide better correlation with theory.

Tensile creep tests were carried out on OFHC copper foils at 850°C and 990°C in the stress range 0.1-0.6 MPa. The stress exponent for creep was found to be close to 2 and measured rates were about two orders of magnitude faster than expected from diffusional creep. Slip lines, approximately 30 μm apart, were observed on the surface after creep. The creep process in these foils under tensile loading is ascribed to glide of dislocations controlled by the rate of generation of dislocations at Bardeen-Herring sources about 30 μm apart.

The creep tests in bending (which are novel) were carried out at 950°C in cantilever configuration loaded under self weight. The measured profile of the crept foils confirmed the linear dependence of strain rate on stress with final curvature 7-13

times lower than predicted from diffusional creep theory. A hundred nanometer thick alumina coating was applied to some copper foils prior to creep exposure. The associated localization of strain at grain boundaries was found to result in fracture of a 100 nm thick alumina coatings there at extremely low applied stress and overall strain.

Tensile creep test of thermomechanically treated 7075 aluminium alloy of initial grain size 48 μm at <5MPa and 350 to 410°C showed a stress exponent close to 1. After correcting for grain growth to 79 μm during the test, the creep rates were within a factor of two of those expected for Nabarro-Herring creep. The creep rates were found to be lower for longer test durations evidently due to grain growth at test temperature and thus indirect evidence for dependence of N-H creep rate on grain size was obtained. True activation energy for creep was found to be close to 165 kJ/mol comparable to the aluminium self diffusivity. For AZ61 magnesium alloy at 250 to 346°C, and stresses upto 6 MPa, Bingham type behaviour was observed with threshold stress decreasing with increasing temperature. The corresponding activation energy for creep was 106 ± 9 kJ/mol comparable with that expected for grain boundary self diffusion in magnesium with the resulting values of grain boundary diffusivity closely matching those obtained previously for Coble creep in pure magnesium. Grain elongation in the direction of the application of tensile stress was observed also to be consistent with operation of Coble creep. Strain rate versus stress for both these materials are shown to be continuous with published results for superplastic flow under comparable conditions.

Dedication

To my father whose belief allowed me to pursue my dreams

Acknowledgments

Table of Content

List of Symbols

a	Wire diameter (m)
A_{CO}	Numerical constant in Coble equation
A_D	Numerical constant in the Dorn equation
A_{HD}	Numerical constant in Harper-Dorn equation
A_{NH}	Numerical constant in Nabarro-Herring equation
b	Burger's vector (m)
B	Numerical constant in Herring equation for creep of bamboo structure
d	Grain size (m)
d_0	Initial grain size (m)
d_t	Grain size after time t (m)
D_0	Pre-exponential factor for diffusivity (m^2s^{-1})
D_{GB}	Grain boundary diffusivity (m^2s^{-1})
D_l	Lattice diffusivity (m^2s^{-1})
D_m	Diffusivity measured from creep tests (m^2s^{-1})
D_r	Lattice self diffusivity measured by radio-tracer experiments (m^2s^{-1})
G	Shear Modulus (Pa)
h	Foil thickness (m)
k	Boltzman's constant ($J\ K^{-1}$)
k_d	Parameter characterizing the rate of grain growth (($\mu m)^2s^{-1}$)
l	Grain length (m)
L	Foil length (m)

$\bar{L}$	Average grain intercept length (m)
$\bar{L}_n$	Average grain intercept length normal to tensile axis (m)
$\bar{L}_P$	Average grain intercept length parallel to tensile axis (m)
M	Bending moment (Nm)
$M_{b,0}$	Maximum bending moment (Nm)
P	Dimensionless test duration
Q_a	Apparent activation energy for creep (J/mol)
Q_c	True activation energy for creep (J/mol)
R	Radius of curvature of crept foil (m)
t	test duration (s)
T	temperature (K)
U	Activation energy for threshold stress dependence on temperature (J/mol)
w	Foil width (m)
w_0	Zero creep load (kg)
α_g	Numerical constant in Eq. (5.12)
α_l	Numerical constant in Eq. (5.12)
δ	Grain boundary width (m)
ε	Measured strain
$\dot{\varepsilon}$	Measured strain rate (s^{-1})
$\dot{\varepsilon}_{CO}$	Coble creep rate (s^{-1})
$\dot{\varepsilon}_{HD}$	Harper-Dorn creep rate (s^{-1})
$\dot{\varepsilon}_{NH}$	Nabarro-Herring strain rate (s^{-1})

γ_{gb}	Grain boundary energy (Jm^{-2})
γ_s	Surface energy (Jm^{-2})
κ	Curvature of the crept foil (m^{-1})
$\dot{\kappa}$	Rate of change of curvature ($m^{-1}s^{-1}$)
Ω	Atomic volume (m^3)
$\dot{\theta}$	Rate of change of angle subtended by the foil at its centre of curvature (s^{-1})
$\dot{\theta}_i$	Rate of change of angle subtended by a grain at the centre of curvature of the foil (s^{-1})
ρ_{foil}	Density of the foil ($kg\text{-}m^{-3}$)
σ	Applied stress (Pa)
σ_0	Threshold stress (Pa)
σ_e	Elastic stress due to bending moment (Pa)
ξ	Numerical factor in grain rotation rate equation (5.12)

List of Acronyms

DFZ   Dispersoid free zone

ECD   Equivalent circle diameter

GBD   Grain boundary dislocation

GBS   Grain boundary sliding

H-D   Harper-Dorn creep

N-H   Nabarro-Herring creep

PFZ   Precipitate free zone

1.0 INTRODUCTION

Time dependant plastic deformation of a material at elevated temperature (>0.4 T_m, where T_m is the melting point of the material) under stress is described as creep. In most common applications, e.g. turbines and nuclear reactors, maximum permissible strain rates are in the range of 10^{-10}-10^{-11} s^{-1}. To design creep resistant materials for such applications, there is a need to understand the mechanical processes governing the creep behaviour at these extremely low strain rates. It is well known that different creep processes dominate under different operating conditions. Therefore, knowledge of the dominant creep mechanism under a particular set of conditions is essential for design of engineering components and structures and also for development of new creep resistant materials.

Creep at high temperatures and low stresses is considered to be controlled by either diffusional creep [1, 2], dislocation-based Harper-Dorn creep [3] or grain boundary sliding accommodated by slip [4, 5]. Out of these three mechanisms only diffusional creep theory is well developed and able to predict the creep rate from first principles. The theory developed independently by Nabarro [1] and Herring [2], for lattice diffusion of vacancies from grain boundaries under tension to those under compression, predicts a linear variation of strain rate with stress and an inverse-squared

dependence on grain size. Coble [6] extended the theory to include the case of stress-directed diffusion of vacancies along the grain boundaries, and predicted an inverse-cubed relationship between strain rate and grain size at intermediate temperatures (0.4-0.6 T_m).

The Harper-Dorn (H-D) creep formulation relies on results obtained by various researchers (e.g. [3]) for pure metals and alloys close to their melting point and is characterised by strain rate linearly dependent on stress and independent of grain size. Strain is generally believed to originate from dislocation movement, though the details of rate controlling processes are unclear. A number of models have been proposed to account for H-D creep, but none have gained general acceptance.

Grain boundary sliding as an independent creep mechanism was developed to account for the superplastic behaviour of materials. A vast amount of experimental data is available for materials deforming by this mechanism. General characteristics of deformation by this mechanism are that the strain rate is proportional to the square of applied stress and inversely proportional to the square of the grain size. A number of phenomenological models are available that match the observations and give good correlation with experimental data.

Recently, there has been renewed interest in creep at high temperature and low stress. Novel techniques like AFM coupled with scratch displacement studies [7] and microstructural data from TEM [8] have been used to provide additional evidence for the dominant creep mechanism. It is clear from these

studies that mechanical data alone from creep tests is not sufficient to identify the operative mechanism. It is for this reason, that after years of research, the issue is still not fully resolved so there is a continuing need to investigate the microstructural aspects of the creep process in conjunction with the mechanical data.

In the present work, creep of high purity copper (>99.99%), 7075 (a superplastic aluminium alloy) and AZ61 (a commercial magnesium alloy) has been studied at high and intermediate homologous temperature and low stress. High purity copper wires (25 to 500 μm in diameter) were creep tested at 990°C (0.93 T_m) and low applied stress (5 to 350 kPa) in an argon-hydrogen atmosphere. Strain was measured at different time intervals and the steady state creep rate determined from the resulting strain-time curves. The creep rates are compared with those predicted from diffusion creep theories and from the Harper-Dorn equation. Profiles of crept wires were examined by scanning electron microscopy to observe changes in individual grain surfaces. Strain contributions from grain boundary sliding were estimated by quantitative metallography. The effect of wire diameter (and consequently grain length) on creep rate is discussed with reference to diffusional creep predictions. The effect of grain aspect ratio is considered in relation to the slight discrepancy between experimental data and theoretical prediction. Recent results of numerical simulations are shown to improve the correlation of experimental data with theoretical rates. Additionally, the surface free energy of copper is estimated from the zero creep stress.

Strips of OFHC (oxygen free high conductivity) copper 600 μm thick were creep tested in tension at 1010-1070°C. Creep strain was measured and microstructural features observed optically and by electron microscopy. OFHC strips 400 μm thick were also creep tested at 850°C in a creep testing rig with data logging facility. Measured creep rates are compared with predictions from competing theories for this set of conditions. The measured creep rates are also compared with results obtained previously for various sample geometries under comparable conditions of stress and temperature. A model based on glide of dislocations is developed to account for this creep behaviour. It is shown that rate of generation of dislocations from Bardeen-Herring sources is rate controlling during this high temperature tensile creep in copper foils..

In a number of engineering applications (e.g. in turbine blades), components are exposed to low stresses at high temperature and undergo plastic deformation in bending. To maintain the specified dimensional tolerance it is necessary to quantify the creep rate in bending. To simulate this kind of loading, creep tests were carried out in bending on high purity (>99.99%) copper foils 100 and 250 μm thick. The foils were tested under small bending loads due to their own weight and allowed to creep for an extended duration. The curvature of the foil after creep was estimated from its measured profile. Observed rate of change of curvature is rationalised in terms of diffusive fluxes of atoms from regions of grain boundary under tension to those under compressive stress. Grain boundary grooves were observed to detect any effect of their orientation with respect to the tensile/compressive axis. For

some samples, alumina coatings of different thicknesses were applied to one of the surfaces of foils before creep testing to observe any crack pattern of the film developed during creep. Localization of strain is a consequence of diffusion creep and was anticipated to provide vital clues to identify the operative mechanism. Calculations of diffusional flux under such loading are performed to theoretically predict the expected diffusional creep rates and the measured creep rates are compared with these.

Finally, constant load creep tests were conducted on two commercial alloys known to exhibit superplasticity to explore the possible connection between diffusional creep and superplastic deformation at low stresses. An aluminium alloy (7075) and a magnesium alloy (AZ61) were used. Stress and temperature dependence of creep rate has been investigated for these two alloys. For both the alloys, measured creep rates at low stresses are compared with those extrapolated from high stresses and those predicted from diffusional creep theory. The effect of grain growth during creep is considered and its effect on creep rates discussed for 7075 Al alloy. For AZ61 alloy, the measured creep rates are shown to be well described by Coble creep incorporating threshold stress and to be in agreement with superplasticity data for higher stress at comparable temperatures.

A major objective of this thesis is to provide specific examples of instances where very low stresses can result in appreciable plastic deformation at relatively high strain rates. In fine grain sized materials (copper wires, thin copper foils and superplastic alloys) diffusional creep was found to be the

dominant creep mechanism at low applied stresses. This observation is a direct consequence of the inverse-squared (or inverse-cubed, in case of grain boundary diffusion control) dependence of diffusional strain rate on grain dimensions. Therefore, it is expected that grain shape and size are important parameters determining the dominant creep mechanism at low stresses and high temperature with diffusional creep expected to dominate at finer grain size. One (fine copper wires), two (thin copper foils) and three dimensional (AZ61 and 7075) grain geometries cover the entire range that can be observed in real materials. Results indicate that increasing complexity of grain size distributions and grain shape increases the discrepancy between experimental observations and theoretical predictions. Therefore it is necessary to further develop diffusional creep theory for polycrystalline material, to take into account the effect of neighbouring grains, to enable creep rates to be accurately predicted.

2.0 LITERATURE REVIEW

2.1 Creep Process

Creep can take place at high temperatures by either dislocation activity or by stress directed diffusion of vacancies, also called diffusional creep. In general, these mechanisms operate in parallel and it is the fastest mechanism under specific conditions that dominates the observed behaviour. Frost and Ashby [9] have developed deformation mechanism maps that indicate the dominant creep mechanism under a given stress-temperature condition. These diagrams and their uses are discussed in detail by Weertman and Weertman [10].

2.1.1 Diffusional Creep

The theoretical background for diffusional creep was introduced independently by Nabarro [1] and Herring [2]. It was pointed out that the application of tensile stress σ lowers the free energy for vacancy generation at grain boundaries under tension by an amount $\sigma \Omega$, where σ is the applied tensile stress and Ω is the volume of a vacancy. This raises the vacancy concentration at the grain boundaries under tension leading to a concentration difference between boundaries under tension and those under compression. This concentration difference, in turn, provides a driving force for diffusion of

vacancies through the lattice. Quantitative analysis of this phenomenon leads to predictions of tensile strain rate, $\dot{\varepsilon}_{NH}$ as follows

$$\dot{\varepsilon}_{NH} = A_{NH} \frac{D_l \Omega \sigma}{d^2 kT} \tag{2.1}$$

where A_{NH} is a numerical factor ~ 10, D_l is lattice self-diffusivity, d is grain size, k is Boltzmann's constant and T is temperature in degrees Kelvin.

Diffusion of vacancies predominantly takes place along grain boundaries at lower homologous temperatures. Analysis of this alternative process for spherical grains leads to a slightly different rate equation, after Coble [6].

$$\dot{\varepsilon}_{Co} = A_{Co} \frac{D_{gb} \delta \Omega \sigma}{d^3 kT} \tag{2.2}$$

where A_{Co} is a numerical factor ~ 50, D_{gb} is grain boundary diffusivity and δ is grain boundary width. The mechanism is illustrated schematically in Fig. 2.1 (from [7]). The values of numerical constants in Eqs. 2.1 and 2.2 depend on the grain geometry used in calculation of the diffusion path and is tabulated in Table 2.1 [11].

Experimental evidence in support of diffusional creep has accumulated over the years in almost all class of materials. The earliest reports supporting diffusional viscous flow at high temperature were published for experiments in fine metal wires of copper [12, 13], gold [14] and beryllium [15]. These experiments were conducted on high purity metal wires (25.4 to 150 μm diameter) with grains extending through the wire diameter ("bamboo

8

structure"). Creep rates were measured close to their melting point under very low stresses. Surface energy was estimated from load required for zero creep based on the procedure developed by Udin *et al.* [12]. Jones [16] reviewed the early high temperature creep data in bamboo structured metal foils and wires close to their melting point and showed that the strain rate was proportional to applied stress and that the strain rate per unit stress was inversely proportional to the product of the two grain dimensions as predicted by Nabarro-Herring (N-H) theory [1, 2]. Radiotracer diffusivity (D_r) was compared to diffusivity estimated from creep tests (D_m) and showed good agreement between theory and experiments in a number of metals when the experiments were conducted for a sufficiently long duration (Fig. 2.2). For short test durations, the experimental creep rates were found to be much faster than those predicted by theory. It was believed that accelerated creep was due to dislocations acting as sources and sinks for vacancies. Burton [17] analysed this enhancement of diffusion creep and developed a model for dislocation climb based on absorption of vacancies at dislocations during primary creep. Jones [18] showed experimentally the operation of diffusional creep by grain boundary diffusion in pure magnesium for two grain sizes (50 and 80 μm). Burton [19] demonstrated inverse cube dependence of strain rate on grain size for copper in the Coble regime and showed that diffusional creep can be significant at much lower temperatures than previously believed. Burton [11] published a monograph containing comprehensive review of early data on diffusional creep in a number of metals (e.g. Cu, Mg, Be, Fig. 2.3) and solid solution alloys (e.g. Fe-3%Si, Cu-Ni, Cu-Zn, Fig. 2.4).

Inman *et al.* [20] measured creep rates in Cu-Sb alloy wires at 950°C and showed that the creep rates were within a factor of three of predictions from the N-H equation. Arzt *et al.* [21] analysed diffusional creep in solid solution alloys limited by mobility of grain boundary dislocations due to solute or impurity drag and showed that the creep in pure and commercially pure nickel (99.5% purity) can be reasonably described by a modified diffusional creep equation [22]. A similar explanation was used to describe qualitatively observed creep behaviour of Al-Cu, Pb-Sn and Al-Zn solid solution alloys. Kloc *et al.* [23] reported creep rates in close agreement with those predicted by the Coble equation for Cu-14at.% Al at intermediate temperatures and low stresses for mean grain intercept lengths less than 270 μm (Fig. 2.5).

Precipitate containing materials provide the most striking evidence for diffusional creep. Diffusive transport of vacancies from grain boundaries under tension to those under compression is expected to lead to formation of precipitate free zones and associated precipitate pile ups. Such an effect has indeed been observed by several investigators [24-30] over a number of years. However, details of creep rate, stress exponent and activation energy are sometimes found to be in disagreement with diffusional creep predictions. Recently, Greenwood [31] and McNee *et al.* [32, 33] have addressed these issues and argued that these discrepancies indicate the need for a better understanding of various aspects of diffusional creep and do not imply that diffusional creep is not operative in those cases.

It has been pointed out that diffusional creep is expected to be even more prominent during creep of ceramics due to difficulty of dislocation motion [11]. Linear stress dependence of grain size compensated creep rate and inverse square dependence of creep rate on grain size has been demonstrated for Al_2O_3, UO_2, SiC, ZrO_2 and MgO as shown in Figs. 2.6 and 2.7 [11, 34]. It has also been suggested that polycrystalline turbine blades under typical operating conditions of gas turbines may be operating under the conditions favouring diffusional creep [35].

Diffusional creep is intimately related to the structure of grain boundaries and free surfaces. Hondros and Lake [36] showed that self diffusivity calculated from zero-creep experiments in copper foils deforming by diffusional creep can vary by almost an order of magnitude depending on oxygen partial pressure in the testing environment. It was shown that under those conditions that favour oxygen chemisorption at interfaces, effectiveness of interfaces as source and sinks of vacancies is reduced, thereby slowing down diffusional creep. Components deforming by diffusional creep can be affected by presence of oxide films on the surface. Burton [37] showed that a particular onset stress must be exceeded before creep commences in thin aluminium foils. The observed threshold stress was related to the strength of the aluminium oxide layer. Similarly, during diffusional creep in materials containing second phase particles, formation of precipitate pile-ups at grain boundaries parallel or nearly parallel to the tensile axis is believed to lead to threshold stresses restricting the onset of diffusional creep [11, 38].

Enhancement of grain boundary diffusional creep has been observed in single phase alloys and materials containing precipitates. During diffusional creep, a counter-flow of vacancies was envisaged in the original theories. Under certain conditions of temperature and applied stress, excess vacancies can condense to form inter-granular cavities at boundaries transverse to the tensile axis. Harris *et al.* [39] and later McNee *et al.* [32] observed cavities in the form of wide blunt cracks within precipitate free zones for ZR55 (Fig. 2.8) and hypothesised that this could enhance observed creep rate and also account for the higher stress exponent observed in these systems. Hanna and Greenwood [40] showed that pre-existing inter-granular voids can result in creep rates in tough pitch copper that were much faster than predicted by diffusional creep. Operation of cavity growth by diffusional creep in these experiments on copper was confirmed by concomitant volume change measurements.

Theoretical analysis of different aspects of diffusional creep has led to significant advancement of the understanding of creep at high temperatures. Lifshitz [41] showed from geometric considerations that grain shape changes that accompany diffusional creep would necessitate grain boundary sliding to avoid cavitation at the grain boundaries as shown in Fig. 2.9 (from [11]). Lifshitz sliding is a consequence of diffusional creep and takes place in conjunction with diffusional creep. Burton [11] demonstrated that, in most metals, since grain boundary sliding involves very small scale diffusion as compared to grain dimensions, it is the diffusional transport of materials across the grain that is rate controlling during creep at low stresses. The

contribution of Lifshitz sliding during diffusional creep has been a subject of a major debate over the years. One view is that both grain boundary sliding and diffusion contribute to the overall strain during diffusional creep and that the two can be distinctly separated. The proponents of this view have developed techniques to estimate the relative contributions of grain boundary sliding and accretion of material normal to the grain boundaries [42-45]. The contribution of GBS to diffusional creep is estimated to be 40-60%. On the other hand, it is held that the strain contribution of sliding and diffusion cannot be distinctly separated as the total strain is zero in the absence of either of the steps of sliding and diffusion [46-50]. According to the latter view the total strain must be fully attributed either to grain boundary sliding or diffusion and diffusional creep should be considered as either diffusion-accommodated sliding or sliding-accommodated diffusion depending on which process is rate controlling. The strain rate, however, is controlled by equations (2.1 and 2.2) irrespective of the contributions from the two processes.

Classical diffusional creep equations assume that the grain boundaries are perfect sources and sinks for vacancies. Recent electron microscope investigations of the structure of grain boundaries, however, have revealed the existence of grain boundary dislocations [51]. The absorption/emission of vacancies involves climb of these grain boundary dislocations to absorb/emit point defects. Arzt *et al.* [21] provided a comprehensive treatment of microscopic processes involved in diffusional creep and their relationship to the nature and number of sources and sinks in the grain boundaries and their

mobility. Expressions were derived for creep rates taking into account the discrete number of grain boundary dislocations in the grain boundary. A small threshold stress was predicted for diffusional creep to become operative in pure metals. In solid solution alloys and precipitate strengthened alloys, the situation becomes more complex. In solid solutions, creep may be controlled by reduced mobility of grain boundary dislocations due to solute redistribution and the consequent effect of solute drag on grain boundary dislocation mobility. The creep rate under these circumstances was proportional to the square of the applied stress and inversely proportional to the grain size [21]. In precipitate containing materials, interfacial reaction considerations at the particle/boundary interface predict a threshold stress due to pinning of grain boundary dislocations. The model was found to predict threshold stresses much higher than those measured experimentally. Predictions of higher apparent stress exponent and activation energy were consistent with experimental observations. However, the observed strong dependences of threshold stress on temperature and on grain size could not be explained by this model.

Further theoretical developments related to the effect of size, shape and distribution of grains deforming by diffusional creep and the relation between individual grain deformation and the macroscopic strain rate are pertinent in accounting for the discrepancy between the experimentally measured rates and those predicted by theory. The method of measuring the grain size is also important. Eqs. 2.1 and 2.2 are applicable to true grain size and not the linear intercept length that is measured experimentally [1, 2, 6]. Classical equations

for diffusional creep were developed assuming circular grains. Gibbs [52] and Greenwood [53] calculated numerical constants for square and orthorhombic grains respectively. Anisotropy in orthorhombic grains for multi-axial applied stress was further analysed and creep compliant coefficient matrices were developed for both N-H and Coble creep [54]. Schneibel *et al.* [55] demonstrated that variations in strain rate by up to a factor of 4.4 were found depending on which grain size distribution was employed in the calculation. Hazzledine and Schneibel [56] developed a procedure for evaluating stress redistribution during Coble creep in irregular grains. Computer simulation of creep by grain boundary diffusion [57, 58] and under locally variable grain boundary properties [59] has been carried to elucidate the phenomenon. A further problem with experimental studies of diffusional creep that has received some theoretical attention is that of concomitant grain growth. Burton [60] showed that there exists a theoretical upper limit to the amount of strain due to Coble creep. During creep test, concurrent grain growth takes place and after a certain total strain is reached, strain rate is controlled by the N-H mechanism. Kim and Hiraga [58] performed computer simulations of diffusional creep accompanied by grain growth in two dimensional structures and showed that grain elongation due to dynamic grain growth results in strain rate decreasing with increasing strain. They, however, assumed completely relaxed shear stresses at grain boundaries and consequently grain rotation was not incorporated. Moreover, N-H creep is expected to become dominant for coarser grains and that has not been included. These shortcomings indicate a further need for more sophisticated simulations to

analyze diffusional creep and emphasise the more varied aspects of diffusional creep in actual materials. Herring [2] realized this in his original paper and commented that his theory *"(is) of course too idealized to apply accurately to any case, but it is hoped that they will sometimes be a fair approximation(s) to the truth"*.

2.1.2 Harper-Dorn Creep

At homologous temperatures greater than 0.3, dislocations are able to climb out of their glide plane thereby allowing deformation to continue. The earliest proposed mechanism of dislocation creep involved climb of dislocations and was shown to be rate-controlling [61]. Dislocation climb may be further divided into lattice diffusion-controlled climb ("high temperature creep"), core diffusion-controlled climb ("low temperature creep"), Harper-Dorn creep and power law breakdown [62]. At the steady state, i.e. during secondary creep, the rate of strain hardening is equal to the rate of recovery. At higher stresses ($\sigma/G > 10^{-4}$), the stress exponent is generally greater than 4. The rate controlling process in this case is believed to be climb of dislocations. The details of the process are not considered here. However, at intermediate and high temperatures and low stresses, dislocation-climb controlled viscous creep has been reported by some investigators and called Harper-Dorn (H-D) creep after initial observations in aluminium close to the melting point by Harper and Dorn [3]. H-D creep is believed to be important under conditions in which the dislocation density does not change with applied stress and is related to equilibrium between the interaction stress between the neighbouring dislocations and the Peierls stress [63].

Harper and Dorn [3] conducted a series of experiments on high purity aluminium (99.99%) at very low stresses (0.02-0.09 MPa) and temperatures close to the melting point (0.98-0.99 T_m). At lower stresses, a linear dependence of strain rate on applied stress was found. A small primary component in the creep curve was also observed. The activation energy for steady state creep was found to be in agreement with that for lattice self-diffusivity of pure aluminium. The experimental creep rates were shown to be about 3 orders of magnitude faster than those predicted by the N-H creep equation and single crystals were shown to creep at the same rate as polycrystalline samples. Experimental observations of marker lines at the grain boundaries showed that the creep strain was not localised to grain boundaries [3]. However, sub-grain formation attending dislocation creep at lower temperatures was found to be absent by Debye- Scherrer and Laue diffraction studies, presumably due to annealing at high temperatures [3] or being greater than the grain size at the low stresses employed in the study [64, 65]. These observations rule out any possibility of a stress-directed diffusional mechanism controlling the creep behaviour and point towards a dislocation-based mechanism. Barrett *et al.* [66] conducted a similar study in pure aluminium and Al-5%Fe alloy and reinforced the conclusions made by Harper and Dorn for aluminium. Barrett *et al.*, however, found evidence for sub-grain formation in their samples which was found to be in agreement with observations at higher stresses and lower temperature. Additionally, they demonstrated that dislocation density measured by etch pitting was independent of applied stress (Table 2.2). Thereafter, a number of other

metals and alloys have been reported to undergo Harper-Dorn creep (e.g. Pb, Sn [67], Al-Mg [65, 68], α-Ti [69], β-Co [70], Pb-Sn, α-Zr, Fe-Si; Fig. 2.10 [71]). Creep rates at 1313K and 0.25 MPa much faster than N-H predictions (Eq. 2.1) have been reported for copper prepared by different processing routes [72] (Fig. 2.11). Ruano *et al.* [73] have interpreted this set of data as evidence of Harper-Dorn creep in copper for large grain sizes and of grain boundary sliding accommodated by slip at smaller grain sizes. Important experimental observations during H-D creep that have been summarized by Yavari *et al.* [65] and Nabarro [63] are reproduced in Table 2.3.

In contrast to diffusional creep, the mechanism of H-D creep is not very well understood. However, for a wide range of materials the creep rate can be empirically described in dimensionless form by

$$\frac{\dot{\varepsilon}_{HD}\, kT}{D_l Gb} = A_{HD}\, \frac{\sigma}{G} \qquad\qquad (2.3)$$

where G is the shear modulus and b is the burgers vector. Experimental values of the coefficient A_{HD} for different metals at high temperature are given in Table 2.4. A number of mechanisms have been suggested to account for the observed creep behaviour and the associated microstructure. The proposed mechanisms were critically analysed by Langdon and Yavari [64]. They concluded that Harper-Dorn creep in Al and Al-Mg alloys is controlled by climb of edge dislocations saturated with vacancies (refer to McNee [7] for a detailed review of the development of Harper-Dorn creep theory). It has more recently been proposed by Wang [74] that Harper-Dorn creep may be

governed by a dislocation process of glide plus climb under a constant dislocation density determined by the Peierls stress. In this model, the strain is contributed by glide of dislocations and the rate controlling process is the climb of dislocations. It was shown that the theoretical predictions were in good agreement with the experimental data for a number of materials (fig. 2.12). More recently, a few important publications reporting new experimental investigations in this field have appeared that, however, question the operation of classical Harper-Dorn creep. Blum and Maier [75] examined the creep behaviour of Al close to its melting point and found creep to be suppressed below the reported transition stress (0.12 MPa) from power-law creep so that no evidence for H-D creep was found. Transition to a lower stress exponent was not observed and the creep behaviour was ascribed to power-law creep. McNee *et al.* [76, 77] conducted a detailed investigation of H-D creep in aluminium of different purities (*99.99-99.999%*) in tensile tests. Below the applied stress of 0.1 MPa, no steady state was observed and the minimum measured creep rates were found to be much lower than those reported for H-D creep. Pre-annealing, prior cold working and prior straining above the transition stress were all found to be ineffective in generating H-D creep behaviour. It is argued that, even when H-D creep is observed, it is limited to rates $\approx 5 \times 10^{-8}$ s^{-1}. Due to independence of strain rate and grain size during H-D creep, this is the fastest creep rate that can be observed and therefore for grain sizes less than 400 μm, diffusional creep would dominate over H-D creep.

Ginter *et al.* [78, 79] reported the results of creep tests in Al of two different purities (99.99 and 99.995%) at large strains (typically > 0.1). The creep tests were carried out on double shear samples with very large grain sizes and in most cases one grain (single crystal) was observed in the whole cross-section of the gauge. With respect to the measured creep rates, significant findings were reported. Below the transition stress for power-law creep, accelerated creep rates associated with H-D creep were not observed for 99.99% purity aluminium. In higher purity aluminium, a lower stress exponent of about 2.5 was observed at lower stresses (shear stress < 0.06 MPa). In this regime, abrupt changes in creep rates at progressive values of strain were observed in the experimental creep curves. It was argued that, for pure aluminium, early data on H-D creep does not represent the steady state due to the test duration being less than 200h (Fig. 2.13). It was proposed that dynamic recrystallization is a necessary condition for H-D creep.

Nabarro [80] has argued in favour of H-D creep claiming that the tests by Blum and Maier [75] were carried at or just above the stress that the power-law creep is expected to predominate and therefore the transition to a Newtonian creep-regime at low stresses was not observed. It was also argued that high dislocation density may suppress H-D creep due to high random internal stress about 0.4 MPa and therefore H-D creep (observed at stresses <0.1 MPa) may not be observed in these cases.

In a recent publication, McNee *et al.* [77] have reported absence of H-D creep in Al, Cu and Sn for long duration tests in tension. A fundamental theoretical

analysis of dislocation mechanisms under the relevant conditions has been undertaken and raises more questions regarding the capacity of H-D creep to generate large strains. It is argued that, at the typical dislocation density of 1×10^{-10} m^{-2} observed during Harper-Dorn creep, a stress of 0.6 MPa would be required to operate Frank-Read or Bardeen-Herring sources. In essence, during H-D creep, these sources are inoperative and therefore creep strain is limited. It is concluded that the dislocation multiplication may take place due to some hitherto unidentified localised stress concentration. Another possibility suggested is that dislocation density is much higher close to the surface compared to the bulk, as has been reported by Nost and Nes [81]. This would allow isolated Frank-Read sources to operate and would consequently lead to inhomogeneous deformation.

2.1.3 Grain Boundary Sliding

Grain boundary sliding described in this section is qualitatively different from Lifshitz sliding [41] described earlier in §2.1.1. Lifshitz sliding takes place concommitantly with diffusional creep and is not an independent process. Rachinger sliding [82], on the other hand is an independent mechanism leading to large tensile strains without fracture at intermediate and high temperatures and is invoked to explain the flow behaviour observed during superplasticity.

Structural superplasticity is observed in a number of metallic alloys exhibiting two features (a) a fine and stable grain size (typically <10 μm) (b) test temperature of the order of at least 0.5 T_m [83]. The experimental

observations of superplasticity are reviewed in great detail elsewhere [83-86] and are beyond the scope of this work. Additionally a critical review of the mechanism of superplasticity was published recently [87]. In the superplastic regime (called region II in the superplasticity literature), the contribution of grain boundary sliding to the total strain is found to be very high (typically 50-70%) [88]. Important experimental observations include an inverse-squared dependence on grain-size and a stress exponent about 2[1]. The grains remain essentially equiaxed even after tensile elongations of a few hundred percents. This observation cannot be explained by either dislocation creep or classical diffusional creep theories which predict grain elongation as macroscopic strain accumulates. It is recognised that grain boundary sliding is the process that allows the grains to remain equiaxed. Sliding is believed to be very rapid and the rate-controlling process is the accommodation required at triple points to allow sliding to continue. The proposed models to explain the observed behaviour fall into two categories based on whether the accommodation process accompanying grain boundary sliding is diffusional flow or dislocation movement. It is the specific accommodation process that is rate controlling.

Ashby and Verall [89] described a diffusional model based on grain switching events of the kind illustrated in Fig. 2.14. It was envisaged that the diffusional accommodation requires a much shorter path length than N-H creep and therefore would lead to much faster rates ($\approx$ 10 times faster). Also, a threshold

---

[1] In superplasticity, constant strain rate tests are generally employed to obtain mechanical data and strain-rate sensitivity, m, is reported. The stress exponent, n is simply the reciprocal of m.

was predicted due to the increase in grain boundary surface area in the intermediate stage. Although this model explains the topological observations during superplasticity, the details of the diffusional path have been shown to be incorrect in the original model [83]. Also, the threshold stresses predicted by the theory are too small and do not account for the strong temperature dependence observed for real materials [11].

The other class of models used to explain superplastic behaviour are based on accommodation-process-controlled dislocation movement. These models are based on situations in which the deformation rate is controlled by climb of dislocations from the head of a pile-up usually at triple points. Models by Ball and Hutchison [4], Gifkins [5] and Mukherjee [90] are three variants on the same theme. Dislocations pile up as the stress at triple point increases and further sliding is controlled by the rate at which the leading dislocation is annihilated by climb into the opposite grain boundary. The process is illustrated schematically in Fig 2.15. The advantage of these models is that they are successful in correctly predicting the grain-size and stress-dependence of strain rate and the activation energy for deformation. The measured experimental rates are frequently in agreement with the predicted rate. Despite the success of these models, Todd [87] has summarised numerous theoretical objections and experimental inconsistencies to pileup models. Also, pile-ups of lattice dislocations are rarely observed experimentally.

An alternate model for superplastic deformation of fine grained mterial has been proposed by Todd [87], based on the geometrical theory of grain boundary structure. The creep rate is proposed to be controlled by the recovery process associated with emission of lattice dislocations from grain boundaries and their annihilation. This process is left unspecified and therefore quantified predictions are not available. However, the model was shown to agree quantitatively with observed primary behaviour.

In the initial stages of superplastic deformation in the low stress regime, there is evidence for grain elongation. In a superplastic 7075 Al alloy a grain aspect ratio approaching 1.7 was measured in the initial stages of superplastic deformation [91]. Grain elongation was observed to stabilize at higher values of strain. Concurrent TEM observation of dispersoid free zones (DFZs) perpendicular to the tensile axis has been reported. The applied stresses were too low to allow dislocation creep. Similar grain elongation was reported by Li et al. [92] and by Pilling and Ridley [85]. The grain elongation reported in these works was at $T > 0.9T_m$ and cannot be ascribed to dislocation creep. This is a markedly different grain elongation to the kind observed by Ma et al. [93] in friction stirred 7075 Al alloy at much higher strain rates and stresses. Shin et al. [91] attribute grain elongation to an accelerated self diffusion process leading to formation of DFZs and locally enhanced plastic deformation of the relatively softer DFZs. Recent theoretical work by Burton [94, 95] has pointed out that grain rotation can occur readily when diffusional creep dominates: because of local irregular grain configurations, bending moments may arise providing the driving force for rotation. During superplastic

deformation, it has been observed that distant grains may come into contact or move apart [89]. It is therefore extremely likely that during large strains any particular grain may have undergone cycles of clockwise and anti-clockwise rotations. Thus only a small grain strain would be observed even after substantial overall strain in the sample [95]. However, in the initial stages of the process, grain elongation would be expected before this cyclic rotation begins.

2.1.4 Low-Stress High Temperature Creep - Search for the Dominant Mechanism?

During the past two decades there has been an extended debate on the existing experimental evidence for diffusional creep in metals and alloys. Alternative explanations based on grain boundary sliding accommodated by slip are offered to account for the low stress data for small grain sized materials. For creep data at larger grain sizes ($d/b > 10^5$) and high temperature, dislocation-based H-D creep was argued to be dominant. The search for such alternative explanations was driven by the observed discrepancies between experimental rates and those predicted by diffusional creep equations (Eqs. 2.1 and 2.2). McNee [7] has provided a chronological description of this prolonged debate which is not repeated here. From a survey of the literature, it is apparent that any amount of mechanical data cannot in itself provide definitive answers. The reason for this is two-fold. On the one hand, diffusional creep that has a strong fundamental basis assumes that grain boundaries can act as perfect sources and sinks. We now know that, except in relatively pure materials, this is not the case and therefore exact agreement of experimental with classical

theories should not be expected. To further complicate matters, grain boundary diffusivity can be fairly sensitive to impurities and the value to be used in Eq. 2.1 and 2.2 must be determined for the same system (use of correlations or values reported for nominally the same compositions will lead to inaccuracy). The other reason is that theoretical knowledge of Harper-Dorn creep, or even grain boundary sliding, is not sufficiently advanced to predict their creep rates from first principles. For this reason alone, a direct comparison with mechanical data is not sufficient and microstructural and other measurements are essential to establish the dominant mechanism (e.g. McNee *et al.* [96] and Thorsen *et al.* [97] who measured movement of grains relative to each other in three-dimensions and directly observed deposition of material at transverse grain boundaries in copper and copper-2 wt.% nickel respectively). There is, again, considerable argument about interpretation of precipitate free zones (PFZs) formed as a result of creep at low stress. Ruano and co-workers [98] initially claimed that PFZs were formed due to a power-law dislocation creep process at high stress. Later this view was modified and PFZs and concurrent pile-ups at longitudinal grain boundaries were attributed to dissolution of precipitates at transverse grain boundaries, diffusion of solute to boundaries parallel to the applied stress and re-precipitation [99]. This particular mechanism has been shown to be unacceptable on three different counts [32, 100]:

a) Dissolution of precipitates of the kind envisaged is thermodynamically unlikely.

b) No driving force exists for diffusion of solute to longitudinal grain boundaries.

c) Re-precipitation at longitudinal grain boundaries would give rise to positive transverse strain. This mechanism acting in isolation would thus result in a negative creep rate.

Furthermore, Wilshire [101] proposed that PFZs are a consequence of fabrication and heat-treatment prior to creep. McNee et al. [32] have provided effective counter-arguments for both these proposals. Firstly, no PFZs were observed prior to creep testing. Secondly, absence of PFZs in regions outside the gauge section on the crept samples implied that PFZs observed during their tests were exclusively due to creep. Based on these microstructural observations, the dominant creep mechanism can be concluded to be diffusional creep. Thus, it can be seen that the potential exists to correctly identify the operative mechanism by using microstructural observations in conjunction with mechanical data.

As indicated previously, in three recent publications, the existence of Harper-Dorn creep itself has come under fire [75-77]. Ginter et al. [78] while studying Harper-Dorn creep at large strains concluded that "*the linear stress dependence of creep rate characterizing Harper-Dorn creep is most probably a direct consequence of short-term measurements (time was less than 200h and total creep strains were less than 0.001) made by previous investigators.*"

A radically different view of the whole situation is held by Wilshire and co-workers[102, 103]. They argue that there is no change in mechanism at low stresses and that creep is still controlled by generation and climb of dislocations as at high stresses. They have argued that since the transition from stress exponent, n, approximately equal to 3 at high stress to 1 at low stress is not accompanied by a sudden change of grain size sensitivity, $m = 0$ to $m \geq 2$, there is no need to invoke diffusional creep mechanism to account for the low stress data in copper [102]. These authors propose a similar approach to rationalize the creep data for Al and reach similar conclusions [103].

2.2 Creep in Copper Wires and Foils

A number of studies have been conducted on creep in fine metallic wires and thin foils very close to their melting point at low applied stresses. The aim of these studies was to estimate surface energy by measuring the stress required to balance the effect of surface tension forces. The experimental procedure involved suspending a very pure (typically 99.95-99.999%) metallic wires or foils with very low attached loads. Knots were applied to the wires to define gauge lengths. The extension/contraction of the sample was measured for each gauge section. The strain thus measured was plotted against the load experienced. The load for "zero-creep" was then used to determine the surface energy value. The technique was developed by Udin and co-workers [12] and used successfully for measurements of creep rates in a number of metals (e.g. copper, gold and silver [16]).

In fine wires (most studies used wire diameter <128 µm), only one grain element was found to occupy the cross-section of the wire. This observation led to these structures being termed "bamboo structure". In these structures, the surface energy γ_s is related to zero-creep load w_0 by the following relation

$$\gamma_s = \frac{w_0}{\pi \frac{a}{2}(1 - \frac{\gamma_{gb}}{\gamma_s}\frac{a}{2l})} \qquad (2.4)$$

where a is the wire diameter, l is the grain length and γ_{gb} is the grain boundary energy. Herring [2] calculated the creep rate of bamboo structures, by diffusion through the lattice assuming flat surfaces of the wire, to be

$$\dot{\varepsilon} = B\frac{D_l\Omega\sigma}{alkT} \qquad (2.5)$$

where B is a numerical constant with value close to 12.37 but dependant on the grain aspect ratio. Burton [95] has analysed the same problem without the assumption of flat surfaces and found that the numerical constant value is more strongly dependant on the grain aspect ratio (Fig. 2.16). Strain rates per unit stress from experimental studies on copper are given in Table 2.5. Comparison with equation (2.5) shows that the measured rates are in close agreement with those predicted from diffusional creep when the test duration was long enough to achieve steady state. Activation energy was measured and found to be close to that for lattice self diffusion. It is worth noting that the experiments on copper foils yield apparently contradictory results. Pranatis and Pound [104] carried out experiments to measure surface energy

and viscosity in copper foils of various thicknesses (38-128 μm) close to the melting point. The measured creep rates were found to be in agreement with diffusional creep theory and strain rate per unit stress was found to be inversely proportional to the product of foil thickness and grain size. Similar experiments by Pines and Sirenko [72] on electrolytic copper foils gave creep rates much faster than diffusional creep predictions. Mohamed [105] reviewed low stress creep data in copper and concluded that the experiments conducted by Pines and Sirenko [72] provided evidence for operation of H-D creep in copper for large grain sizes. Ruano et al. [106] reached same conclusion for creep data at large grain sizes and further added that the creep rates reported for small grain size could be interpreted in terms of grain boundary sliding. Jaeger and Gleiter [107] also conducted some experiments on alumina coated copper foils. They showed that the alumina coating fractured at high angle boundaries and concluded that only these boundaries were operative as vacancy sources and sinks during the creep process. The operative creep rates, however, were not reported.

The conclusions of Mohamed [105] and Ruano et al. [106] raised questions regarding interpretation of early creep data in copper and other pure metals. Various authors provided counter arguments in defence of diffusional creep. Specifically, regarding the creep data of Pines and Sirenko in copper, Owen and Langdon [108] argued that these experiments were carried out in the range where the strain rate was linearly proportional to applied stress and therefore grain boundary sliding cannot have been the rate controlling process. The observed discrepancy of two orders of magnitude between

experimental rates and those predicted by diffusional creep was explained on the basis of substantial inter-granular porosity inherent in these samples made by powder metallurgy. No comments were made regarding the data where the measured creep rate was apparently independent of grain size. These could still be regarded as evidence for H-D creep in copper.

2.3 Role of diffusional creep in superplasticity

As indicated earlier, Rachinger grain boundary sliding is believed to be the dominant mechanism of strain generation during superplastic deformation. The accompanying accommodation process at low and intermediate strain rates is, however, not so unambiguously known. Raj and Ashby [46] contend that the rate of sliding is not controlled by the intrinsic properties of the boundary but *"almost always it is the accommodation of the (planar) incompatibilities that controls the extent and rate of sliding"*. Accordingly, accommodation may be either purely elastic, a diffusional flux of matter or plastic flow involving dislocation motion.

Elastic accommodation results in a very small amount of sliding and cannot be of any major significance during grain boundary sliding. On the other hand, accommodation by plastic flow is expected to dominate at higher stresses (Region II). At lower stresses and strain rates, a diffusional flux of vacancies from those regions of the boundary that are under tensile stress to those under compression can relieve back stresses and allow sliding to continue. However, numerical comparison of measured creep rates with those predicted from the N-H and Coble equations shows that the measured

rates are generally about an order of magnitude faster. An attempt to account for this discrepancy was made by Ashby and Verrall [62, 89] based on a grain switching model. It was claimed that since the diffusional paths were shorter, the overall rate was about an order of magnitude faster. The rates thus estimated are then in better agreement with experimental rates.

Gifkins [5] calculated the overall strain rate by considering various accommodation processes individually and assuming that they act in parallel. The total strain rate can thus be calculated by simply summing the contributions from triple-point folds, diffusional accommodation, dislocation climb and glide. The calculated rates were compared to those measured experimentally for a number of single phase alloys in the superplastic regime. Based on this comparison, they concluded that, although diffusional accommodation was never actually the dominant mechanism in regime II, it makes a significant contribution. Similar calculations were performed by Shin *et al.* [109] to account for their data on superplastic behaviour of the 7475 Al alloy. They concluded that diffusional accommodation according to the Ashby-Verrall model [89] controlled the rate of sliding at lower stress for the two lowest grain sizes (5.5 and 8 μm) used in their work while, at increasing stress, the contribution due to accommodation by slip appears to increase. Accordingly, the stress exponent gradually increases with increasing stress, albeit without a sharp transition. They have argued that a high stress exponent (>2) observed at lower stresses may result from a temperature dependent threshold stress. This has been demonstrated to be the case for

superplastic deformation of a 7475 Al alloy with relatively coarse grain size [110].

Other experimental evidence is available to support the claim that diffusional accommodation is of significant importance during superplastic deformation, particularly at low stresses and strain rates. Quantitative metallographic studies of superplastic deformation of Zn-Cu-Mn and Al-Zn-Mg alloys indicate that the contribution of diffusional flow increases at decreasing strain rates [111]. Almost 40% of total strain was attributed to diffusional flow at the lowest strain rate of $3 \times 10^{-4} \text{ s}^{-1}$. Backofen et al. [112] observed striations in a Mg-6 Zn-0.5 wt.% Zr (ZK60) alloy perpendicular to the stress axis and attributed their presence to diffusional transport of matter. For the very fine grain sizes employed in their work (mean linear intercept grain size 0.55 μm), they observed that a "diffusional strain" calculated from the width of the striations was approximately equal to the strain due to grain elongation up to about 100% strain. This diffusional strain was also well correlated with total sample strain and accounted for approximately half the sample strain. They contended that diffusional flow may have an important role in superplastic theory. Valiev and Kaibyshev [113] found a strong dependence of grain boundary sliding on the angle between the axis of the specimen and the traces of sliding boundary on the surface from their tensile tests on a Mg-Mn-Ce alloy. In region I, sliding occurred mainly at transverse boundaries, whereas in regions II and III the largest amount of sliding was measured for boundaries lying at 45° to the specimen axis. This observation can be easily

understood in terms of an increasing contribution from diffusional accommodation at decreasing strain rates.

Similarly, Li et al. [114] concluded that diffusional creep controlled deformation of superplastic Al-4.5% Mg alloy at strain rates $<10^{-5}$ s^{-1}. Experimental creep rates were found to be in good agreement with those expected from the N-H equation. The activation energy for superplastic deformation was found to be close to that for aluminium self-diffusion. Grain elongation was observed during superplastic deformation, with grain aspect ratio approaching 1.7 at a strain rate of 10^{-4} s^{-1}. The ratio of grain elongation to total strain was estimated at various strain rates and was found to exhibit a minimum at intermediate strain rates. At high applied stresses, grain elongation can be attributed to dislocation motion while at low stresses, diffusional motion can provide a ready explanation for large grain elongation. The above-mentioned observation of grain elongation in a fine grained aluminium alloy motivated Shin et al. [91] to study the microstructural evolution of 7075 aluminium alloy during superplastic deformation in more detail. The observations of Li et al. [114, 115] were confirmed by Shin et al. TEM observation of microstructure after deformation revealed the presence of dispersoid free zones (DFZs) in the vicinity of grain boundaries perpendicular to the stress axis at a strain rate of 2 x 10^{-4} s^{-1}. The authors attribute DFZs to a diffusional creep process on the basis of the earlier observation [109] that associated flow stresses were too low for dislocation creep to be operative. They observed that the width of DFZs was dependent

on strain rate. They postulate that a larger DFZ at lower strain rate is a consequence of an increased contribution of diffusional flow to overall strain.

Two superplastic alloys studied in the present work were the aluminium-zinc-magnesium-copper alloy 7075 and the magnesium-6 wt.% aluminium-1 wt.% zinc alloy AZ61. Fine grained 7075 has been extensively shown to exhibit superplasticity [91, 93]. Various techniques to produce fine grain sizes have been developed including thermo-mechanical treatment [116], equal channel angular pressing [117] and friction stir processing [93].

Recently magnesium alloys of the AZ series (AZ31 and AZ61) have also been shown to exhibit superplasticity [118-123] at intermediate temperatures and stresses. The associated mechanical data, however, did not extend to the very low stresses at which Coble creep is expected to be the dominant mode of deformation of magnesium alloys [18, 24, 27, 124-126]. This was therefore explored further in the present work. Since superplastic behaviour of aluminium and magnesium alloys is an area of some practical importance, a better understanding of its mechanism is crucial for future development.

3.0 EXPERIMENTAL PROCEDURE

3.1 Wire Testing

Experiments to establish the experimental conditions under which diffusional creep is dominant were carried out on copper. Copper was selected for this work because some of the strongest evidence for diffusional creep has been found for this material. Reels of high purity (>99.99%) copper wires of diameter 25-500 microns were purchased from Goodfellow Cambridge Ltd. in the as-drawn condition. The nominal composition of the as-supplied material is given in Table 3.1. The as-received wires were examined under an optical microscope for surface defects. The portions of wire that were damaged were discarded. Pieces of as-received wire were mounted in Bakelite and the diameters of the wires measured from their cross-sections. The resulting values of wire diameter are reported in Table 3.2. Creep samples were prepared by cutting short lengths of wire from these reels. The gauge length for the finer wires (25, 50 and 125 microns diameter) was marked by tying two knots on the wire approximately 80 mm apart. For thicker wires (250 and 500 micron diameter), annular scratches were made by rolling the wire over a vertical razor blade. Copper weights were tied to each sample to obtain the desired stress. The samples were suspended on a temporary stand and the gauge lengths were measured using a travelling

microscope. Each sample was then cleaned in a soap solution, washed and then dried with alcohol.

The creep tests were carried out in a vertical tubular furnace. The general arrangement of the creep testing furnace is shown in Fig. 3.1. A ceramic disc was cement bonded near one end of a K type thermocouple. Four holes were drilled through this disc to allow four samples to be tested simultaneously. Four hooks, made of Ni-Cr wire, were attached via these holes. The loaded copper wires were tied to these hooks. The tip of the thermocouple was positioned to be close to the mid-point of the gauge length of the creep samples. Prior calibration of the furnace established that the hot zone of the furnace was maintained to within $\pm 1K$ over the specimen gauge length of 80 mm. Temperature was controlled by a Eurotherm 118P type controller and the variation in temperature during testing was $<2K$. The specimen assembly was placed in the furnace tube, through which a slowly flowing gas could be passed.

The furnace containing the samples was first flushed with argon-5% hydrogen for 6 h. The wires were then given an annealing treatment at 450°C under load for 1 hour and then removed for measurement of the gauge length to within $\pm$ 20 μm at room temperature using a travelling microscope. The creep tests were then carried out in the flowing Ar - 5% H_2 atmosphere at 990°C. The samples were withdrawn and the gauge length remeasured initially after 24 h and then repeatedly after longer durations to obtain satisfactory levels of strain.

For the thinnest wires, on completion of each test, the wire was cut at the lower end of the gauge length and the parts were weighed. The applied stress was calculated from the weight below the gauge length with a correction for the self-weight of the sample, i.e. half the weight of the remaining sample up to the midpoint of the gauge length. The gauge length was then examined under an optical microscope. The average grain length of the "bamboo" structure was measured by counting the number of grain boundaries (approximately 100) over a length of wire. Optical and scanning electron microscopy was carried out to observe the changes in profile of the wire and any surface features that developed during the test. Scanning electron microscopy was carried out at operating voltage of 10 kV. For thicker wires, longitudinal and transverse sections were mounted in Bakelite, then ground and polished to observe the grain geometry.

Optical observation of wires showed evidence of offsets at grain boundaries not closely perpendicular to the wire axis. To estimate the contribution of grain boundary sliding to total creep strain, random photographs of the as-crept wires were taken in a scanning electron microscope. Each horizontal offset and the angle of the grain boundary with the tensile axis was measured from the photographs. This was converted to vertical strain and compared with the total measured strain. Images of grain boundary grooves were also taken and the ratio of surface energy (γ_s) and grain boundary energy (γ_{gb}) computed from the angle at the groove boundary root using the force balance shown in Fig 3.2.

3.2 Foil Testing

3.2.1 Tensile Tests

The initial cross-section of the OFHC copper bar used was 100 mm wide by 100 mm thick. Pieces were hot-rolled at 700°C longitudinally to 8 mm thickness. The surface was thereafter ground and polished down to 6 μm finish using diamond paste to remove the oxide formed during hot rolling followed by cold-rolling to 600 μm thick. For thinner foils the cold rolling was continued down to 400 μm thick. The measured foil thicknesses were within ±20 μm of the quoted thicknesses. The cold-rolled sheets were re-polished to 6 μm finish and creep samples were punched out. The dimensions of these samples are shown in Fig. 3.3. Edges were filed using a jeweller's file to remove flash from punching. Small cross wire scratches were placed 3.0 and 3.1 mm from the vertical and horizontal edge respectively at both ends on one surface. Punch marks were applied at the intersection and holes (1.5 mm diameter) were drilled near both ends. These samples were placed in silica tubes, which were evacuated and back filled with argon (400 mbar), then sealed off, placed in a furnace and annealed at 1075°C for 40 hours with an initial heating rate of 1°C/min. Some samples were annealed for 1 hour at 1075°C to obtain finer grain size. These samples were introduced into the furnace once the desired temperature was reached. The complete sequence of operations is summarised in Fig 3.4.

Before creep testing, indentations were applied to the gauge section using a Vickers microhardness tester. The gauge length ~20 mm was measured to

±0.02 mm, from both the micro-indents and the end-holes, using a travelling microscope. During creep testing, the micro-indents tended to anneal out, therefore in later tests, 3-4 indents were applied in a line across the width of the gauge length. Each sample was weighed prior to testing and an identification number marked in ink at one end.

Grain size was measured using the linear intercept method. Grain boundary intersections with the surface were revealed by thermal etching during annealing. These grain boundary positions were very well defined after annealing. It was noted that the corresponding grain boundary groove was observed at the opposite surface implying that the grains extended through the thickness of the sheet. However, the grains did not extend across the width of the gauge section.

Creep testing was carried out in the vertical tubular furnace described earlier. Weights were applied directly to each sample using a piece of Ni-Cr wire. The measurement of strain was carried out by withdrawing the sample at the end of the test and measuring the gauge length under a travelling microscope.

To compare the grain sizes estimated from the thermally etched grain boundaries at the surface with chemical etching, annealed samples were mounted face up in bakelite and prepared conventionally to 1 μm finish using diamond paste. The repolished face was then chemically etched with alcoholic ferric chloride to reveal the grain boundaries. Sections were also made of copper foils 600 μm thick through their thickness after giving an annealing treatment similar to that of the creep samples. These were thereafter

prepared for metallography and it was confirmed that there were no grain boundaries parallel to the surface and that all grains were through thickness.

The creep-tested samples were characterised by optical and electron microscopy. For low magnification photography, a zoom microscope was used. However, sample bending led to difficulty in uniformly illuminating the sample and the quality of photographs obtained was very poor.

3.2.2 Bending Tests

Foils 100 and 250 microns thick of high purity (>99.99%) copper were used in this work. The thicknesses of the foils were found to be within ±5 μm of the nominal thicknesses. The nominal composition of the as-received material is given in Table 3.1. The tests were conducted either by supporting the foil on two posts at either end or by clamping it at one end. A schematic of the test assembly for the creep tests carried out on two supports (these tests are hereafter described as bridge-type tests) is shown in Fig. 3.5a. 6 mm wide foils were placed on a sample holder machined out of OFHC copper. The foil was supported by the two endposts 20 mm apart. Scratch marks were applied on the base of the sample holder and the vertical distance of the sample holder from the foil was measured using a travelling microscope. These measurements were used to estimate the amount of strain accumulated during creep, as described below. The foil was thus loaded only under its own weight. This loading leads to normal stresses on planes normal to the long axis of the foil, which were compressive on the top surface and tensile at the bottom surface. The maximum bending moment in the foil acts at the

midpoint of the span (10 mm from either end, Fig. 3.5a). The magnitude of the maximum bending stress was estimated to be 2.62×10^{-6} Nm. The corresponding unrelaxed normal stresses at the top and bottom surfaces were estimated to be ± 0.26 MPa. Shear stresses were largest at the two ends of the foil but these were estimated to be about an order of magnitude lower than the maximum normal stress. In this case, the ends of the foil were found to have sintered to the copper sample holder by the end of the test.

For the bending tests carried out using only one support (hereafter referred to as cantilever tests), the foil was held on a graphite/OFHC copper sample holder by tightly winding it with (a long) copper wire (Fig 3.5b). In this case, the top surface of the foil was under tension while the lower surface was under compressive stress. The bending stress acting on the foil was maximum at the supported end and decreased parabolically to zero at the other end. The value of bending moment depends linearly on the foil width and thickness and on the square of foil length

$$M_b(x) = \frac{\rho_{foil}\, g w h}{2}(L - x)^2 \qquad\qquad (3.1)$$

where w and h are the foil width and thickness respectively, x is the horizontal distance along the foil and L is the total length of the foil (Appendix 1).

In both these types of tests, the assembled creep specimen was placed in a silica tube along with a titanium getter. The tube was then evacuated and back filled with argon (400 mbar), then sealed off. The sealed tube was placed in a

horizontal tubular furnace and held at 1000°C for the test duration. The heating rate was set to 3°C/min.

For the bridge-type tests, the base of the sample holder was scratch marked 5 mm apart before sealing off. The distance of the foil from the base of the holder was measured at these 5 different locations before the test, after 24 hours at 1000°C and then after completion of the test. The profile of the foil thus measured at the end of the test was curve fitted to a circular equation of the form $(x-a)^2 + (y-b)^2 = R^2$ to obtain the radius of curvature (R) of the foil after the test. Curvature (κ) of the foil is simply the reciprocal of the radius of curvature. Strain at the surface is thus

$$\varepsilon = \pm \kappa \frac{h}{2} \tag{3.2}$$

To measure the profile of the foil crept during cantilever tests, the foils were placed under an optical microscope such that the edge of the foil was observed under reflected light. The supported end of the foil was aligned to be parallel to the graduated scale on the eyepiece. One edge of the foil was positioned at the central crosswire that served as zero point. Thereafter, the sample stage was displaced by 500 μm along the longitudinal axis and displacement of the edge from the horizontal scale was recorded. This process was repeated after moving the stage another 500 μm. Thus, the profile of the foil was discretised over the whole length. The procedure for estimating the curvature, κ, for the cantilever tests from the measured profile is described in Appendix 1.

To study the effect of localization of strain during diffusion creep, an alumina coating (approximately 100 nm thick) was applied to one of the surfaces of the foil. The alumina coating was deposited by plasma sputtering using an aluminium target in an oxygen-argon atmosphere. The substrate was pre-treated with plasma to clean the surface. During coating the substrate reached a maximum temperature of about 150°C. Four coating runs were carried out. For bridge type tests, the coating was applied to the foils by plasma deposition at an operating power of 0.9 kW for either 12 or 25 min. For samples used for cantilever tests, the coating was applied at an operating power of 4 kW for 40s. To estimate the coating thickness, a long duration coating experiment (10 min at an operating voltage of 570 V, total current being 7A) was carried out. The thickness of this coating was measured to be about a 1.6 μm using a nano-identation machine. The coating was observed to be uniform and adhesive. Based on previous experiments, it was known that the coating deposited has a number of point defects and was non-stoichiometric. Both bridge-type and cantilever tests were carried out on samples which were either uncoated or coated on one surface. After the tests, the rate of change of curvature was estimated in the manner described above and microscopic observations of the coated and uncoated surface were carried out by both optical and scanning electron microscopes.

3.3 Creep tests on superplastic alloys

To study the low stress creep behaviour of superplastic alloys some constant load creep tests were conducted. It was essential to use single phase superplastic alloys to be able to make any theoretical comparison of measured

creep rates and those predicted by theory. It has been shown that suitably fine-grained aluminium 7075 and magnesium AZ61 alloys exhibit superplasticity and were therefore used in this work.

3.3.1 Aluminium alloy 7075

Hot extruded bars 50 mm in diameter of 7075 aluminium alloy were obtained from an external supplier. The nominal composition of the as-received alloy is given in Table 3.3. To obtain fine grain size, a thermomechanical treatment was carried out. Two surfaces of the rod were first machined flat to enable rolling. The treatment was based on that developed by Wert *et al.* [116]. The four stages involved in the process are:

(a) Solution treatment at 482°C for 3 hours followed by water-quenching.

(b) Age hardening at 400°C for 8 hours followed by water-quenching.

(c) Hot rolling at 220°C. During this step the thickness was reduced from 40 mm to 10 mm (75% reduction in thickness) in 5 passes. The stock was reheated to 220°C between passes.

(d) Recrystallization treatment at 482°C for 30 minutes followed by water quenching.

Steps (a-c) were carried out on successive days and Vickers hardness values were recorded before and after each step. A small increase in hardness was observed due to age hardening at room temperature after (a) and before (b).

Samples were prepared for microstructural observations by grinding off about 2 mm from the surface. Cross-sections were also prepared for metallography

by grinding and polishing down to 1 μm finish. Polished samples were electro-etched using 25% nitric acid/75% methanol electrolyte for 30 seconds with a potential of 12-15 V at -30°C.

Thermomechanically treated 10 mm thick bars were machined to produce creep samples. The dimensions of the creep samples used for constant load tests are shown in Fig. 3.6. Creep tests were carried out in two Mayes rigs. The details of the creep testing rigs and the data acquisition system used for this work are described in detail elsewhere [7]. Three K type RS 219-4365, stainless steel sheathed thermocouples were attached to monitor the temperature along the gauge length. A three-zone furnace was used with each rig. The temperature variation of the set point was found to be within 1K and temperature difference along the gauge length was maintained to be less that 2K. The elongation of the sample was measured using a RDP group type D5/200AG transducer at intervals of 2 minutes and recorded using a Datascan technology type 7220 16 channel datalogger. No water cooling was required at the temperatures used during the course of this work.

As-machined samples were polished to 1 μm finish prior to creep testing. Scratch marks were applied parallel and perpendicular to the tensile axis. Two gauge marks were applied to the sample and the gauge length was measured under a travelling microscope. The weight of the sample was measured and the width and thickness of the gauge section measured using a vernier calliper. Creep samples were then assembled for creep testing. For this aluminium alloy, it was found that application of an anti-seize compound

(Omega-99) at the grips and the screws ensured easy disassembly. It was possible to change stress and temperature during the test. This allowed stress and temperature dependence of the creep rate to be investigated on the same sample.

The elongation-time data thus obtained was transferred to a spread-sheet programme (EXCEL) and converted to strain-time curves. The steady state creep rates were calculated from these curves. The total elongation indicated by the transducer was compared to that measured from the gauge marks applied prior to testing. The values measured by both methods were found to be in reasonable agreement. Surface features were observed under an optical microscope and also in a scanning electron microscope (Camscan) operating at 20 kV.

3.3.2 Magnesium Alloy AZ61

This material was supplied by Magnesium Elektron Limited in the form of hot-rolled plate 10 mm in thickness. The composition of the as-supplied alloy is given in Table 3.3. Flat creep specimens were machined from the plate with the gauge length parallel to the rolling direction. The dimensions of the creep sample are shown in Fig. 3.6. The machined samples were polished to 1 μm finish and then scratch marks were applied parallel and perpendicular to the tensile axis. The general procedure for the creep testing was the same as described in §3.3.1 for aluminium alloy 7075. Tensile creep tests were carried out at 250 to 346°C with applied stress between 0.9 and 4 MPa.

A longitudinal-section of the as-received material was polished to 1 μm finish and etched using 2% nital solution. Mean linear intercept grain size was measured by counting the number of intercepts to a set of given lines parallel and perpendicular to the rolling direction. At least 200 grains were measured in each case. An annealing treatment was carried out for 5 h at 325°C to investigate grain growth behaviour. After creep tests, the grain boundaries were exposed due to thermal etching. The grain size measurements were carried out in the grip and the gauge areas after creep. The measurements were made normal and parallel to the direction of the tensile axis, to check for any developing grain elongation during creep. Topological features and scratch displacements during creep were examined under an optical microscope and in a CamScan scanning electron microscope.

4.0 RESULTS

4.1 Creep of copper wires

4.1.1 Strain-time curves

Typical strain-time curves at seven stress levels, showing creep strain measured in 25 μm diameter wire as a function of time at 990°C are shown in Fig. 4.1. The primary component was negligible for finer wires ($\leq$ 125 μm in diameter) with a steady state achieved early (i.e. within 24 h) during creep. Errors involved in the measurement of stress and strain were within 2% and 3-9% respectively.

4.1.2 Dependence of strain rate on stress

Steady state creep rates were determined from the slopes of the strain-time curves (e.g. Fig. 4.1). Figs. 4.2(a-e) show strain rate as a function of applied stress on linear coordinates for the five different wire diameters used. It is evident that the strain rate varied linearly with stress. Negative creep rates were observed for smaller wire diameters ($\leq$ 125 μm) at the lowest applied stresses. For the larger diameter (250 and 500 μm) wires the primary strain component was larger. The creep rates measured towards the final stages of a much longer test (1060 h) on 500 μm diameter wire were found to be considerably lowered (by a factor of about 3) compared to creep rates

measured after 360h. The lower rates were believed to represent steady state and were used in further calculations.

The slopes of the strain rate-stress curves were determined by linear regression. A summary of results from the mechanical data is given in Table 4.1. For the calculation of N-H creep rates, the following values were used in Eq. (2.5):

B = 12 [2];

$D_l = 2.0 \times 10^{-5} \exp(-197,000/RT) \, m^2/s$ (R in J/mol-K) [9];

$\Omega = 11.8 \times 10^{-30} \, m^3$ [9].

4.1.3 Dependence of strain rate on grain dimensions

Strain rate per unit stress, $d\dot{\varepsilon}/d\sigma$, compensated for grain dimensions according to N-H theory, is plotted versus wire diameter in Fig. 4.3. In smaller diameter ($\leq$ 125 microns) wires, grain length exceeded the wire diameter and therefore $d\dot{\varepsilon}/d\sigma$ in those cases was normalised by the product of grain length, l, and wire diameter, a. For 500 μm diameter wires, grain size was smaller than the wire diameter. Longitudinal sectioning of these wires revealed numerous longitudinal grain boundaries and therefore square of grain size (l^2) was used in construction of the graph for the data on this wire diameter. Fig. 4.3 shows $d\dot{\varepsilon}/d\sigma$ about twice the predicted value for N-H creep for all the wire diameters tested in the range 25-500 microns.

To identify the effect of grain dimensions, $d\dot{\varepsilon}/d\sigma$ was plotted against the product of grain dimensions on a double log plot (Fig. 4.4). Data from other sources [12, 13, 20, 104] for creep of copper close to its melting point at low stresses were also plotted. Only those data points from literature were plotted for which the parameter $P(=\sqrt{D_l t/al}$, where t is test duration) was greater than 2 and therefore believed to indicate that the steady state had been achieved [16]. The creep data from the shorter test on 500 μm diameter wire (360 h) was also plotted for comparison. This allowed direct comparison of steady state creep rates measured by different researchers on bamboo-structured copper wires with different diameters and grain structure. Data from creep tests on thin copper foils by Pranatis and Pound [104] were plotted in Fig. 4.4 using the product of grain size and foil thickness for the abscissa.

4.1.4 Profile of wire

The wires after creep testing were examined by SEM to observe microstructural features generated during creep. Profiles of three wires tested at different stresses are shown in Fig. 4.5. For negative effective stress (i.e. when applied stress was less than the zero creep stress), bulges were observed on the surface close to the grain boundary (Fig. 4.5a). At such low applied stresses, the wire was effectively under axial compression and led to diffusion of copper atoms from the grain boundary to the surface (or correspondingly, a flux of vacancies from the surface to the grain boundary). In Fig. 4.5(b), for which the applied stress balances the surface

tension forces, there was no effective mass transport and the wire diameter remained relatively uniform. Under net tension along the wire axis, vacancy diffusive flux was established from the grain boundary to the free surface resulting in the profile observed in Fig. 4.5(c).

4.1.5 Effect of grain aspect ratio

When the deformation was controlled by surface tension forces (i.e. applied stress less than zero creep stress), contraction of the wire was observed. At higher stresses, when the applied stress was greater than the zero creep stress, elongation of wires was observed. However, an effect of grain aspect ratio on the profile of the wire was observed both below and above the zero creep stress. Deformation in grains with large aspect ratios was found to be confined to a small region in the vicinity of grain boundaries. In Fig. 4.6 it is seen that the surface of the wire is uniformly straight over most of the length of the grain and only changes in the profile of the wire are observed close to the grain boundary. For grains with smaller aspect ratio (close to unity), Fig. 4.7 shows that the profile of the wire changes continuously over the whole length of the grain. It can thus be deduced that the whole length of the grain contributes to the grain deformation. This effect of grain aspect ratio was also observed at higher stresses. For grains with a larger aspect ratio, the deformation was found to be confined to the region close the grain boundary as shown in Fig. 4.8. Again, as in Fig. 4.6, it was observed that the profile of the wire remains unchanged far away from the grain boundary and the diffusion is restricted to the region in the vicinity of the grain boundary.

4.1.6 Grain boundary sliding

No slip features were observed on the surface of individual grains that would suggest dislocation activity. Grain boundary sliding to form grain offsets was not observed in 25 μm diameter wires where grain boundaries were essentially perpendicular to the wire axis. In 50 to 500 μm diameter wires, however, grain boundary sliding events to form offsets were observed to an increasing degree, as shown in Figs. 4.9 and 4.10. To estimate the contribution to strain due to grain boundary sliding, the offsets in some creep samples were measured. A series of photographs of the gauge length of the crept sample were taken. The vertical components of the offsets were summed and the strain due to sliding was estimated. This strain was compared to the total strain measured on the sample. The estimated percentage contribution of GBS to total creep strain for different samples is given in Table 4.2. The contribution from GBS was found to be minor for all wire diameters. On longitudinal sections of the wire samples, no evidence for inter-granular or intra-granular cavitation was found.

4.2 Creep of foils in tension

4.2.1 Heat treatment

The grain size of the original as-received OFHC copper bar was estimated as 504 ± 101 μm. Elemental analysis of the as received material showed that metallic impurities were each less than 50 ppm while phosphorus level was

0.018 wt.%. Heat treatment of the punched foil samples derived from this bar was carried out at 1075°C. The microstructures after annealing for 1 h and 40 h are shown in Fig. 4.11. Resulting grain sizes after annealing were estimated as 0.71 ± 0.09 mm and 1.05 ± 0.1 mm respectively. Annealing at 1075°C for 100h showed further grain growth to 4 mm indicating that the grain structure was not stable and that grain growth may have continued during creep testing.

4.2.2 Dependence of strain rate on stress

A summary of creep results is given in Table 4.3. The creep rates were estimated assuming no primary stage. Pranatis and Pound [104] measured creep strain vs time in copper under similar conditions and reported linear variation of strain with time without a significant primary component. Errors involved in the measurement of stress and strain rate are 2% and 8-10% respectively. An example of a typical calculation in shown in Appendix 2. The complete data set for creep strain rate as a function of stress is shown in Fig. 4.12 . The test temperature, grain size and thickness of the samples are also shown. One sample was annealed at slightly higher temperature and had only three grains in the gauge length after annealing. The data point for that sample is marked with an arrow. The result for another sample coated with a layer of alumina few nanometers thick and creep tested at 1336 K at an applied stress 0.40 MPa is also marked with an arrow.

From the double lograthmic

plot the stress exponent for the entire stress and temperature range was determined to be 1.7 ± 0.3.

Two tests were carried out at 850°C in a coil testing rig, where it was possible to change stress during the test and strain was measured continuously using a linear transducer. The results of these tests are given in Table 4.4. Plotting the results on a double log scale (Fig. 4.13) gives a slope of 1.5 ± 0.2. Low stress dependence of creep rates at low stresses and high temperatures in foils was thus reconfirmed.

4.2.3 Dependence of strain rate on grain size

Effect of grain size was investigated for 0.6 mm thick foils. One sample was produced by annealing at a slightly higher temperature and the resulting grain size was 10 mm. The creep rate for this sample was only about two times slower than creep rate for foils of grain size ≈ 1.5 mm tested at similar stress and temperature, even though the grain size for this sample was about an order of magnitude larger.

After creep testing, grain sizes measured from thermally etched boundaries did not indicate significant grain growth during testing. However, when one sample was mounted, repolished and chemically etched, only three grains were observed in the gauge length. This observation suggests significant grain growth in that test.

For tests conducted at 850°C, two grain sizes were investigated as shown in Table 4.4. The measured strain rates were comparable for both grain sizes

tested (0.4 and 0.8 mm). The large experimental scatter made it difficult to draw firm conclusions about the grain size dependence of the creep rate. Additionally, the grains extended across the foil thickness and testing for grain size dependence is thus less conclusive. However, on the basis of very limited evidence, the creep rate appears to be independent of grain size in this range.

4.2.4 Microstructural observations

Microscopic observation of the surface after creep revealed presence of slip lines as shown in Fig. 4.14. These were initially believed to arise from bending of the sample during its removal from the furnace after creep testing. However, the possibility of a dislocation based creep mechanism, suggests that these slip features may have contributed to creep strain. Localised slip bands close to the edge of the sample were observed in some samples. These slip bands were associated with surface steps as shown in Fig. 4.15. Formation of localised slip bands can be expected to lead to scatter in the creep strain as is seen in Figs. 4.12 and 4.13. Substructure formation was also observed even after fairly low strain (Fig. 4.16). One sample that was mounted and polished to observe grain growth behaviour showed void formation at the grain boundaries as shown in Fig. 4.17. In conjunction with these observations, direct confirmation of deposition of material at transverse grain boundaries was obtained in one sample (Fig. 4.18).

4.3 Creep of foils in bending

Two types of tests were conducted on high purity copper foils (100 and 250 μm thick) as described earlier in §3.2.2. These are referred to as bridge type tests and cantilever tests.

4.3.1 Bridge type tests

4.3.1.1 Curvature of foils

The grain size of the uncoated foil (100 μm thick) after creep tests up to 200h was 280 ± 84 μm. The results for creep of the uncoated and coated samples are given in Table 4.5. It is noted that the average rate of change of curvature ($\dot{\kappa}$) decreased with increasing test duration for the uncoated sample. As discussed later, the measured $\dot{\kappa}$ values were about 1-2 orders of magnitude lower than expected from the N-H mechanism. It was observed after the creep test that the ends of the foil were sintered to the copper sample holder. This was believed to have restricted the creep of the foil. In an effort to compensate for this effect, local curvature of the central span of the foil was estimated as shown in Fig. 4.20. The local curvatures are also given in Table 4.5.

4.3.1.2 Surface observations

On the uncoated sample, grain boundary grooves were observed on both the tensile and the compressive surfaces. There was no obvious effect of the

orientation of the grain boundary with respect to the stress axis on the groove width as is shown in Fig 4.21.

Initially a thin alumina coating was deposited on the copper foil by plasma sputtering for approximately 12 min. A large amount of this coating was lost during creep testing. To overcome this problem, sputtering time was increased to 25 min to obtain a thicker coating. The thicker alumina coating was found to be stable and still adherent to the copper foil after creep. It was observed that the presence of the coating on the foil restricted grain growth. After creep testing, the grain size of the samples that had been alumina-coated prior to tests was found to be 178 ± 42 μm compared to measured value of 280 ± 84 μm for the uncoated sample. This may be due to the fact that the grain boundaries were pinned to the surface when the coating was applied. The creep rates of the coated samples were found to be two-thirds of those of the uncoated samples. Microstructural observation of the coated surface was carried out to ascertain the fracture characteristics of the coating and the salient features of the deformation process. In Fig. 4.22(a) the effect of orientation of the grain boundary with respect to the tensile axis is illustrated. The coating applied on this sample was thinner than that applied to the other sample and the underlying structure of the crept sample was exposed. It can be seen that the grain boundaries that were perpendicular/nearly perpendicular to the tensile axis showed much larger cracks in the coating than those that were parallel to the tensile axis. The cracks were observed to be highly elongated perpendicular to the tensile axis (Fig. 4.22b). Fig. 4.22(c) is a photograph from one of the ends of the

foil, where the bending stresses were much lower and cracking of the coating is negligible. Such cracks that are observed towards the end were more equiaxed compared with those in Fig. 4.22(b). Jaeger and Gleiter [107] studied creep at high temperatures and low stresses in alumina–coated copper foils under tension and observed that the coatings fractured only at high-angle grain boundaries.

4.3.2 Cantilever tests

The measured $\dot{\kappa}$ values from the bridge type creep rates were about two orders of magnitude lower than expected from the N-H mechanism (Table 4.5). This is believed to have been due to the sintering of copper foils to the copper endposts, which restricted creep. To overcome this limitation, a new set of tests was designed. In these tests (designated cantilever tests), only one support was used at one end leaving the other end free. Also, graphite sample holders were fabricated to avoid sintering. An additional advantage of this test design is that it was possible to conduct tests at different values of bending moment (and therefore axial stress) by simply varying the length of the foil to be tested. In addition, a more accurate procedure for estimation of curvature κ was developed as described in Appendix 1.

4.3.2.1 Curvature of foils

A complete summary of the results of tests carried on copper foils in cantilever mode is given in Table 4.6. Test conditions, corresponding

curvature of the crept foils and the curvature expected from the N-H mechanism are also given. The calculations of the theoretical curvatures are discussed in the next chapter. It was observed that the experimental curvatures were 7-13 times slower than those expected from the N-H mechanism. The expected curvatures were calculated assuming only one grain in any cross-section of the sample (i.e. a bamboo structure). For polycrystals, the theory includes a numerical factor ξ (<1) in Eq. 2.6 [94, 95]. The average value of ξ can be calculated by comparing the measured rates with the rates predicted by theory. From tests 9 to 18 (Table 4.6), ξ is determined to be 0.09 ± 0.01 from these experiments. Tests 2, 3 and 8 have been ignored for calculations since they were conducted for shorter duration and the deflection of the foil was very small.

4.3.1.2 Surface observations

Due to the curvature of the foils, it was difficult to obtain good quality photographs of the coated surface of the foil. SEM was not effective for this because the alumina coating was found to be transparent to the electron beam. Penetration depth of the electrons at a typical accelerating voltage of 20 kV was calculated to be of the order of a micron and therefore the coating could not be observed. Figs. 4.23-4.25 show the salient features of the coating fracture due to the creep of the substrate. Fig. 4.23 shows micrographs from the bottom surface of a 100 μm thick foil after creep. Fig. 4.23 (a) taken from an area close to the support (where the compressive stress on the foil was close to its maximum) shows that only slight thermal grain boundary

grooving had taken place. In contrast, the grain boundary was clearly visible in a corresponding area close to the unsupported end (where the compressive stress approaches zero) in Fig. 4.23 (b). Similarly, in Fig. 4.24 taken from the two ends of the top surface of a 100 μm thick foil (the top surface was coated in this case) after creep, the coating fracture pattern was quite distinct. Fig. 4.24a shows an area close to the support (the tensile stress is a maximum here), at which the coating had fractured revealing the underlying grain boundaries clearly while for an area close to the unsupported end, Fig. 4.24b shows that the coating was relatively intact and the grain boundary was visible only as a result of thermal grooving. Comparison of Fig. 4.23 (a) and Fig 4.24 (a) shows the effect of stress on the width of the grain boundary grooves. The grain boundary grooves were found to be much wider when the stress was tensile than when the substrate was under compressive stress.

Fig. 4.25 shows SEM micrographs from the top surface of a 250 μm thick foil. Due to the extremely low strains achieved for the thicker foils, the coating did not fracture. However, the application of stress had an effect on the thermal grooving behaviour of the grain boundaries. Figs. 4.25 (a) shows that the grooves were more easily visible in areas where the tensile stress on the substrate was appreciable than in Fig. 4.25(b) for the unloaded end. This suggests that the grooves were wider/deeper in the areas under small tensile stress.

4.4 Low stress creep of two superplastic materials

Structural superplasticity is observed at small grain sizes and low/moderate stress levels. The role of diffusional creep during superplasticity has been a subject of curiosity. Creep behaviour of two alloys known to exhibit superplasticity at low stresses was investigated as part of this work. The results of the creep tests are reported in this section.

4.4.1 Aluminium alloy 7075

4.4.1.1 Thermo-mechanical treatment

The microstructure of the as-received material is shown in Fig. 4.26 (a). It can be seen that the as-received material was in a severely cold-deformed condition. Thermomechanical processing of the as-received bars was carried out to attain grain refinement as described in § 3.3.1. During warm rolling, it was found to be essential to exceed an optimum rolling speed else the stock cooled down rapidly during the pass and underwent extensive cracking leading to failure.

Fig. 4.26(b) shows the microstructure of the material after recrystallization treatment. It is observed that precipitates at the grain boundary pin the boundary resulting in finer grain sizes. To obtain an accurate measure of the grain size, an orientation map of the surface was obtained by Electron Back Scattered Diffraction (SEM-EBSD) pattern. The microstructure of the sample after the recrystallization treatment as obtained from EBSD patterns is shown in Fig. 4.26 (c). The equivalent circle diameter (ECD) thus measured was 39.3±1.4 μm. ECD, however, is estimated from only the surface of the sample and is thus an underestimate of the true grain size due

to sectioning effect. The true grain size is 1.224 times the ECD [146] and evaluated to be 48.2 μm. To investigate the stability of the microstructure, an annealing treatment was carried out at 350°C for about 50 hours. The microstructure of the sample after annealing is shown in Fig. 4.26(d). It can be seen that the microstructure is generally stable at 350°C.

4.4.1.2 Strain vs. time curves

Creep curves at low stresses and at 350°C are shown in Fig. 4.27. It is seen that the sample shows an appreciable amount of primary stage after each stress change. On stress reduction from 6.5 MPa to 5.5 MPa, a small component of anelastic creep was also observed. Thereafter the creep proceeds, albeit at a lower rate than expected from interpolation of the creep rates at 5 and 6 MPa. On further stress reduction, anelastic creep was not observed.

4.4.1.3 Dependence of strain rate on stress

To investigate the stress dependence of creep rates, stress jump tests were carried out. In the first cycle, the stress on the sample was changed at increments of 1 MPa. The steady state creep rates were determined from the creep curves as shown in Fig. 4.27. The stress exponent measured during the increasing stress cycle was 1.3 ±0.4. Once a transition to a high stress exponent (close to 5) was observed, the stress was reduced by 1 MPa at a time. The steady state creep rates are plotted as a function of stress in Fig. 4.28. The complete sequence of testing and the results are given in Table 2.7. It is readily seen that the creep rates measured during the unloading cycle

were about 2-3 times lower than those measured during the increasing stress cycle.

McNee [127] conducted stress jump tests on thixo-forged 7075 aluminium. The creep rates obtained for the material in its thixo-forged condition are also shown in Fig. 4.28. Microstructure of thixo-forged 7075 after creep testing is shown in Fig. 4.29. The grain size of the thixo-forged sample after creep was measured to be 144 ± 9 μm. The rates predicted by N-H, H-D creep mechanism and by extrapolation of creep data for the same alloy at higher stresses are also given in Fig. 4.28 for comparison.

4.4.1.4 Temperature dependence

To investigate the temperature dependence of creep at low stresses, temperature change tests were carried out on one sample. The applied stress was 3 MPa during this test, in the low stress regime. The Arrhenius plot of $\dot{\varepsilon}T$ vs. 1000/T is shown in Fig. 4.30. The activation energy at 3 MPa determined from the slope of the plot is 110 ± 39 kJ/mol.

4.4.1.5 Microstructural observations

An anti-seize compound was used during creep testing of this aluminium alloy to prevent reaction of the sample with the threads. The presence of this compound made it impossible to retain a clean surface after creep. After the creep tests, the samples had to be repolished and therefore, no direct surface observations could be carried out after creep. After grinding and polishing, the grain size after test 2 was measured to be 78.4 ± 6.7 μm.

4.4.2 Magnesium alloy AZ61

4.4.2.1 Strain vs. time curves

The test conditions and resulting incremental strains with associated secondary creep rates are set out in Table 4.8. A typical strain vs. time curve (for test number 2 at 303°C) is shown in Fig. 4.32. Significant primary creep was exhibited only by the initial condition for this test (28 h at 0.9 MPa), the subsequent stages at 1.8, 2.7 and 0.9 MPa showing minimal primary components.

4.4.2.2. Dependence of strain rate on stress

Strain rates were determined from the strain vs time curves. When the rates are plotted against stress on a linear scale, the extrapolated curves intersect the abscissa indicating a threshold stress. Fig. 4.33 shows that secondary creep rates exhibited a linear dependence on applied stress between 1 and 4 MPa at all temperatures with a temperature dependant threshold stress σ_0.

Values of strain rate per unit stress $d\dot{\varepsilon}/d\sigma$ and of σ_0 from Fig. 4.33 are given in Table 4.9 along with other parameters. The lowest stress level that could be applied in the creep rigs was 1 MPa. Therefore, the behaviour of the material below this stress could not be investigated.

4.4.2.3 Temperature dependence

To investigate the temperature dependence of creep rate, tests were carried out at six temperatures between 250°C and 346°C. Fig. 4.34 shows Arrhenius plots of $Td\dot{\varepsilon}/d\sigma$ versus 1000/T for the temperature regime

involved. The activation energy determined from the slope of the curve was found to be 106 ± 9 kJ/mol. Threshold stress σ_o was also found to be temperature dependent. σ_o was found to vary from 1.25 ± 0.6 MPa at 250°C to 0.50 ± 0.15 MPa at 346°C. An Arrhenius plot was constructed for this temperature dependence of threshold stress (Fig. 4.35). The corresponding material constant was found to be 23.1 ± 5.7 kJ/mol.

4.4.2.4 Microstructural observations

The microstructure after creep comprised equiaxed α-Mg grains with a small volume fraction of presumed $Mg_{17}(Al,Zn)_{12}$ particles a few microns in size at grain boundaries. Table 4.10 shows mean linear intercept grain size $\overline{L}$ parallel and normal to the rolling direction and direction of creep loading. The initial equiaxed grain structure did not change significantly from its initial $\overline{L}$ of 25 μm, in a 5h heat treatment at 325°C or during tests 1 and 2 (a small increase to about 30 μm resulted from test number 3). More significantly, after creep, in the gauge length, the grain dimension in the direction of creep loading was 10 to 15% larger than in the transverse direction, whereas grains remained equiaxed in the grip areas. For the 13% strain of sample 2 and the 8% strain of sample 3, the measured average grain aspect ratio is sufficient to account for the measured sample strain. For the 31% strain of sample 3, however, the measured aspect ratio is not sufficient to account for the measured strain, indicating that some additional process has made an appreciable contribution at this larger strain. Finally, there was evidence from the reorientation of scratch marks made parallel to

the direction of loading that some rotation of grains has occurred during creep. An example is shown in Fig. 4.36.

5.0 DISCUSSION

5.1 Creep of copper wires

5.1.1 Dependence of strain rate on stress

The observation (Fig. 4.1) that strain varied linearly with time is consistent with the observations of Regnier and Felsen [128] and Pranatis and Pound [104] for copper wires and foils respectively, under conditions of stress and temperature similar to ours. In addition, during diffusional creep of polycrystalline samples, primary creep is generally found to be absent [15, 19]. The steady state strain rates, thus determined, were found to vary linearly with applied stress (Fig. 4.2). This observation confirms that creep is in the viscous regime and that power-law dislocation creep is not operative. Based solely on this observation, both N-H and H-D creep could be viable creep mechanisms.

5.1.2 Dependence of strain rate on grain size

According to Eq. (2.5), $d\dot{\varepsilon}/d\sigma$ can be compensated for variation in grain dimensions by multiplying it by the product of wire diameter and grain length and this value should be a constant at a given temperature for any given wire diameter if N-H creep is operative. It is shown in Fig.4.3 that the grain size compensated creep rate per unit stress is nearly constant over more than an order of magnitude variation in grain size. (In fact, grain size compensated

68

creep rate decreases slightly with increasing wire diameter. This trend is explained in §5.1.5 in terms of the effect of grain aspect ratio on creep rate). This dependence of $d\dot{\varepsilon}/d\sigma$ on grain dimensions would not be observed if the operative mechanism was dislocation-based H-D creep, which proceeds at the same creep rate for single crystals as for polycrystals [3].

Fig. 4.4 compares the results of several workers on the effect of grain geometry on the creep rate. Pranatis and Pound [104] conducted their experiments on pure copper foils with varying foil thickness and found that the viscosity of foils varied inversely with the product of foil thickness and grain size. Regnier and Felsen [128] reported linear dependence of strain rate on the reciprocal of product of wire diameter and grain size for 10-250 μm diameter wires creep tested at 800-1018°C. According to Eq. (2.5), the diffusion creep mechanism predicts a straight line with a slope of −1, for $T / D_l (d\dot{\varepsilon}/d\sigma)$ versus the product of grain dimensions (either la or l^2 as appropriate), if N-H creep was solely operative over the whole range of wire diameters that were studied. The corresponding slope in Fig. 4.4 for the wires studied in this work is -1.12 ± 0.02 in reasonable accord with diffusional creep theory. A transition from diffusional creep to Harper-Dorn creep is predicted for wire diameters exceeding 125 microns from Fig. 4.4. No such transition was, however, observed in this study for steady state conditions. It is concluded that diffusional creep describes the steady state creep behaviour for the entire range and that Harper-Dorn creep was not found to be operative at the steady state. This conclusion is reinforced by

comparing the actual creep rate with the predictions of theory according to Eqs. (2.3) and (2.5) in the next section.

5.1.3 Comparison of experimental creep rates with theory

The numerical value of B in Eq. 2.5 has been estimated for specific grain geometries. For bamboo structures, the asymptotic value of $B_\infty = 12.37$ for $a \gg l$ and "does not begin to depart seriously from this value until a/l has become smaller than any value likely to be encountered frequently in wires whose crystal grains occupy the whole cross section" [2]. Therefore, a value of 12 was used for B for the grain aspect ratios >1 observed in this work for wire diameters ≤ 125 μm. For 250 and 500 micron diameter wires, the grain size was typically smaller than the wire diameter and the structure cannot be termed bamboo structure, so the applicable value of B is 12 for equi-axed grains [11] and product of grain length and wire diameter (al) in Eq. (2.3) is replaced by square of grain size (l^2).

Using b=2.56 $\times 10^{-10}$ m [9] for copper and $A_{HD} = 3 \times 10^{-11}$ [65] in Eq. (2.3), $d\dot{\varepsilon}/d\sigma$ for H-D creep is calculated to be 6.25 $\times 10^{-14}$ (Pa-s)$^{-1}$. In Table 4.1 the measured creep rates are 1-2 orders of magnitude faster than those predicted from Harper-Dorn creep (Eq. 2.3) for wire diameters less than 250 μm. Thus, measured creep data was within a factor of 2 of Harper-Dorn creep rates only for 250 μm diameter wires and for 500 μm diameter wires tested for shorter durations. However, it must be noted that creep data for 250 μm diameter wires are also in close agreement with creep rates predicted by diffusional creep theory. Additionally, for 500 micron diameter

wire, the measured $d\dot{\varepsilon}/d\sigma$ after 1061h was found to be about 5 times lower than for Harper-Dorn creep for a test that was carried out for a very long duration to achieve steady state creep (Table 4.1). This fact together with the evident grain size dependence (Fig. 4.4) discounts the possibility of Harper-Dorn creep in bamboo structures for all wires achieving steady state under the testing conditions used in this work. Furthermore, after plotting the experimental conditions used in this study on the deformation mechanism map developed in Fig. 2 of ref. [71], it was confirmed that the conditions for in this work fall unambiguously in the diffusion creep regime except for 500 µm diameter wires. The results for 500 µm wires lie close to the N-H/H-D boundary but it has been shown in this work that the measured steady state creep rates are about 5 times lower than those predicted by Harper-Dorn creep.

The measured steady state rates are within a factor of 1.5 to 2.6 of predicted rates for diffusion creep (Table 4.1). This is considered good confirmation of the operation of N-H diffusional creep. When the effect of grain aspect ratio is included in the theoretical prediction, the agreement is found to be even better (§ 5.1.5). When data from the shorter (356h) test for 500 µm diameter wires are considered, it is noted that creep was about 5 times faster than for diffusional creep and in closer agreement with the Harper-Dorn rate. P was calculated to be 1.01 at 356h for this particular test. It has been demonstrated [16] that, for P < 2.5, measured creep rates can be orders of magnitude faster than N-H predictions. During the initial stages of low

stress creep, dislocations can climb by absorption and emission of vacancies that leads to primary creep rates faster than N-H rates [17]. At P=1.01, the transient creep rate by this mechanism is calculated to be ≈10 times the N-H creep rate, assuming that dislocations climb about 100 μm before annihilation. It is therefore important to conduct creep tests for sufficiently long durations to avoid misinterpretation of dominant steady state creep mechanism, particularly in the low strain-rate regime.

5.1.4 Profiles of the wires

Microstructural features observed in Figs. 4.5 and 4.9 provide further evidence that N-H creep is the dominant deformation mechanism. In Fig. 4.5, for 25 μm diameter, it can be readily seen from the profile of the crept wires that diffusion currents have been established under stress. Most notably, the direction of flux is observed to have reversed (c.f. Fig. 4.5(a) and Fig. 4.5(c)) when the effective axial stress changes from compressive to tensile upon increasing the applied stress.

5.1.5 Effect of grain aspect ratio

Recent numerical calculations by Burton [95] for creep in bamboo structure wires have shown that value of B is more strongly dependant on the aspect ratio of the grain than previously thought (Fig. 2.16). This is ascribed to the fact that, for grains of larger aspect ratio, the diffusion path may be confined to a smaller region in the vicinity of grain boundary. Experimental confirmation of the numerical simulation [95] is reported for the first time in Figs. 4.6-4.8. It is therefore interesting to look at the quantitative predictions

of Burton's simulation. For example, consider the results for 25 μm wires from Table 4.1. The average value of the aspect ratio for these wires is 2.2. The value of B for this aspect ratio from Fig. 2.16 is approximately 20. Using this value of B, the ratio of experimental creep rates to predicted rates for 25 μm diameter wires is calculated to be 1.6. Similar calculations for 50 and 125 μm wires show that the measured rates are respectively 1.6 and 1.7 times faster than expected from diffusional creep predictions. These calculations show that the agreement between the measured and expected rates is better if the effect of grain aspect ratio is included. These results of the present work emphasize the need for incorporation of newer findings into the classical framework of diffusional creep to achieve better quantitative agreement of experiments with theory.

5.1.6 Grain Boundary Sliding

When diffusive motion of vacancies is the prominent mode of deformation, the closest quantitative agreement between theory and experiment is observed as demonstrated in Table 4.1 and Fig. 4.4. For 50 and 125 μm diameter wires, grain boundary sliding was observed as shown in Fig. 4.9, which became more prominent in 250 and 500 μm diameter wires (Fig. 4.10). It should however be noted that this process occurs in parallel with diffusional creep as shown in Figs. 4.9(c) and (d) in which both diffusional creep and offset grain boundary sliding are seen to operate simultaneously in the same sample. Additionally, the strain contribution from grain boundary sliding has been found to be a minor one (<20 %) for the range of

wire diameters studied, although its contribution increased with increasing wire diameter (Table 4.2). This observation can be readily explained in terms of the orientation of grain boundaries in these specimens. As the sample diameter increased, the grain boundaries were no longer entirely perpendicular to the wire axis and so the grain boundaries became susceptible to sliding.

5.1.7 Zero creep stress results

From the linear plots of strain rate versus applied stress (Fig. 4.2), the zero creep stress, σ_0, can be obtained by interpolation. The zero-creep stresses, thus obtained (Table 5.1), can be compared to the values expected from surface tension effects. After Udin et al. [12], σ_0 can be expressed as

$$\sigma_0 = \frac{\gamma_s}{a/2}[1 - \frac{a}{2l}(\frac{\gamma_{gb}}{\gamma_s})] \tag{5.1}$$

where a is the radius of the wire, γ_s is the surface tension, γ_{gb} is the grain boundary energy and l is the mean grain length. The ratio γ_{gb}/γ_s is estimated, by force balance at a grain boundary groove as shown in Fig. 3.2, to be 0.36 ± 0.04 over 10 grooves in 25 and 50 μm diameter wires. Inman et al. [20] measured this ratio in pure copper by electron shadowgraphs for OFHC 50 μm diameter wires tested at 950°C and reported a mean value of 0.34. Hoage [13] concluded, from data reported by other researchers, that the ratio between the grain boundary energy and surface energy at 900°C is close to 1/3. The average grain length for each sample was measured and is reported in Table 4.1 along with the zero creep stress.

Using the ratio γ_{gb}/γ_s and the number of grains per unit length, the surface energy calculated from the zero creep stress can be corrected for grain boundary energy according to Eq. (5.1). Resulting values can be compared with values reported by other researchers for "pure" copper at similar temperatures close to the melting point as in Table 5.1. In ref. [128] the surface energy was calculated from zero-creep stress but was corrected for thermal grooving resulting in a much higher value for the surface energy compared to those reported by other investigators. Jones [129] has reviewed surface energy measured by the zero creep method and concluded that the "preferred value of solid/vapour surface energy at the melting point of copper is 1720 ± 100 mJ/m^2". It is noted that the values of surface energy measured in the present study are slightly lower than reported elsewhere. This could be attributed to presence of contaminants, e.g. oxygen, within the furnace atmosphere. Hondros and Lake [130] have shown that chemisorption of oxygen on copper can lower both the zero creep stress and the $d\dot{\varepsilon}/d\sigma$ in the diffusion creep regime. Further evidence consistent with the presence of oxygen comes from observation of thermal etching on the copper wire surfaces after creep. In silver, it has been shown that presence of oxygen is a necessary condition for thermal etching to take place [130]. Oxygen, therefore, is believed to have been present in the atmosphere and responsible for the slightly reduced surface energy in this work.

5.2 Foil tests in tension

5.2.1 Dependence of strain rate on stress

The value of stress exponent for creep of copper foil at low stress was found to be 1.7 ± 0.3 and 1.5 ± 0.2 from tests conducted on virgin samples at 1070°C and from stress change tests conducted at 850°C respectively.

Figs. 4.12 and 4.13 show that the creep rate has low stress dependence at the stresses investigated in this work. If we ignore the one data point in Fig. 4.12 that shows negative strain rate, then the entire data set can be plotted on log scales. We have ignored this data point because this data was obtained from the very first creep test conducted so confidence in this data point is less than for the other two data points for the same stress level. For the present calculations we also exclude the creep rates for the sample with initial grain size 10 mm and the alumina coated sample. The two sets of data at 850°C and 1070°C can be integrated by compensating for temperature using an activation energy = 197 kJ/mol [9] and using non-dimensionalized strain rate and stress. As discussed in the next section (§ 5.2.2), the observed creep behaviour is evidently independent of grain size and therefore no correction for grain size is applied for evaluation of the stress exponent. By performing a non-linear regression of the data in the low stress regime at 1070°C, along with the data obtained at 850°C from stress-jump tests, it was determined that the stress exponent for creep in the low stress regime was 1.9 ± 0.3. Both sets of data can then be best described empirically by

$$\frac{\dot{\varepsilon}kT}{D_lGb}=5.0\times10^{-7}\left(\frac{\sigma}{G}\right)^{1.9} \qquad (5.2)$$

Based on the calculated stress exponent, the observed creep behaviour cannot be ascribed to power-law creep for which the expected stress exponent is

close to 5 [9]. The other possible mechanisms from the literature [9] are diffusional creep (Eqn. 2.1) and H-D creep (Eqn. 2.3). Bingham type behaviour is not considered since the measured threshold stress ($\approx$0.015 MPa) is negligible compared to applied stress.

By equating the power-law creep rates with those expected from low stress creep observed in our work, the expected value of the transition stress to power law creep can be estimated. The power law data for copper was obtained from the compilation by Frost and Ashby [9]. The transition stress expressed in non-dimensional form was thus calculated to be $\sigma/G = 8 \times 10^{-5}$. At 1065°C, this transition stress was calculated to be 2 MPa. Thus, all the data obtained in this work is expected to lie within the regime of the as yet unidentified low stress mechanism.

5.2.2 Dependence of strain rate on grain size

The observation that the tensile creep rates of foils at 1065°C for two different grain sizes (1.4 mm and 10 mm) are similar within the experimental scatter suggests that the creep rates are independent of grain size in this range. The chemically etched sample however revealed much larger grain size (6-7 mm) than the 1.4 mm measured for the thermally etched sample. It thus appears that grain growth occurred during the test so that the actual grain size was larger than indicated by thermal etching. As indicated earlier, the grains extended across the thickness of the foil. For such grain structures, the thickness as well as grain size is relevant. The evidence for the dependence of strain rate on grain size is thus inconclusive.

However, results from creep tests conducted at 850°C indicate that the observed creep phenomenon in foils under these conditions was grain size independent. Two grain sizes employed in these tests were 0.42 and 0.81 mm corresponding to 0.4 and 0.6 mm thick foils respectively. The measured strain rates for both the grain sizes can be reasonably expressed by a single straight line (Fig. 4.13). These observations indicate that the tensile creep of copper foils at 1065°C or 850°C is probably not controlled by a grain size dependent N-H type mechanism. This conclusion is confirmed in the next section where the measured rates are compared with those expected from the N-H mechanism.

5.2.3 Comparison of experimental rates with theory

For calculation of the dimensionless creep rate, the following values (all from Frost and Ashby [9] for copper) were used, with d =1mm:

$D_l = 2.0*10^{-5}\exp(-197,000/RT)$ m^2/s;

$G = 4.21*10^{10}$ [1- 0.54(T-300)/T$_m$] Pa;

$\Omega = 11.8*10^{-30}$ m^3;

and $b = 2.56*10^{-10}$ m.

The least squares fit for the data assuming linear stress dependence was found to be

$$\frac{\dot{\varepsilon} kT}{D_l Gb}\left(\frac{d^2 b}{\Omega}\right) = 322\left(\frac{\sigma}{G}\right); without\ a\ threshold\ stress \qquad (5.3)$$

$$or\ \frac{\dot{\varepsilon} kT}{D_l Gb}\left(\frac{d^2 b}{\Omega}\right) = 317\left(\frac{\sigma - \sigma_0}{G}\right); with\ \sigma_0 = 0.014\ MPa \qquad (5.4)$$

The proportionality constant A_{NH} from theory was calculated to be 7.5 for foils [52]. The relation between strain rate and stress based on Nabarro-Herring theory can thus be expressed as

$$\frac{\dot{\varepsilon}kT}{D_lGb}(\frac{d^2b}{\Omega}) = 7.5\left(\frac{\sigma - \sigma_0}{G}\right) \qquad (5.5)$$

where $\sigma_0 = 0.015$ MPa from the expected value of surface tension. Calculation of threshold stress σ_0 based on the surface tension effect is shown in Appendix 3. It can be seen by comparing Eqns. 5.4 and 5.5 that the experimental creep rates were nearly 40 times faster than predicted by the Nabarro-Herring theory. Experimental creep rates one order of magnitude faster than theory are normally reported for pure metals at short test durations [11, 16]. Similar calculations for creep of the sample with initial grain size of 10 mm showed that the experimental creep rate was 4 orders of magnitude faster than theoretical predictions.

In Fig. 5.1a, the creep rate compensated for grain size according to Nabarro-Herring theory from the present work, other data from the literature on creep of copper under similar temperature and stress ranges in fine wires and foils and the N-H prediction (A_{NH} =7.5) are plotted for comparison. The grain size for the work by Udin *et al.* [12] has not been reported in the original paper. Jones [16] while analysing this set of data has reported the values of grain sizes that were used for comparison with the Nabarro-Herring theory. From their data a best-fit value for A_{NH} of 43.5 was evaluated (i.e observed rates were about 4 times faster than expected from the N-H equation). Pranatis and Pound [104] reported the viscosity of copper in the linear stress

regime at temperatures of 1233-1324 K, but the actual values of strain rate and stress were reported for only one data set. Comparison of their data with the Nabarro-Herring equation (Eq. 2.1) shows that the observed creep rates were nearly 2 times *slower* than the prediction. The best fit of their data into an equation of the form of Eq. 5.3 yields

$$\frac{\dot{\varepsilon} kT}{D_l Gb}(\frac{d^2 b}{\Omega}) = 5.54\left(\frac{\sigma}{G}\right) \tag{5.6}$$

The grain-size and temperature compensated creep rates obtained in the present work are seen to be about an order of magnitude faster than reported previously [12] for copper wires at similar temperatures where diffusional creep was the dominant creep mechanism. Other reported data, by Pines and Sirenko [72] for rolled strip (their specimen number 6), which has been interpreted as evidence of Harper-Dorn creep in copper, is also shown to be faster than the predictions of Nabarro-Herring creep. Their data, however, has a major shortcoming that the duration of their tests was only a few minutes (non- dimensionalised test duration P ≈ 0.01-0.06, see Table 2.5) and so cannot possibly represent steady state creep rates. Jaeger and Gleiter [107] conducted tensile tests on samples similar to ours and observed that the coating cracked at high angle grain boundaries. They concluded that the operating deformation mechanism was N-H creep and that only the high angle boundaries took part in the deformation. Our analysis of their result (though the measured strain rates for their tests were not reported, it was indicated that the extension at some grain boundaries was about 5 μm after 100 h), however, gives strain rate approximately two orders of magnitude

faster than those calculated from the N-H equation (in agreement with our own measurements). The preceding comparison of data from different researchers, along with the discussion on dependence of strain rate on grain size, suggests that diffusional creep cannot account for the tensile creep rates of copper foils observed in the present work.

Based on the above discussion it seems unlikely that diffusional creep dictates the observed creep behaviour in coarse-grained copper foils. This may be related to the foil thickness used in this study. The works of Udin *et al.*[12] and Pranatis and Pound [104] were conducted on much thinner wires and foils respectively. The sample geometry thus restricted grain growth in their creep samples. Udin *et al.* [12] annealed their samples prior to creep testing at a temperature slightly higher than the creep test temperature to stabilize the grain structure. Diffusional creep is known to dominate at finer grain sizes [9].

Another possible mechanism is grain boundary sliding accommodated by slip, with a stress exponent of 2, close to the value found in this work. However, this mechanism can be discounted for the following reason. In the sample that was repolished and chemically etched, the grain boundaries were observed to be at an angle 80-90° to the faces of the sample, which contains the tensile axis. This is expected since the grain boundary area would be a minimum for this configuration. The boundaries were also observed to run across the width of the gauge section as for bamboo structures in wires. Grain

boundary sliding is not expected to play a very dominant role under this grain boundary geometry.

In Fig. 5.1b, the creep rates are plotted without compensating for the grain size (i.e. in accordance with H-D creep). The coefficient A_{HD} (Eq. 2.3, H-D coefficient in terms of shear stress and shear strain) can be evaluated as $6.39*10^{-11}$. Ruano *et al.* [73] evaluated $A_{HD} = 3.7*10^{-11}$ for copper after analysing the data of Pines and Sirenko [72] at 1040°C. Both these values compare well with the value of A_{HD} observed for other materials as given in Table 2.4. One major distinction, however, is that the stresses employed in the present work and also in the work by Pines and Sirenko, are about an order of magnitude larger than those used in classical H-D creep studies in Al and its alloys. Satisfactory theoretical models of H-D creep are not available to compare these A_{HD} with a theoretical value.

5.2.4 Microstructural observations

Presence of slip lines on the surface of the sample after creep suggests that the applied stress was sufficiently high to initiate dislocation glide resulting in plastic strain. To confirm this observation, it is relevant to consider the magnitude of the Peierls stress, τ_p, at these temperatures. Wang [74] has estimated the magnitude of the Peierls stress for a number of metals at temperature close to their melting point as

$$\left(\frac{\tau_p}{G}\right)_{Tm} = \frac{1}{13}(\frac{1}{1-\nu})\exp(\frac{2\pi}{(1-\nu)}\frac{b}{d_{hkl}}) \qquad (5.7)$$

where d_{hkl} is the inter-planar spacing of the particular slip plane. For slip in copper in its close packed plane, the value of τ_p from Eq. (5.7) is estimated to be 0.06 MPa. Therefore, glide is possible at the low stresses (>0.2 MPa) applied in this study. However, this glide motion of dislocations can result in only a limited amount of strain without multiplication, given by:

$$\gamma = \rho b \bar{x} \qquad\qquad (5.8)$$

where $\bar{x}$ is the average distance of dislocation glide (equal to specimen thickness in our case). Using a value of dislocation density ρ typical for well-annealed material at high temperature ($=10^9$ m^{-2}), the total strain is only of the order of 10^{-4}, which is about an order of magnitude lower than the strain measured in this work.

Average slip line spacing was measured in a number of grains and found to be 30.2 ± 8.2 μm. Accordingly, to operate Frank-Read or Bardeen-Herring sources, the required applied stress would be given by

$$\tau = \frac{Gb}{\lambda} \qquad\qquad (5.9)$$

where λ is the average dislocation link length. Substituting the appropriate values for copper, we obtain the stress required to operate these sources to be 0.22 MPa. This is exceeded by the applied stress in out work so that these dislocation sources would be expected to operate.

Therefore, the suggested mechanism for the observed creep behaviour is based on dislocation glide and dislocation multiplication by the operation of

Frank-Read (or Bardeen-Herring) sources 30 μm apart. Out of the two sequential processes in operation (i.e. glide and multiplication), glide is strongly stress dependent [131] and therefore cannot be rate-controlling during the low stress dependent creep observed in this work. If we consider dislocation generation by diffusion controlled climb (Bardeen-Herring sources), the dislocation generation rate, $\dot{\rho}$ is expressed as

$$\dot{\rho} = \frac{\rho_0 \vartheta_c}{\Gamma} \qquad (5.10)$$

where $\rho_0 \, (=10^9 \, m^{-2}$ for a typically well annealed material) is the dislocation source density, $\vartheta_c \, (= \dfrac{2D_i b^2 \tau}{kT \ln(R/r_0)}; R/r_0 = 10^8)$ [132] is the dislocation climb velocity and Γ is the dislocation climb length ($=\lambda$). The strain rate can thus be estimated simply using the following relation

$$\dot{\gamma} = \dot{\rho} b \bar{x} \qquad (5.11a)$$

where $\bar{x}$ is the average glide distance (= 400 or 600 μm in our samples) and $\dot{\gamma}$ is shear rate. Expressing in terms of tensile stress and strain and using Eq. (5.10), we obtain after rearrangement

$$\frac{\dot{\varepsilon} kT}{D_i Gb} = \frac{2\rho_0 b \bar{x}}{3\sqrt{3} \ln(R/r_0)} (\frac{\sigma}{G})^2 \qquad (5.11)$$

Eq. (5.11) has a stress exponent of 2, which is in good agreement with the observed stress exponent (1.9 ± 0.3). The magnitude of strain rate predicted by Eq. (5.11) is found to be in reasonable agreement with the rates measured experimentally in this work. All the data are found to be within a factor of 3

84

of the expected rate as shown in Fig. 5.1b. As a typical example, Eq. (5.11) predicts a strain rate of 2.7×10^{-8} s^{-1} at an applied stress of 0.23 MPa at 1335K. The measured creep rate under these conditions (test 1, specimen 1 in Table 4.3) was 5.37×10^{-8} s^{-1}. The rates predicted by this model are in good agreement with the measured rates. The model also provides a satisfactory explanation for the observed microstructural features. Other models, e.g. Nabarro's model [133] for steady state creep due to dislocation climb, give strain rate about 10 orders of magnitude lower than those observed here [77]. Alternatively, Barrett's model [134] based on dislocation annihilation at sub-grains is inconsistent with the observation of very large slip spacings at the surface so is inconsistent with both the measured creep rates and the microstructural observations. Furthermore, as seen in Fig. 4.13, the strain rates at 850°C for a 0.6 mm thick sample are about 1.5 to 2 times faster than those for 0.4 mm thick samples. This observation is entirely consistent with the proposed model, which predicts that the strain rate is directly proportional to glide distance, which in the present case is equal to the foil thickness. Interestingly, the proposed model can also reasonably account for the creep rates obtained by Pines and Sirenko [72] as shown in Fig. 5.1(b).

McNee *et al.* [77] have hypothesised that since the dislocation density closer to the surface may be higher than that measured in the bulk of the sample; it is likely that this will allow localised slip to take place. Such slip bands close to the edge of the sample have been observed in some samples (e.g.

Fig. 4.15). In the instances where these slip bands were observed, they were sufficient to account for almost all of the strain measured in the sample. Observation of these localised slip bands, close to the edge of the sample is believed to be evidence in support of the hypothesis of McNee *et al.* Substructure was also observed in these regions after fairly low overall strain. This is an expected consequence of strain localization in these slip bands.

Additionally, in some samples deposition of material and cavitation was observed at grain boundaries (Figs. 4.17 and 4.18). This can be regarded as evidence for stress directed diffusion of vacancies, though it is not the dominant creep mechanism in this case because of the very large grain sizes involved.

5.3 Foil tests in bending

As discussed above, for creep behaviour in foils 400 and 600 μm thick, the creep behaviour in tension cannot be ascribed to diffusional creep. One of the objectives of the present work was to assess the effect of diffusional creep on the stability of coatings applied to the creeping substrate. Therefore tests were conducted under bending loads on copper foils 100 and 250 μm thick. The sample geometry was able to restrict grain growth and the grain sizes were small enough to allow diffusional creep to dominate the creep process. Grain boundary sliding takes place only when there is a shear force acting along the grain boundary. In the thin foils studied here, the normal to each grain boundary is expected to be in the same plane as the normal stress.

Thus, there would negligible stress (or driving force) acting along the grain boundary for GBS to operate. The two complicating factors of grain growth and grain boundary sliding generally encountered during testing of foils in tension were thus eliminated.

5.3.1 Bridge type tests

5.3.1.1 Curvature of foils

Burton [94, 95] has analysed grain rotation for a bicrystal under bending moments by grain boundary diffusion and lattice diffusion. The mechanism is analogous to that proposed by Nabarro [1] and Herring [2] but the diffusion paths are different. The analysis by Burton was carried out assuming a single grain boundary extending across the foil thickness as well as the width of the foil. The resulting expression in terms of the rotation rate, $\dot{\theta}$ [95], is

$$\dot{\theta} = \alpha_l \frac{M\Omega D_l}{wh^4 kT}(1 + \frac{\alpha_g}{\alpha_l}\frac{\omega D_g}{dD_l})$$ (5.12)

where $\alpha_g = 720$, $\alpha_l = 6.35\ \alpha_g$ and M is the bending moment. The relative contributions of grain boundary and lattice diffusion can be calculated for the present situation using the following values for copper [9]

$\omega D_g = 5 \times 10^{-15} \exp(-104,000/RT) = 1.8 \times 10^{-19}\ m^3/s$;

$D_l = 2 \times 10^{-5} \exp(-197,000/RT) = 7.7 \times 10^{-14}\ m^2/s$ and

$d = 250\ \mu m$.

The second term in Eq. (5.12) is thus found to 1.47 x 10^{-3} (<<1). Therefore, neglecting the term for grain boundary diffusivity at high homologous temperature, Eq. (5.12) can be rewritten as

$$\dot{\theta} = \alpha_1 \frac{M\Omega D_1}{wh^4 kT} \qquad (5.13)$$

By comparison of the predicted rates with the rates measured experimentally in the bridge-type tests on 100 μm thick copper foils, it was observed that the measured creep rates were 1-2 orders of magnitude lower than predicted. This was attributed to sintering of the copper foils to the endposts of the sample holder. Such sintering of the ends of the foils is likely to have restricted creep. As discussed earlier, local curvatures from the central span of the foils were also estimated. However, these curvatures were not significantly different from the overall curvature. Thus, it was decided to conduct further tests on cantilever samples so that any sintering would not restrict creep.

5.3.1.2 Surface observations

Grain size was found to be restricted to ≈150 microns when an alumina coating was applied prior to creep testing (Table 4.5). This is believed to be due to limited mobility of the grain boundaries caused by interaction with the coating. Examination of the uncoated sample showed that there was no effect of orientation of the stress axis on the grain boundary grooves developed on the surface of the foil due to thermal etching. It must be noted that diffusional creep under applied tension leads to wider grooves perpendicular to the tensile axis compared to those parallel to the tensile

88

axis. However, in these tests conducted under bending moment, the motion of vacancies is from the top surface to the bottom surface of the foil. Therefore, there should be no major effect on the width of grain boundary grooves of the orientation of the grain boundary with respect to the tensile axis as is seen in Fig. 4.21.

Comparison of Figs. 4.22 (b and c) from the stressed and unstressed region of the foil respectively confirms that the coating fracture is due to the applied stress. The few cracks in the coating in the unstressed region of the foil may be due to thermal stresses and are qualitatively different from those observed in the stressed region. Fracture behaviour of the coating in the stressed region provides evidence that the deformation of the substrate is localised at grain boundaries. At high temperature and low stresses, one of three deformation mechanisms are generally considered to be rate controlling [9], namely Nabarro-Herring (N-H), Harper-Dorn (H-D) creep or grain boundary sliding (GBS) accommodated by slip. H-D creep is believed to be a lattice dislocation creep process [63] and does not lead to localization of strain [3]. Observation of fracture of coatings localised at grain boundaries in Fig. 4.22 (a and b) is contrary to prediction of any dislocation based creep process. Therefore, H-D creep cannot account for these observations. As discussed earlier in this section, grain boundary sliding is not expected to be operative for the applicable grain geometry. The microstructural observations of the cracking of the coating confirms that the foils in bridge type tests were deforming by stress directed

diffusion of vacancies, though this process was restricted by sintering of the ends of the foil to the sample holder.

5.3.2 Cantilever tests

5.3.2.1 Curvature of foils

In the present case (see Appendix 1), the bending moment M is given as

$$M = -\frac{q}{2}(L-x)^2 \tag{5.14}$$

Using Eq (5.14) in (5.13), we get

$$\dot{\theta} = \alpha_1 \frac{\rho_{foil} g \Omega D_1}{2h^3 kT}(L-x)^2 \tag{5.15}$$

From geometry (see Fig. 5.2),

$$\frac{d^2 y}{dx^2} = \frac{1}{R} = \Delta\theta\Big/ d \tag{5.16}$$

Intergrating (5.15) once w.r.t time and twice with x over length L, gives

$$y = \alpha_1 \frac{\rho_{foil} g \Omega D_1 t}{2h^3 dkT}\left(\frac{L^2 x^2}{2} - \frac{Lx^3}{3} + \frac{x^4}{12}\right) \tag{5.17}$$

Comparing Eq. (5.17) with the equation of profile in Appendix 1 (Eq. 13) gives

$$K = \alpha_1 \frac{\rho_{foil} g \Omega D_1 t}{2h^3 dkT} \tag{5.18}$$

The theoretical value of K thus calculated for each test condition is shown in Table 4.6 along with the measured values of K from the profile measurements of the crept foil.

It is seen that the measured rates are 7-13 times lower than those expected from the theory. Using the ratio of the measured to the expected rates, the

average value of α_1 is estimated to be 425 ± 62 (compared to 4572 estimated theoretically by Burton [95]). Eq. (5.12) was calculated for a bi-crystal, assuming grain boundaries to be perpendicular to the long axis of the foil [95]. In our experiment, however, there were about 10 grains across the width of the sample. Grain boundaries were randomly oriented with respect to the long axis of the foil and therefore the contribution of each grain boundary to bending is expected to be less than the upper bound for the idealised case used in calculating the expected rate. The component of the stress that is normal to the grain boundary will be the effective stress for any particular boundary. The overall creep rate should, therefore, be compensated to take into account the variation of grain boundary orientation in a polycrystalline material. Additionally, the presence of neighbouring grains is expected to restrict independent deformation of each grain. These two factors are believed to be responsible for the lower rates observed in our experiments. Unfortunately, no other experimental work is available to compare the value of numerical factor α_1.

It is interesting to compare the measured creep strains with the predictions of the classical diffusional equation as developed by Nabarro and Herring if these equations are simply applied to the tensile and compressive stress respectively on the upper and lower surfaces of the foils. The relevant equation is expressed as

$$\dot{\varepsilon}_{NH} = B \frac{D_l \Omega}{d^2 kT} \sigma_e \qquad\qquad (2.1)$$

where B=12 [52] and σ_e ($=\dfrac{3\rho_{foil}g(L-x)^2}{h}$) is the value of elastic stress at the tensile surface. Eq. (8) can be converted into a form comparable to Eq. (4)

$$\dot{\theta}_{NH} = \frac{\dot{\varepsilon}_{NH}\, d}{h/2}$$

$$= 6B\frac{\rho_{foil}g\Omega D_l(L-x)^2}{dh^2kT} \qquad\qquad (5.19)$$

The rates estimated by the classical diffusional creep equation on the basis only of tensile and compressive stresses (Eq. 5.19) are thus seen to be about two orders of magnitude slower than those predicted by a more rigorous analysis for the case of bending moments presented by Burton [95]. This is about 20 times lower than the rate measured from cantilever tests in the present work. This discrepancy can be readily understood if we consider the diffusional paths for grain deformation under bending moments. Fig. 5.3a shows the schematic equipotential plot within an equiaxed grain subjected to a bending moment[2]. Atomic diffusive fluxes can be calculated from the gradient of the potentials and are shown in the figure. It can thus be easily visualised that under the present situation the grain size no longer dictates the creep rate. The foil thickness becomes the all-important parameter and governs the diffusion distance. The creep rate is dependent only on

---

[2] The potentials, μ, were calculated by solving the Laplace equation

$$\nabla^2\mu = 0$$

subjected to the following boundary conditions
At the horizontal boundaries

$$\mu = 0$$

At the grain boundaries

$\hat{n}.\vec{\nabla}\mu = \beta y$ (Rate of deposition/depletion is linear)

$w\int\mu y\,dy = \Omega M$ (Boundary constraint)

diffusional path assuming that the grain boundaries act as perfect source and sinks for vacancies. Shorter diffusion distance in thin foils therefore leads to more rapid creep in the present work. This aspect of the present work is fundamentally different from other reported observations of diffusional creep, although the basic mechanism still remains the same, viz. stress directed migration of vacancies. Fig. 5.3b shows contours of the potential for a grain that is 2.5 times larger in x direction than the foil thickness. It is seen that grain size is not such an important parameter since the foil thickness dictates the diffusion distance. Fig. 5.4 shows the schematic variation of relaxed stress along the grain boundary. It should be noted in Fig. 5.4 that the variation of stress is quite different than in elastic case due to stress relaxation by vacancy diffusion.

5.3.2.2 Surface observations

Figs. 4.23-4.25 show micrographs of the foil surfaces after creep in the cantilever mode. When bending load is applied to the foil in cantilever mode, the top and bottom surfaces are under tensile and compressive loads respectively. Due to this loading variation through the thickness of the foil, the grain boundary has excess vacancies close to the top surface, while there is a deficiency of vacancies close to the bottom surface. This will result in diffusion of vacancies from the top surface to boundary and from boundary to the bottom surface via the lattice or grain boundary at high or low temperature corresponding to Nabarro-Herring and Coble creep respectively [95] as shown in Fig. 5.3.

The effect of low compressive stress can be seen in Fig. 4.23. It is seen that the grain boundary is hardly visible in the region where there is a compressive stress (Fig. 4.23a) while in the unstressed region a grain boundary is easily visible due to thermal etching. This observation is consistent with diffusional creep theory which predicts that under compressive stress the grain boundary grooves would be narrower due to migration of atoms from these grain boundaries. More importantly, at the grain boundaries under tensile stress, matter would deposit at the grain boundary resulting in wider grooves. This is indeed observed in our experiments as seen in Fig 4.24 (a). This deposition of matter at grain boundaries under tension leads to localization of strain leading to fracture of the alumina coating. Fig. 4.24 (b) confirms that fracture of the coating is due to the effect of the small tensile stress alone, other conditions being the same in the two micrographs.

An interesting observation in Fig. 4.24 (a) is that the coating was found to fracture even at grain boundaries that were parallel to the long axis of the foil. This occurs because during bending of beams the top surface is under normal stress even in the transverse direction. This effect is due to Poisson's ratio and leads to anti-syntactic surfaces in a bending foil. Since the foil was clamped to the end post, there would be additional stresses acting in the transverse direction. This effect is magnified close to the supported end due to clamping of the foil. Thus it is expected that diffusional creep is operative

even at grain boundaries that are parallel to the long axis of the foil and a finite positive value of strain is expected at these boundaries.

In the cantilever tests conducted on 250 µm thick foils, the total strain was not sufficient to produce coating fracture of the kind observed in Fig. 4.24. However, operation of the same mechanism as described above was confirmed from the comparison of the width of grain boundary grooves from the stressed and unstressed regions of the foil. The consistency of mechanical data for the two foil thicknesses reported in Table 4.6 supports this conclusion.

5.4 Creep of superplastic alloy at low stresses

5.4.1 Aluminium alloy 7075

5.4.1.1 Strain vs. time curves

The creep curves of the 7075 aluminium alloy at all the stresses applied in this work showed renewed primary creep on increasing the stress. The origin of the primary component is probably bowing out of dislocations but was not investigated in this work.

5.4.1.2 Dependence of strain rate on stress

Fig. 4.28 shows that for the thermomechanically treated sample the stress exponent was close to 1 at low stresses (<5 MPa). Above the transition stress, the value of stress exponent was close to 5 normally associated with power-law creep. An analysis of available creep data for Al-7075 (temperature range 373-723K and stress range 3-450 MPa) from the

literature [135-140] was carried out. The available data was fitted to the Dorn Equation and the high stress data was best expressed as

$$\frac{\dot{\varepsilon}\,kT}{GbD_0\exp(-\dfrac{Q}{RT})}=A_D(\frac{\sigma}{G})^n \tag{5.20}$$

where the best fit values of various parameters are given as follows: $D_0 = 1.7\times10^{-4}\exp(-142,000/RT)$, $n = 4.1\pm0.2$ and $A_D = 7.23$. Our data from the TMT samples is plotted in Fig. 5.5 along with this data from other sources for comparison. The observed discontinuity in Fig. 5.5 is most probably due to grain size. Power law creep data is obtained from publications before 1970. The thermomechanical treatment to produce small grain sizes were not so well developed and therefore these creep data presumably were obtained for coarse grained material. This is believed to be the reason for the apparent discontinuity close to the transition stress.

It is observed that our data on TMT 7075 aluminium alloy at lower applied stress ($\sigma/G < 2.6\times10^{-5}$) shows a transition to a lower stress exponent ($=1.3\pm0.4$, Fig. 4.28). For a thixo-forged sample [127], the corresponding stress exponent was 4.3 and the transition to a lower stress exponent was not observed. It is interesting to note that low stress tests conducted by Embury et al. [138] at 450°C also did not show a transition to a low stress exponent. The tests by Embury et. al. were conducted on as-rolled plates which did not have a fine recrystallised grain-structure. Therefore, it can be surmised that the transition to a viscous regime for this alloy is observed only for finer

grained microstructures. This observation suggests that H-D creep is not operative in this alloy even for large grain sizes.

Another interesting observation was that on reducing stress, the creep rates were about 2-3 times lower than the rates observed in the preceeding increasing cycle (Fig. 4.28). Also, a substantial amount of negative strain was observed on first decreasing the stress in the power law regime as seen in Fig. 4.27. Two possibilities considered here are strain assisted grain growth and intra-granular cavitation. Grain growth would result in decreasing creep rates with increasing time if the creep rate is grain size dependent. This aspect is discussed in more detail in § 5.4.1.4. Anelastic creep observed in Fig. 4.27 can be explained by the presence of voids in the cross-section of the crept sample. At lower stresses, sintering of these voids can result in negative creep. In our tests, voids were observed at the end of the tests in cross-sections of the crept sample. These voids could have been formed in either the viscous regime or during exposure to high stress. It is not yet clear, however, whether lowering of stress leads to sintering of these voids.

5.4.1.3 Dependence of strain rate on temperature

The activation energy measured from low stress creep tests was 110 ± 39 kJ/mol (Fig. 4.30) compared to 150 kJ/mol for self diffusion in aluminium [9]. The values reported by other investigators for creep deformation of 7075 at high stresses lie in the range of 160-236 kJ/mol. The best fit value

of activation energy for the high stress region for all the available data was estimated to be 142±14 kJ/mol close to that for aluminium self diffusion. The value measured in this work at lower stresses is thus lower than that estimated from analysis of creep data for 7075 at higher stresses. This may be due to grain growth during creep. The diffusional creep rate at a temperature T_1 (modified from Eq. 2.1) is given by

$$\dot{\varepsilon}_1 = \frac{A}{d_1^2 T_1} \exp(\frac{-Q_c}{RT_1}) \tag{5.21}$$

If creep rates are measured at two temperatures, T_1 and T_2, then true activation energy for creep, Q_c, can be calculated to be

$$Q_c = -R \ln(\frac{\dot{\varepsilon}_1 d_1^2 T_1}{\dot{\varepsilon}_2 d_2^2 T_2}) \frac{T_1 T_2}{(T_2 - T_1)} \tag{5.22}$$

Apparent activation energy for creep, Q_a, calculated without compensating for grain size is similarly written as

$$Q_a = -R \ln(\frac{\dot{\varepsilon}_1 T_1}{\dot{\varepsilon}_2 T_2}) \frac{T_1 T_2}{(T_2 - T_1)} \tag{5.23}$$

Substituting, Eq. (5.23) in Eq. (5.22), we get

$$Q_c = Q_a \left[\ln(\frac{\dot{\varepsilon}_1 d_1^2 T_1}{\dot{\varepsilon}_2 d_2^2 T_2}) \Big/ \ln(\frac{\dot{\varepsilon}_1 T_1}{\dot{\varepsilon}_2 T_2}) \right] \tag{5.24}$$

Substituting the values for strain rates and grain sizes for 350°C and 410°C in Eq (5.24), we get $Q_c=1.51$ $Q_a=165$kJ/mol, in reasonable agreement with the activation energy for aluminium self-diffusion.

5.4.1.4 Comparison with theory

The rates measured in this work are plotted in Fig. 4.28 along with the N-H rates (Eq. 2.1) for the two respective grain sizes (50 and 144 μm), Harper-Dorn rates (Eq. 2.3) and power law rates (Eq. 5.20). It can be seen that the measured creep rates are in very good agreement (all the data for TMT 7075 at low stresses are within a factor of two of the N-H rates) with rates predicted by the diffusional creep mechanism at low stresses. On stress reversal (as indicated in Fig. 4.28), the creep rates were about 2-3 times lower than those measured in the increasing load cycle. This may be due to grain growth during testing. The grain size measured at the end of test 2 was found to be 78.4 ± 6.7 mm. This 50% increase in grain size would reduce the creep rates by nearly a factor of 2 and the results would then be close to those expected from N-H theory.

The creep data can be normalised for grain size assuming that grain size varies parabolically with time [60] according to

$$d_t^2 = d_o^2 + k_d t \qquad\qquad (5.25)$$

where d_0 is the initial grain size, d_t is the grain size after time t and k_d is a parameter characterizing the kinetics of grain growth. Using the value of grain size before the test and that measured at the end of the test 2 (48.2 and 79 μm respectively), the operative value of parameter k is calculated to be 10.6 $(\mu m)^2 h^{-1}$. Using this value of k_d in Eq (5.25), expected grain size was calculated at the beginning of each stress change. Similar calculations for test 1 [127] (on thixo-forged material) could not be performed because the

test durations were not known. However, the final grain size of the sample was measured and this data point then normalised accordingly. The strain rates thus normalised for grain size according to the N-H equation (Eq. 2.1) are plotted against stress in Fig. 5.6. The normalised rate predicted by the N-H equation and those a factor of 2 above and below the predicted rate are also shown. It is seen that the creep rates for both, thixo-forged and thermo-mechanically treated 7075 alloy, at low stress (< 5 MPa) are in good accord with N-H rates. Some difference still remains with regard to the effect of increasing and decreasing stress cycles. The reason for this remains unclear.

It is worth noting that the creep rates for the finer grain size are about an order of magnitude faster than that expected for Harper-Dorn creep, which has frequently been associated with creep of aluminium and its solid solution alloys at high temperature and low stresses [3, 66, 67], although this interpretation has been questioned [75, 77].

Creep data from superplasticity literature for 7075 aluminium alloy was compared with those measured in this work. Kwon and Chang [141] reported the creep data for superplastic 7075 aluminium alloy for grain sizes in the range of 9-45 μm at temperatures 445-515°C. Yang *et al.* [142] reported strain rate-stress dependence of as-rolled 7075 alloy. Typical data from these works are plotted in Fig. 5.5 along with the data from the present work. It can be seen that superplasticity data of Kwon and Chang is within the same order of magnitude as the creep rates measured in the present work

that is ascribed to diffusional creep. Therefore it is expected that the diffusional creep would play a significant role during superplastic deformation of such fine-grained materials in the low stress regime. Superplasticity data of Yang *et al.* [142] is about 3-4 orders of magnitude faster than those obtained from conventional creep tests. A note-worthy feature in the work of Yang *et al.* is that the superplasticity experiments were carried out on cold rolled material. It is, therefore, difficult to compare creep rate from their work to those measured in the present work and by Kwon and Chang due to the different microstructures involved.

5.4.2 Magnesium alloy AZ61

5.4.2.1 Strain vs. time curves

Fig. 4.32 shows that the primary component of creep is minimal in all tests after the initial exposure to stress and high temperature. As discussed previously, this observation is consistent with diffusional creep as it indicates that steady state was achieved rapidly. It was likewise observed by Vagaralli and Langdon [125] that the primary stage was absent for creep of commercially pure magnesium at low stresses and high temperature.

5.4.2.2 Dependence of strain rate on stress

The results of Fig. 4.33 are characteristic of Bingham creep behaviour, where $\dot{\varepsilon} \propto (\sigma - \sigma_0)$ and σ_0 ranges from 1.25 ± 0.6 MPa at 250°C to 0.50 ± 0.15 MPa at 346°C. Similar behaviour has been reported for several metals [124, 143, 144] under comparable conditions. The results for pure

magnesium [124], for example, range from 1.5 MPa at 152°C to 0.16 MPa at 323°C and show a reasonable fit with the empirical equation:

$$\sigma_o = \frac{A}{\overline{L}} \exp\left(\frac{U}{RT}\right) \tag{5.26}$$

where A and U are material constants. The results of Fig. 4.33 give A = 0.15 ± 0.02 N/m and U = 23.1 ± 5.7 kJ/mol for AZ61 with $\overline{L}$ = 25 μm, compared with A = 0.04 ± 0.01 N/m and U = 23 kJ/mol for Mg [124] with $\overline{L}$ = 15 μm.

5.4.2.3 Dependence of strain rate on temperature

The activation enthalpy of 106 ± 9 kJ/mol yielded by the temperature-compensated strain rate per unit stress results in Fig. 4.33 is ~ 0.7 of the activation enthalpy for lattice diffusion of Mg in Mg [145], which would be consistent with a major role for grain boundary diffusion in determining the creep rate. This is also consistent with the findings of Crossland [124] for pure magnesium, that grain boundary diffusion creep (Coble creep) dominated over the ranges 152 < T < 323°C and 15 < $\overline{L}$ < 104 μm at low stresses comparable with the conditions in our experiments for AZ61.

5.4.2.4 Grain Boundary diffusivity

Radiotracer grain boundary diffusivity in either AZ61 or Mg is not available from the literature, therefore a direct comparison of the creep rates measured in this work with those expected from theory could not be made. However, Crossland and Jones [124] showed that grain boundary diffusional creep (Coble creep) was the dominant creep mechanism in Mg at low stresses and intermediate temperature. The grain boundary diffusivity of Mg were thus

evaluated assuming that diffusional creep was rate controlling. The relevant equations are then

$$(d\dot{\varepsilon}/d\sigma)_L = \frac{12\,\Omega\,D_L}{d^2 kT} \tag{5.27}$$

and

$$(d\dot{\varepsilon}/d\sigma)_B = \frac{48\,\Omega\,D_B\delta}{d^3 kT} \tag{5.28}$$

for lattice diffusion (Nabarro-Herring) [1, 2] and grain boundary diffusion (Coble) creep [6], respectively. Taking $\Omega = 2.33 \times 10^{-29}$ m^3/atom, k = 1.38 x 10^{-23} J/atom K, d = 1.76 $\overline{L}$ and $D_L = 5.9 \times 10^{-16}$ m^2/s [145], Eq. (5.27) predicts

$(d\dot{\varepsilon}/d\sigma)_L = 1.0 \times 10^{-14}$ m^2 N^{-1} s^{-1} at our highest test temperature, 346°C, which is less than one percent of the measured value, implying a negligible contribution from Nabarro-Herring creep. Our results for $d\dot{\varepsilon}/d\sigma$ can be compared with those of Crossland and Jones [124] by substituting them for $(d\dot{\varepsilon}/d\sigma)_B$ in Eq. (5.28) to yield

$$D_B\delta = (d^3 kT/48\Omega)d\dot{\varepsilon}/d\sigma \tag{5.29}$$

at each test temperature. The resulting $D_B\delta$ values are included in Table 4.9 and plotted as log ($D_B\delta$) versus 1/T in Fig. 5.7, yielding $D_{OB}\delta = (7.7 \pm 1.6)$ x 10^{-10} m^3/s and $Q_B = 106 \pm 9$ kJ/mol for AZ61. This result is in excellent agreement with the corresponding values obtained by Crossland and Jones

[124] for pure magnesium, $D_{OB} \delta = 8 \times 10^{-10}$ m^3/s and Q = 105 kJ/mol. The resulting values of $D_B \delta$ given for our test temperatures are given for comparison in Table 4.9. The value of $D_b\delta$ measured in this work is found to be within a factor of two to that calculated from the data of Crossland and Jones assuming that Coble creep is the dominant creep mechanism. It was established that the observed creep behaviour in Mg under these conditions represents Coble creep [124]. Our work was carried out under similar conditions of stress and temperature and is expected to be controlled by the Coble creep mechanism also. Similarity of measured creep rates reinforces this proposition. Additionally it is concluded that the content of Al and Zn in AZ61 has negligible effect on the magnitude of grain boundary diffusivity indicated by the Coble creep process.

5.4.2.5 Comparison with superplasticity data

It is of interest to compare the findings of the present creep work with results for superplastic deformation of AZ61 of similar grain size at similar stresses and temperatures. Watanabe et al. [118] used AZ61 with grain size ($\overline{L} \approx 20$ μm) similar to that of our material in the comparable temperature range (250 to 400°C). Their stress range extended up to ~ 70 MPa, however, and stresses below our maximum of 4 MPa were explored only at their highest temperatures (375 and 400°C), with the operative activation energy being 90 kJ/mol at ($\sigma - \sigma_o$) = 25 MPa, similar to our 106 ± 9 kJ/mol, in the range 250 to 300°C. Grain size was also found to be relatively stable up to about 380°C, consistent with our findings. The subsequent publication by Kim et al. [122]

used AZ61 with $\overline{L}$ = 5 and 9 μm at 325 to 420°C, again with stresses down to our maximum of 4 MPa reached only at the highest temperature. At the lower temperatures, and σ = 22 MPa, activation energy was near to 90 kJ/mol, similar to our 106 ± 9 kJ/mol, and grain size was relatively stable up to nearly 400°C. Figs. 5.8a-e shows strain rate versus stress for the five lowest temperatures employed by Watanabe *et al.* and Kim *et al.* in their superplasticity work for comparison with our creep data at lower stresses for the same or near equivalent temperatures. The continuity between our creep and their superplastic strain rates is notable. This continuity is reinforced by the corresponding plot of temperature compensated strain rate versus σ/E where E is Young's modulus, in Fig. 5.9, using our value of activation energy, 106 kJ/mol. The increase in stress exponent at σ/E > 10^{-3} is indicative, however, that the mechanism of superplastic flow involves more than diffusional creep.

5.4.2.6 Microstructural observations

The implication that Coble creep with a threshold stress controls the creep process operating under the conditions studied is confirmed by the increase in aspect ratio of grains along the direction of applied stress from 1.00 ± 0.02 as received and in the grip areas to 1.10 to 1.15 as a result of creep (Table 4.10). Some rotation of grains evident in Fig. 4.36 is a further expected consequence of diffusional creep deformation of an assembly of quasi equiaxed grains that remain in mutual contact during transfer of matter to and from grain faces. Mutual rotation of grains can provide the link between diffusional creep and

the observation that grains remain essentially equiaxed after superplastic deformation.

6.0 CONCLUSIONS AND FUTURE WORK

6.1 Conclusions

The following conclusions are drawn from the present work.

1. Viscous creep behaviour was observed in copper wires 25–500 µm in diameter at low stress (5 - 300 kPa) and high temperature (990°C). This creep in copper wires is found to be entirely consistent with diffusional creep. Strain rate per unit stress was inversely proportional to the product of wire diameter and grain length for finer wire diameters and to square of grain size for larger wire diameter. The measured steady state creep rates were within a factor of 2 of the rates predicted by classical diffusional creep theory for all wire diameters tested. Microstructural observations of the wire profiles after creep has provided also direct evidence for this diffusion of vacancies under the influence of stress.

2. No transition from diffusional creep to Harper-Dorn creep was observed for the steady state creep of copper wire at 990°C for increasing wire diameters within the range of wire diameters (25-500 µm) employed in this study. Though, the largest diameter wires crept significantly faster than predicted by diffusion creep theory when the

test duration was not sufficiently long to achieve steady state, steady state creep rates remained in close agreement with those expected from diffusional creep. Grain boundary sliding to form offsets was noticed in all wires except for the smallest diameter (25 μm). Although the contribution to strain from grain boundary sliding was found to increase with wire diameter, it was a minor one (<20%).

3. Surface energy of copper at 990°C determined from zero creep stress measured for copper wires was found to be 1.49-1.60 J/m^2 which is slightly lower than values measured by other investigators. This discrepancy is attributed to the presence of residual oxygen in the Ar-5% H$_2$ furnace atmosphere.

4. The stress exponent for tensile creep of copper foils of two thicknesses (0.4 and 0.6 mm) during creep in the stress range 0.1 to 0.6 MPa at 1065°C was found to be 1.7 ± 0.3. Similarly, for creep at 850°C, the stress exponent was measured to be 1.5 ± 0.2. The grain sizes employed varied from 0.58 to 10 mm and no significant effect of grain size was observed. The measured creep rates were found to be about 40 times faster than for diffusional creep. After creep, slip lines 30.2 ± 8.2 μm apart were observed on the surface of the sample. A model based on the rate of generation of dislocations at Bardeen-Herring sources satisfactorily accounts for the measured strain rates and microstructural observations.

5. Creep rates were measured from changes in the profile of thin copper foils (100 and 250 μm in thickness) in the form of cantilever under self loading at 950°C. The profile of foils after creep was measured and the curvature of each foil was evaluated from the discretised profile. The shape of a foil crept in cantilever mode confirmed that the rate of deformation was linearly dependent on stress.

6. A simple model based on the rate of rotation of grains due to diffusion of vacancies was used to estimate the rate of change of curvature of foils that were subjected to bending loads. The rates predicted by the model were about 7-13 times faster than the rates from cantilever tests. The discrepancy could most probably be accounted by the variation in grain boundary orientation and restriction of neighbouring grains. Creep in the corresponding bridge-type tests, which involved clamping at both ends, was restricted presumably due to sintering of the foil to the end supports of the sample holder.

7. The measured rates were about 20 times faster than the classical diffusional creep formulation based solely on tensile and compressive stresses respectively at the top and bottom surfaces of the foil. This is due to shorter diffusional distances involved when diffusional creep is operative by diffusion across a single grain boundary.

8. Microstructural investigation of the fracture behaviour of an alumina coating previously applied to a creeping foil showed that cracking of the coating was localised to those parts of the foil that were under

small tensile stress. Small compressive stress was observed to nullify the effect of thermal grooving. In the unstressed regions of the foil the coating did not fracture but thermal grooving at grain boundaries took place. All these features are consistent with operation of diffusive fluxes of vacancies from regions of the grain boundary under tension to those under compression.

9. Thermomechanical treatment of 7075 aluminium alloy was found to result in a fine equiaxed grain structure (grain size ≈ 48 μm). The resulting stress exponent for creep at 350°C for the stress range 1-5 MPa was found to be close to 1 (≈ 1.3) and a transition to power law creep was observed at higher stress (>5 MPa).

10. After correcting for grain growth during creep, creep rates for 7075 aluminium alloy, in the low stress regime, were found to be within a factor of two of those expected from diffusional creep theory. The activation energy for creep of 7075 aluminium alloy at an applied stress of 3 MPa in the temperature range 350-410°C was found to be 110 ± 39 kJ/mol.

11. Steady state creep of AZ61 magnesium alloy at $250 < T < 346°C$ and $0.9 < \sigma < 4$ MPa and an intercept grain size $\overline{L}$ of ~ 25 μm exhibited Bingham behaviour with threshold stress σ_0 decreasing with increasing T from ~ 1.25 MPa at 250°C to ~ 0.5 MPa at 346°C, in good accord with earlier measurements for pure magnesium under similar conditions.

12. The Arrhenius plot of log $(T d\dot{\varepsilon}/d\sigma)$ versus T^{-1} yields an activation energy for creep of AZ61 magnesium alloy similar to that expected for control of creep by grain boundary diffusion, and consistent with the expectation that Coble rather than Nabarro-Herring diffusion creep should dominate for the conditions of testing. The resulting values of $D_B\delta$ obtained from measurements of $d\dot{\varepsilon}/d\sigma$ match closely those obtained earlier by Crossland [124] for pure magnesium, and give $D_{OB}\delta = 7.7 \times 10^{-10}$ m^3/s with $Q_B = 106 \pm 9$ kJ/mol for the range $250 < T < 346°C$.

13. Measurements of grain aspect ratio of AZ61 magnesium alloy after creep show grain elongation in the direction of application of the tensile stress and contraction in the transverse direction dependent on strain. There was no such elongation in the unstressed grip areas after creep or in the material, as heat treated, or as received. This is consistent with stress-directed diffusive deposition of material at boundaries under normal stress, a key indicator of the operation of a diffusional creep mechanism.

14. The results for strain rate versus stress for this AZ61 alloy are shown to be continuous with those of Watanabe *et al.* [118] and Kim *et al.* [122] for superplastic flow of AZ61 at comparable temperatures but higher stresses.

6.2 Future work

During the experiments involving tensile creep tests of copper foils, considerable experimental scatter was observed. Any future work should try to use electronic data-logging to allow stress-jump tests to be carried out on the same sample. Additionally, more information regarding the shape of the creep curve can be obtained. This would also allow estimation of steady state creep rates and the corresponding stress–exponent to be made with more precision. Additionally, investigation of tensile creep behaviour of foils should focus on the effect of foil thickness as there was experimental evidence obtained in this work from creep tests at 850°C that the creep rate may be directly proportional to foil thickness as predicted by the glide-climb model proposed in this work (Eq. 5.11). Another aspect of the proposed work should involve comparison of results obtained by other investigators for gold foils and other materials. Relationship of the proposed mechanism to Harper-Dorn creep could be another area of investigation, although three areas of conflict are readily seen.

1) The present model predicts a stress exponent of 2. Although, a stress exponent of 1 is commonly used to characterize Harper-Dorn creep, recent analysis of Harper-Dorn creep by Ginter *et al.* [79] concludes that the true stress exponent for Harper-Dorn creep evaluated from longer tests is closer to 2.

2) The applied stresses typical of Harper-Dorn creep are generally in the range of 10^{-2} to 5×10^{-2} MPa. These are about an order of magnitude

lower than stresses applied in the present work. While it has been shown that the applied stresses used in the present work are sufficient for glide to take place, the situation for Harper-Dorn creep is not clear.

3) The present model predicts that the creep rate for cold-deformed material would be higher than that for annealed material, a prediction in contrast with experimental observation that accelerated Harper-Dorn creep is not observed in materials with high dislocation densities [79]. This raises a bigger question concerning absence of Harper-Dorn creep in some recent experimental work.

The technique developed to measure the rate of change of curvatures of foils due to grain rotation is in its formative stage. There is a plenty of scope for development of this technique to gather more information related to creep due to bending moments. Firstly, for measurement of the profile of crept foils, it might be advantageous to use an optical technique for substrate curvature measurements based on laser scanning to generate profile data easily and more accurately. An entirely different way to measure strain rates would be to apply a micro-grid to both the surfaces of the foil and then evaluating the strain after creep from the distance between consecutive gridlines. This method could be used to estimate strain rates over a range of applied stresses from just one sample.

A direct comparison of cracking of alumina coatings under diffusional creep and power-law creep can be made be using samples of larger length. Under power-law creep, the equations developed here for calculating curvature from

the profile would no longer be valid and therefore new equations will have to be developed. Additionally, practical issues like the depth of the sample holder (in the present work, the sample holder was only 8 mm deep) and, consequently, difficulties in sealing off the assembly, would need to be addressed.

In the present work, the relationship between creep and superplasticity has been only very slightly explored and the results seem to be promising. From the results of work in both 7075 aluminium alloy and AZ61 magnesium alloy, there is evidence that diffusional creep is the dominant mode of deformation of these alloys at relatively coarse grain sizes and lower stresses. Future work should attempt to obtain finer microstructures. For 7075 aluminium, a transition to power law creep was observed at 5 MPa because the grain size was not fine enough. Use of techniques like equal channel angular pressing is attractive, but complicated due to highly unstable grain structures with a large propensity for grain growth during creep testing. During creep of AZ61, no transition to power law creep was observed due to finer grain size. Thus, to further investigate the relationship between creep and superplasticity, attempts must be concentrated towards developing finer microstructures (grain sizes in the range of 5 to 15 μm) that remain stable at creep testing temperatures.

The creep tests themselves must seek to address two issues

1) Can grain elongation be directly related to the total sample strain under superplastic conditions?

2) The role of grain rotation in maintaining low grain aspect ratio even after large specimen elongation.

Surface profiling techniques like AFM, coupled with scratch displacement, could be a valuable tool in distinguishing between or relating grain boundary sliding and diffusional creep.

References

1. Nabarro, F.R.N. *Deformation of single crystals by the motion of single ions*. In *Report of a conference on the strength of solids*. 1948, Bristol: The Physical Society, London: p. 75-90.

2. Herring, C., *Diffusional viscosity of a polycrystalline solid*. J. Appl. Phys., 1950. **21**: p. 437-445.

3. Harper, J. and J.E. Dorn, *Viscous creep of aluminum near its melting temperature*. Acta Metall., 1957. **5**: p. 654-665.

4. Ball, A. and M.M. Hutchinson, *Superplasticity in the aluminium-zinc eutectoid*. Metal Science J., 1969. **3**: p. 1-7.

5. Gifkins, R.C., *Grain boundary sliding and its accommodation during creep and superplasticty*. Metall. Trans. A, 1976. **7**: p. 1225-1232.

6. Coble, R.L., *A model for boundary controlled creep in polysrystalline materials*. J. Appl. Phys., 1962. **34**(6): p. 1679-1682.

7. McNee, K.R., Ph. D. thesis, *Microstructural features of low stress creep in pure metals and precipitation hardened alloys*, 2000, Dept. of Engineering Materials, University of Sheffield.

8. Norbygraard, T. and J.B. Bilde-Sorensen. *Σ=3 grain boundaries in Cu-Ni subjected to diffusional creep*. In *Proc. 9th International conference on creep and fracture of engineering materials and structures*. J.D. Parker, 2001, Swansea, UK: Institute of Metals: p. 15-20.

9. Frost, H.J. and M.F. Ashby, *Deformation mechanism maps*. 1982, Oxford: Pergamon Press.

10. Weertman, J. and J.R. Weertman, *Mechanical properties-strongly temperature-dependant*, In *Physical Metallurgy*, R.W. Cahn and P. Hassen, Editors. 1983, Elsevier Science Publishing: Amsterdam. p. 1309-1340.

11.   Burton, B., *Diffusional creep in polycrystalline materials*. Defects in metals and alloys. 1977, Aedermannsdorf: Trans Tech Publications.

12.   Udin, H., A.J. Shaler, and J. Wulff, *The surface tension of solid copper*. Trans. AIME, 1949. **185**: p. 186-190.

13.   Hoage, J.H., *Surface tension studies on uranium and copper*. U. S. Atomic Energy Commission, 1963. **Report HW-78132**: p. 1-16.

14.   Alexander, B.H., M.H. Dawson, and H.P. Kling, *The deformation of gold wire at high temperatures*. J. Appl. Phys., 1951. **22**: p. 439-443.

15.   Borsch, R. and J.R. Hauber, *Creep study of high-purity polycrystalline beryllium*. Trans. Met. Soc. AIME, 1968. **242**: p. 1933-1936.

16.   Jones, H., *A comparison of theory with experiments for diffusion creep in metal foils and wires*. Mater. Sci. Eng., 1969. **4**(2-3): p. 106-114.

17.   Burton, B., *The enhancement of diffusional creep by dislocation climb*. Mater. Sci. Eng., 1975. **18**: p. 245-247.

18.   Jones, R.B., *Diffusional creep in polycrystal magnesium*. Nature, 1965. **207**: p. 70.

19.   Burton, B., Ph. D. thesis, *The contribution of vacancy flow to deformation*, 1969, Department of Metallurgy, University of Sheffield.

20.   Inman, M.C., D. McLean, and H.R. Tipler, *Interfacial free energy of copper-antimony alloys*. Proc. Roy. Soc. A, 1963. **273**: p. 538-557.

21.   Arzt, E., M.F. Ashby, and R.A. Verall, *Interface controlled diffusional creep*. Acta Metall., 1983. **31**(12): p. 1977-1989.

22.   Burton, B., I.G. Crossland, and G.W. Greenwood, *Creep of nickel at low stresses*. Metals Science, 1980. **14**: p. 134-136.

23. Kloc, L., J. Fiala, and J. Cadek, *Creep in a Cu-14 at.% Al solid solution alloy at intermediate temperature and low stresses.* Mater. Sci. Eng. A, 1990. **A130**: p. 165-172.

24. Greenfield, P., C.C. Smith, and A.M. Taylor, *The creep behaviour of heat treatable magnesium base alloys for fuel element components.* Trans. Met. Soc. AIME, 1961. **221**: p. 1065-1073.

25. Squires, R.L., R.T. Weiner, and M. Phillips, *Grain boundary denuded zones in a magnesium-0.5% zirconium alloy.* J. Nucl. Mater., 1963. **8**(1): p. 77-80.

26. Haddrell, V.J., *Diffusion creep deformation in a magnesium reactor component.* J. Nucl. Mater., 1966. **18**: p. 231-232.

27. Hines, G.F., V.J. Haddrell, and R.B. Jones, *Importance of diffusion creep in the deformation of magnox fuel-element components*, In *Physical metallurgy of reactor fuel elements*, J.E. Harris and E. Sykes, Editors. 1975, The Metals Society: London. p. 72-78.

28. Jones, R.B., *Diffusion creep and strength of a magnesium-manganese alloy*, In *Quantitative relationship between properties and microstructure*, D.G. Brandon and A. Rosen, Editors. 1969: Haifa. p. 343-351.

29. Karim, A., D.A. Holt, and W.A. Backofen, *Diffusional flow in a hydrided Mg-0.5 wt.% Zr alloy.* Trans. Met. Soc. AIME, 1969. **245**: p. 1131-1133.

30. Karim, A. and W.A. Backofen, *Some observations of diffusional flow in a superplasctic alloy.* Metall. Trans., 1972. **3**: p. 709-712.

31. Greenwood, G.W., *Denuded zones and diffusional creep.* Scripta Metall. Mater., 1994. **30**(12): p. 1527-1530.

32. McNee, K.R., G.W. Greenwood, and H. Jones, *Changes in precipitate distribution during the low-stress creep of a hydrided magnesium-zirconium alloy.* Phil. Mag., 2002. **82**(15): p. 2773-2790.

33. McNee, K.R., G.W. Greenwood, and H. Jones, *The effect of stress orientation on the formation of precipitate free zones during low stress creep*. Scripta Mater., 2002. **46**: p. 437-439.

34. Kottada, R.S. and A.H. Chokshi, *The high temperature tensile and compressive deformation characteristics of magnesia doped alumina*. Acta Mater., 2000. **48**(15): p. 3905-3915.

35. Lupinc, V. *Creep Strengthening mechanisms*. In *Proceedings of High Temperature Alloys for Gas Turbine*. R. Brunetaud, D. Coutsouradis, and R. Stickler, 1982, London: D. Reidel Publishing Company: p. 395-421.

36. Hondros, E.D. and C.R. Lake, *Inhibition of diffusion creep in copper by dissolved oxygen*. J. Mater. Sci., 1970. **5**: p. 374-378.

37. Burton, B., *The low stress creep of aluminium near to the melting point: the influence of oxidation and substructural changes*. Phil. Mag., 1972. **25**: p. 645-659.

38. Harris, J.E., *The inhibition of diffusional creep by precipitates*. Metal Science J., 1972. **7**: p. 1-6.

39. Harris, J.E., M.O. Tucker, and G.W. Greenwood, *The diffusional creep strain due to growth of intergranular voids*. Metal Science J., 1974. **8**: p. 311-314.

40. Hanna, M.D. and G.W. Greenwood, *Cavity growth and creep in copper at low stresses*. Acta Mater., 1982. **30**: p. 719-724.

41. Lifshitz, I.M., *On the theory of diffusion-viscous polycrystalline bodies*. Soviet Physics, 1963. **17**: p. 909-920.

42. Eigeltinger, E.H., *A technique for the meaurement of diffusion creep from marker line displacements*. J. Mater. Sci., 1974. **9**: p. 644-650.

43. Eigeltinger, E.H. and R.C. Gifkins, *Grain boundary sliding during diffusional creep*. J. Mater. Sci., 1975. **10**: p. 1889-1903.

44. Cannon, W.R., *The contribution of grain boundary sliding to axial strain during diffusion creep.* Phil. Mag., 1972. **25**: p. 1489-1497.

45. Kim, B.-N. and K. Hiraga, *Contribution of grain boundary sliding in diffusional creep.* Scripta Mater., 2000. **42**: p. 451-456.

46. Raj, R. and M.F. Ashby, *On grain boundary sliding and diffusional dreep.* Metall. Trans., 1971. **2**: p. 1113-1127.

47. Speight, M.V., *Mass transfer and grain boundary sliding in diffusion creep.* Acta Metall., 1975. **23**: p. 779-781.

48. Beere, W.B., *Stress distribution during Nabarro-Herring and superplastic creep.* Metal Science, 1976. **10**: p. 133-139.

49. Sahay, S.S. and G.S. Murty, *Uncertainty in separating the strain contributions of sliding and diffusion in diffusional creep.* Scripta Mater., 2001. **44**(5): p. 841-845.

50. Gibbs, G.B., *Sliding contribution to the total strain of a polycrystalline aggregate.* Metal Science, 1977. **11**(2): p. 65-67.

51. Gleiter, H., *Microstructures*, In *Physical Metallurgy*, R.W. Cahn and P. Hassen, Editors. 1983, Elsevier Science Publications: Amsterdam. p. 650-662.

52. Gibbs, G.B., *Diffusion creep of a thin foil.* Phil. Mag., 1966. **13**: p. 589-593.

53. Greenwood, G.W., *An analysis of the effect of multiaxial stresses and grain shape on Nabarro-Herring creep.* Phil. Mag. A, 1985. **A51**(4): p. 537-542.

54. Greenwood, G.W., *A formulation for anisotropy in diffusional creep.* Proc. Roy. Soc. London A, 1992. **436**: p. 187-196.

55. Schneibel, J.H., R.L. Coble, and R.M. Cannon, *The role of grain size distributions in diffusional creep.* Acta Metall., 1981. **29**(7): p. 1285-1290.

56. Hazzledine, P.M. and J.H. Schneibel, *Theory of Coble creep for irregular grain structures.* Acta Metall., 1993. **41**(4): p. 1253-1262.

57. Ford, J.M., J. Wheeler, and A.B. Movchan, *Computer simulation of grain-boundary diffusion creep.* Acta Mater., 2002. **50**(15): p. 3941-3955.

58. Kim, B.-N. and K. Hiraga, *Simulation of diffusional creep accompanied by grain growth in two dimensional polycrystalline solids.* Acta Mater., 2000. **48**(16): p. 4151-4159.

59. Tong, W.S., J.M. Rickman, H.M. Chan, and M.P. Harmer, *Coble creep response and variability of grain boundary properties.* J. Mater. Res., 2002. **17**(2): p. 348-352.

60. Burton, B., *A theoretical upper limit to Coble creep strain resulting from concurrent grain growth.* J. Mater. Sci., 1993. **28**(18): p. 4900-4903.

61. Weertman, J., *Theory of steady state creep based on dislocation creep.* J. Appl. Phys., 1955. **26**: p. 1213-1217.

62. Ashby, M.F. *Diffusion accommodated flow and superplasticity.* In *3rd International Conference of strength of Metals and Alloys.* 1973, Cambridge: p. 8.

63. Nabarro, F.R.N., *The mechanism of Harper-Dorn creep.* Acta Metall., 1989. **37**(8): p. 2217-2222.

64. Langdon, T.G. and P. Yavari, *An investigation of Harper-Dorn creep-2. The flow process.* Acta Metall., 1982. **30**(4): p. 881-887.

65. Yavari, P., D.A. Miller, and T.G. Langdon, *An investigation of Harper-Dorn creep-1. Mechanical and microstructural characteristics.* Acta Metall., 1982. **30**: p. 871-879.

66. Barrett, C.R., E.C. Muehleisen, and W.D. Nix, *High temperature-low stress creep of Al and Al-0.5%Fe.* Mater. Sci. Eng., 1972. **10**: p. 33-41.

67.   Mohamed, F.A., K.L. Murty, and J.W. Morris, *Harper-Dorn creep in Al, Pb and Sn.* Metall. Trans., 1973. **4**: p. 935-939.

68.   Murty, K.L., F.A. Mohamed, and J.E. Dorn, *Viscous glide, dislocation climb and newtonian viscous deformation mechanisms of high temperature creep in Al-3Mg.* Acta Metall., 1972. **20**: p. 1009-1019.

69.   Malakondaiah, G. and P. RamaRao, *Creep of alpha-titanium at low stresses.* Acta Metall., 1981. **29**: p. 1263-1275.

70.   Malakondaiah, G. and P. RamaRao, *Grain size independent viscous creep in alpha titanium and beta cobalt.* Scripta Metall., 1979. **13**: p. 1187-1190.

71.   Fiala, J. and T.G. Langdon, *An examination of the metals deforming by Harper-Dorn creep at high homologous temperatures.* Mater. Sci. Eng. A, 1992. **151**(2): p. 147-151.

72.   Pines, B.Y. and A.F. Sirenko, *Diffusion creep rate in metals at sub-melting temperatures.* Fiz. Metal. Metalloved., 1963. **15**(4): p. 584-591.

73.   Ruano, O.A., J. Wadsworth, J. Wolfenstine, and O.D. Sherby, *Evidence for Nabarro-Herring creep in metals:fiction or reality?* Mater. Sci. Eng., 1993. **A165**: p. 133-141.

74.   Wang, J.N., *A microphysical model of Harper-Dorn creep.* Acta Mater., 1996. **44**(3): p. 855-862.

75.   Blum, W. and W. Maier, *Harper-Dorn creep - a myth?* Physica Stat. Sol. A, 1999. **171**: p. 467-474.

76.   McNee, K.R., H. Jones, and G.W. Greenwood. *Low stress creep of aluminium at temperatures near to T_m.* In *Proc. 9th International Conference on Creep & Fracture of Engineering Materials and Structures.* J.D. Parker, 2001, Swansea: The Institute of Metals, London: p. 185-195.

77.   McNee, K.R., V. Srivastava, G.W. Greenwood, and H. Jones. *Departures from model predictions for creep in pure metals at low*

stresses near their melting temperatures. In *Proc. of 2002 TMS annual meeting "Creep deformation: Fundamentals and Applications".* R.S. Mishra, J.C. Earthman, and S.V. Raj, 2002, Seattle, Washington: TMS: p. 95-104.

78.   Ginter, T.J., P.K. Chaudhary, and F.A. Mohamed, *An investigation of Harper-Dorn creep at large strains.* Acta Mater., 2001. **49**(2): p. 263-272.

79.   Ginter, T.J. and F.A. Mohamed, *Evidence for dynamic recrystallisation during Harper-Dorn creep.* Mater. Sci. Eng. A, 2002. **A322**(1-2): p. 148-152.

80.   Nabarro, F.R.N., *Harper-Dorn creep - a legend attentuated.* Physica Stat. Sol. A, 2000. **182**(2): p. 627-629.

81.   Nost, B. and E. Nes, *Dislocations in aluminium under stress observed by Lang X-Ray topography.* Acta Metall., 1969. **17**: p. 13-20.

82.   Rachinger, W.A., *Relative grain translations in the plastic flow of aluminium.* J. Inst. Met., 1952. **81**: p. 33-41.

83.   Langdon, T.G., *The physics of superplastic deformation.* Mater. Sci. Eng. A, 1991. **A137**: p. 1-11.

84.   Padmanabhan, K.A. and G.J. Davies, *Superplasticity.* 1980, Berlin, Germany: Springer.

85.   Pilling, J. and N. Ridley, *Superplasticity in Crystalline Solids.* 1989, London, England: The Institute of Metals.

86.   Chokshi, A.H., A.K. Mukherjee, and T.G. Langdon, *Superplasticity in advanced materials.* Mater. Sci. Eng. R, 1993. **R10**: p. 237-274.

87.   Todd, R.I., *Critical review of mechanism of superplastic deformation in fine grained metallic materials.* Mater. Sci. Technol., 2000. **16**(11-12): p. 1287-1294.

88. Lin, Z.-R., A.H. Chokshi, and T.G. Langdon, *An investigation of grain boundary sliding in superplasticity at high elongations.* J. Mater. Sci., 1988. **23**: p. 2712-2722.

89. Ashby, M.F. and R.A. Verall, *Diffusion accommodated flow and superplasticity.* Acta Metall., 1973. **21**: p. 149-163.

90. Mukherjee, A.K., *The rate controlling mechanism in superplasticity.* Mater. Sci. Eng., 1971. **8**: p. 83-89.

91. Shin, D.H., Y.J. Joo, C.S. Lee, and K.-T. Park, *Grain elongation in a superplastic 7075 Al Alloy.* Scripta Mater., 1999. **41**(3): p. 269-274.

92. Li, F., H. Bae, and A.K. Ghosh, *Grain elongation and anisotropic grain growth during superplastic deformation in an Al-Mg-Mn-Cu alloy.* Acta Mater., 1997. **45**: p. 3887-3895.

93. Ma, Z.Y., R.S. Mishra, and M.W. Mahoney, *Superplastic deformation behaviour of friction stir processed 7075 Al alloy.* Acta Mater., 2002. **50**(17): p. 4419-4430.

94. Burton, B., *Diffusional rotation of crystals about a common interface.* Phil. Mag. A, 2002. **82**(1): p. 51-64.

95. Burton, B., *Lattice diffusion controlled rotation of crystals about a common interface.* to be published, 2003.

96. McNee, K.R., G.W. Greenwood, and H. Jones, *Microstructural evidence for diffusional creep in copper using atomic force microscopy.* Scripta Mater., 2001. **44**: p. 351-357.

97. Thorsen, P.A. and J.B. Bilde-Sorensen, *Deposition of materials at grain boundaries in tension interpreted in terms of diffusional creep.* Mater. Sci. Eng. A, 1999. **A265**: p. 140-145.

98. Ruano, O.A., O.D. Sherby, J. Wadsworth, and J. Wolfenstine, *Diffusional creep and diffusion-controlled dislocation creep and their relation to denuded zones in $Mg-ZrH_2$ materials.* Scripta Mater., 1998. **38**(8): p. 1307-1314.

99. Wadsworth, J., O.A. Ruano, and O.D. Sherby, *Deformation by grain boundary sliding and slip versus diffusional creep*, In *Creep Behaviour of Advanced Materials for the 21ˢᵗ Century*, R.S. Mishra, A.K. Mukherjee, and K.L. Murty, Editors. 1999, TMS, Warrendale. p. 425-440.

100. Nabarro, F.R.N., *Particle distribution after diffusional creep*, In *Creep Behaviour of Advanced Materials for the 21ˢᵗ Century*, R.S. Mishra, A.K. Mukherjee, and K.L. Murty, Editors. 1999, TMS, Warrendale. p. 391-396.

101. Wilshire, B., *Case Studies in diffusional creep*, In *Creep Behaviour of Advanced Materials for the 21ˢᵗ Century*, R.S. Mishra, A.K. Mukherjee, and K.L. Murty, Editors. 1999, TMS Warrendale. p. 451-460.

102. Wilshire, B. and C.J. Palmer, *Grain size effects during creep of copper.* Scripta Mater., 2002. **46**: p. 484-488.

103. Wilshire, B. and C.J. Palmer. *Deformation processes during creep of pure aluminium.* In *Creep Deformation: Fundamentals and Applications. TMS Annual Meeting.* R.S. Mishra, J.C. Earthman, and S.V. Raj, 2002, Seattle: p. 51-60.

104. Pranatis, N.L. and G.M. Pound, *Viscous flow of copper at high temperatures.* Trans. AIME, 1955. **203**: p. 664-668.

105. Mohamed, F.A., *Analysis of creep data on copper at very low stresses.* Mater. Sci. Eng. A, 1979. **40**: p. 101-104.

106. Ruano, O.A., J. Wadsworth, and O.D. Sherby, *Harper-Dorn creep in pure metals.* Acta Metall., 1988. **36**(4): p. 1117-1128.

107. Jaeger, W. and H. Gleiter, *Grain boundaries as vacancy sources in diffusion creep.* Scripta Metall., 1978. **12**: p. 675-678.

108. Owen, D.M. and T.G. Langdon, *Low stress creep behavior: An examination of Nabarro-Herring and Harper-Dorn creep.* Mater. Sci. Eng. A, 1996. **A216**(1-2): p. 20-29.

109. Shin, D.H., C.S. Lee, and W.-J. Kim, *Superplasticity of fine-grained 7475 Al alloy and a proposed new deformation mechanism.* Acta Mater., 1997. **45**(12): p. 5195-5202.

110. Shin, D.H., K.T. Park, and E.J. Lavernia, *High-Temperature Deformation in a Superplastic 7475-Al-Alloy with a Relatively Large Grain-Size.* Mater. Sci. Eng. A, 1995. **201**(1-2): p. 118-126.

111. Matsuki, K., N. Hariyama, M. Takizawa, and Y. Murakami, *Quantitative metallographic study on superplastic deformation in Zn-Cu-Mn alloy.* Metal Science, 1983. **17**: p. 503-510.

112. Backofen, W.A., G.S. Murty, and S.W. Zehr, *Evidence for diffusional creep with low strain rate sensitivity.* Trans. Met. Soc. AIME, 1968. **242**: p. 329-331.

113. Valiev, R.Z. and O.A. Kaibyshev, *Mechanism of superplastic deformation in a Mg alloy-I. Structural changes and operative deformation mechanism.* Physica Stat. Sol. A, 1977. **44**(1): p. 65-76.

114. Li, F., *Microstructural evolution and mechanisms of superplasticity in an Al-4.5%Mg alloy.* Mater. Sci. Technol., 1997. **13**(1): p. 17-23.

115. Li, F., W.T. Roberts, and P.S. Bate, *Superplasticity and the development of dislocation structures in an Al-4.5% Mg alloy.* Acta Mater., 1996. **44**: p. 217-233.

116. Wert, J.A., N.E. Paton, C.H. Hamilton, and M.W. Mahoney, *Grain refinement in 7075 aluminium by thermomechanical processing.* Metall. Trans. A, 1981. **12A**: p. 1267-1276.

117. Horita, Z., T. Fujinami, M. Nemoto, and T.G. Langdon, *Improvement of mechanical properties for Al alloys using equal-channel angular processing.* J. Mater. Proc. Tech., 2001. **117**: p. 288-292.

118. Watanabe, H., T. Mukai, M. Kohzu, S. Tanabe, and K. Higashi, *Effect of temperature and grain size on the dominant diffusion process for superplastic flow in an AZ61 magnesium alloy.* Acta Mater., 1999. **47**(14): p. 3753-3758.

119.   Watanabe, H., H. Tsutsui, T. Mukai, K. Ishikawa, Y. Okanda, M. Kohzu, and K. Higashi, *Superplastic behavior in commercial wrought magnesium alloys.* Mater. Sci. Forum, 2000. **350**: p. 171-176.

120.   Kim, W.J. and S.W. Chung, *Superplasticity in fine-grained AZ61 magnesium alloy.* Met. Mater., 2000. **6**(3): p. 255-259.

121.   Kim, W.J., S.W. Chung, C.W. An, and K. Higashi, *Superplasticity in a relatively coarse-grained AZ61 magnesium alloy.* J. Mater. Sci. Lett., 2001. **20**(17): p. 1635-1637.

122.   Kim, W.J., S.W. Chung, C.S. Chung, and D. Kum, *Superplasticity in thin magnesium alloy sheets and deformation mechanism maps for magnesium alloys at elevated temperatures.* Acta Mater., 2001. **49**(16): p. 3337-3345.

123.   Bussiba, A., A. Ben Artzy, A. Shechtman, S. Ifergan, and M. Kupiec, *Grain refinement of AZ31 and ZK60 Mg alloys- towards superplastic studies.* Mater. Sci. Eng. A, 2001. **A302**: p. 56-62.

124.   Crossland, I.G. and R.B. Jones, *Grain boundary diffusion creep in magnesium.* Metal Science, 1977. **11**: p. 504-508.

125.   Vagarali, S.S. and T.G. Langdon, *Deformation mechanisms in H.C.P. metals at elevated temperatures-I. Creep behaviour of magnesium.* Acta Metall., 1981. **29**: p. 1969-1982.

126.   Vagarali, S.S. and T.G. Langdon, *Deformation mechanisms in H.C.P. metals at elevated temperatures-II. Creep behaviour of Mg-0.9% Al solid solution alloy.* Acta Metall., 1982. **30**: p. 1157-1170.

127.   McNee, K.R., *Creep of thixo-forged 7075 aluminium alloy.* Pvt. Communication, University of Sheffield, 2002.

128.   Regnier, P. and M.F. Felsen, *Creep of bamboo-structure copper wires in and out of stress range of diffusion controlled deformation.* Phil. Mag. A, 1981. **A43**: p. 29-41.

129.   Jones, H., *The surface energy of solid metals.* Metal Science J., 1971. **5**: p. 15-18.

130. Hondros, E.D. and A.J.W. Moore, *Evaporation and thermal etching.* Acta Metall., 1960. **8**: p. 647-653.

131. Johnston, W.G. and J.J. Gilman, *Dislocation velocities, dislocation densities and plastic flow in Lithium Floride crystals.* J. Appl. Phys., 1959. **30**: p. 129-144.

132. Friedel, J., *Dislocations.* International Series of Monographs on Solid State Physics, ed. R. Smoluchowski and N. Kurti. Vol. 3. 1964, London: Pergamon Press. 491.

133. Nabarro, F.R.N., *Steady state diffusional creep.* Phil. Mag., 1967. **16**: p. 231-237.

134. Barrett, C.R. and W.D. Nix, *A model for steady state creep based on the motion of jogged screw dislocations.* Acta Metall., 1965. **13**: p. 1247-1258.

135. Dix, E.H.J., *Aluminium alloys for elevated temperature service.* Aeronaut. Engng. Review, 1956. **15**: p. 40-48.

136. Voerhees, H.R. and J.W. Freeman, *Report on the elevated temperature properties of Al-Mg alloys.* 1960. p. 147-159.

137. Takeuchi, K. and F. Tanaka, *Creep and stress-rupture properties of wrought aluminium alloys.* Metals Abstract, 1968 (1) 31-2043, 1968. **9/2**: p. 61-75.

138. Embury, J.D., B.A. Wilcox, and A.H. Clauer, *The influence of microstructure on high-temperature creep and tensile deformation of Al-Zn-Mg-Cu alloys.* J. Inst. Met., 1972. **100**: p. 153-162.

139. Park, J.G., D.Y. Lee, and J. Choi, *Static creep behaviour of Al-Zn-Mg and Al-Zn-Mg-Cu alloys.* J. Mater. Sci., 1996. **31**: p. 2719-2723.

140. Kauffman, J.G., *Properties of Aluminium Alloys*, ed. J.G. Kauffman. 1999, Ohio: ASM International. 211-217.

141. Kwon, Y.N. and Y.W. Chang, *The effect of grain size and temperature on the superplastic deformation of a 7075 Al alloy.* Metall. Mater. Trans. A, 1999. **30A**(8): p. 2037-2047.

142. Yang, X., H. Miura, and T. Sakai, *Continous dynamic recrystallization in a superplastic 7075 aluminium alloy.* Mater. Trans., 2002. **43**(10): p. 2400-2407.

143. Towle, D.J. and H. Jones, *The creep of alpha-iron at low stresses.* Acta Metall., 1976. **24**: p. 399-407.

144. Sritharan, T. and H. Jones, *The creep of beta-cobalt at low stresses.* Acta Metall., 1979. **27**(1979): p. 1293-1300.

145. Fujikawa, S.I., *Diffusion in Magnesium.* J. Jap. Inst. Light Met., 1992. **42**: p. 822-825.

146. Underwood, E. E., *Quantative stereology*, 1970: Addison-Wesley

147. Ardell, A. J. and S. S. Lee, *A dislocation network theory of Harper-Dorn creep-1. Steady state creep of monocrystalline Al.* Acta Metall., 1986. 34: p. 2411-2423.

148. Timeshenko, S. and D. H. Young, *Elements of Strength of Materials*, 1968, 5th Edition. London: Van Nostrand.

APPENDIX 1

Calculation of stresses and profile during cantilever tests

(a) Estimation of bending moment and stress

For the cantilever tests described in §3.2.2. a procedure for estimation of rate of change of curvature from the profile of the foil was developed. This procedure is described in this section. Firstly it is important to estimate the bending moment and axial stress in the foil. The foil is loaded only under its self weight (q) as shown in Fig. A1.
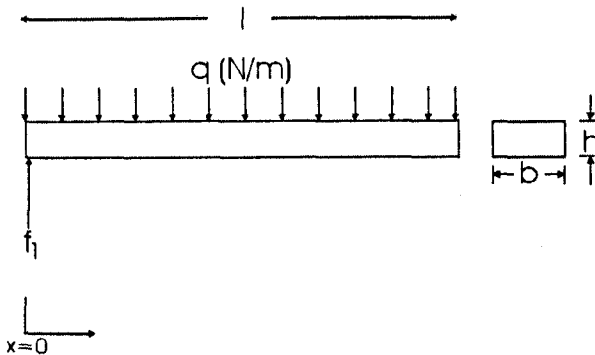
Figure A1. Schematic of the loads acting on the cantilever foil.

For equilibrium,

$$f_1 = q*L = \rho_{foil}*L*b*h*g \qquad (1)$$

where f_1 is the reaction forces from the support post, ρ_{foil} is density of copper, and g is the acceleration due to gravity.

Taking a transverse section at x, as shown in Fig. A2, where the shear force is given as V(x) and the bending moment $M_b(x)$
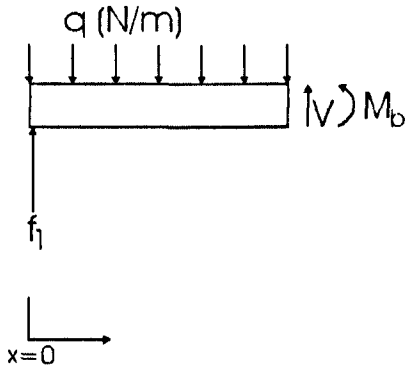
Figure A2. Free body diagram for the cantilever foil.

Force equilibrium can be written as

$$f_1 - q*x + V(x) = 0 \qquad (2)$$

Combining (1) and (2)

$$V(x) = q*(x - L) \qquad (3)$$

Now,

$$\frac{dM_b(x)}{dx} = -V(x) \qquad (4)$$

$$M_b(x)\big|_0^x \quad = \int_0^x -q*(x-L)dx$$

$$= -q*[\frac{x^2}{2} - Lx]_0^x \qquad (5)$$

$$M_b(x) - M_{b,0} = -\frac{q}{2}[x^2 - 2Lx]$$

At x = L, $M_b(x) = 0$

131

$$\Rightarrow M_{b,0} = \frac{qL^2}{2} \qquad (6)$$

Using (6) in (5),

$$M_b(x) = -\frac{q}{2}(L-x)^2 \qquad (7)$$

In pure bending, i.e. when there is no shear stress, the axial stress σ_x in the beam is given by

$$\sigma_x(x) = \frac{M_b(x)y}{I_{yy}} \qquad (8)$$

where I_{yy} is the second moment of inertia given by $\int_A y^2 dA = \dfrac{bh^3}{12}$ and y is the distance of the point from the neutral line. However, this expression can be used as a first approximation in the present case, after calculations by Timoshenko and Young [148] showed that the error involved in estimation of the normal stress is very small. The maximum tensile (or compressive) stress is at the convex (or concave) surface where y would be $\pm h/2$.

Using (1) and (8),

$$\sigma_x(x, surface) = \pm \frac{M_b(h/2)}{I_{yy}}$$

$$= \pm \frac{(-\frac{q(L-x)^2}{2})(\frac{h}{2})}{\frac{bh^3}{12}} \qquad (9)$$

$$= \pm 3\rho_{foil} g \frac{(L-x)^2}{h}$$

(b) Estimation of Profile of Foil Undergoing Diffusional Creep

During diffusional creep, strain rate is directly proportional to stress. Using (9),

$$\dot{\varepsilon} \propto (L-x)^2$$

Curvature of the foil, κ, is defined as approximately equal to d^2y/dx^2 where x is the horizontal distance along the foil and y is the vertical deflection of the foil edge from its original position. After Timoshenko and Young [148],

$$\varepsilon_x = \kappa \frac{h}{2}$$
$$= \frac{d^2y}{dx^2}\left(\frac{h}{2}\right)$$

Combining (10) and (11) gives

$$\frac{d^2y}{dx^2} \propto (L-x)^2$$
$$= K(L-x)^2$$

Integrating Eq. (12) twice under appropriate limits gives

$$y = Kx^2\left[\frac{L^2}{2} - \frac{Lx}{3} + \frac{x^2}{12}\right]$$

The measured profile is curve-fitted to Eq. (13) to obtain the best-fit value of constant, K. At x =0,

$$\kappa(x=0) = KL^2; \qquad \varepsilon(x=0, surface) = \kappa\frac{h}{2} \qquad (14)$$

Assuming a minimal primary component (under diffusional creep regime), rate of change of curvature of the foil is obtained by dividing the calculated curvature (14) by total test duration. An example of the success of this procedure is shown in Fig A3.
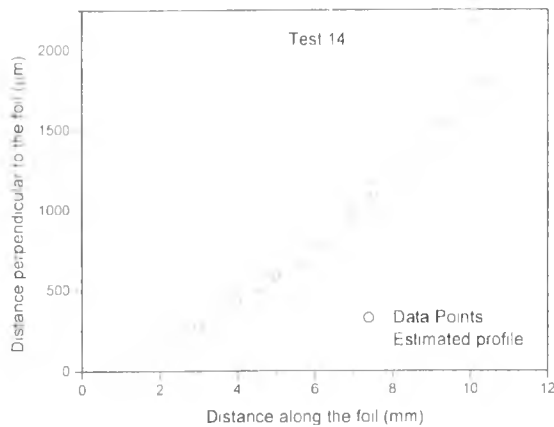
Figure A3 Curve fitting of the measured profile to estimate the curvature due to bending.
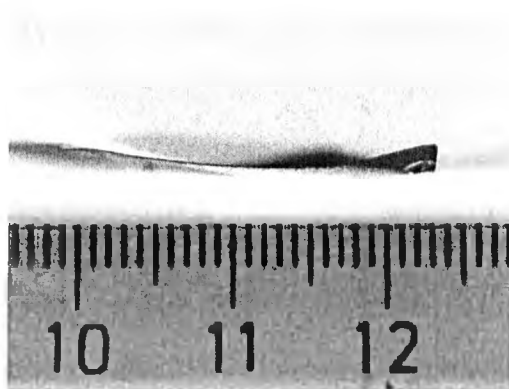
Figure A4 Profile of a bridge type sample after creep testing.

APPENDIX 2

Calculation of error in measurement of creep rates of copper wires

The strain rate $\dot{\varepsilon}$ is expressed as

$$\dot{\varepsilon} = \frac{\Delta l}{l_0 t} \qquad (1)$$

where Δl is the increase in gauge length after creep, l_0 is the initial gauge length and t is the test duration.

Partially differentiating (1)

$$d\dot{\varepsilon} = \frac{d(\Delta l)}{l_0 t} - \frac{\Delta l}{t}\frac{dl_0}{l_0^2} - \frac{\Delta l}{l_0}\frac{dt}{t^2} \qquad (2)$$

Dividing both sides by $\dot{\varepsilon}$, gives

$$\frac{d\dot{\varepsilon}}{\dot{\varepsilon}} = \frac{d(\Delta l)}{\Delta l} - \frac{dl_0}{l_0} - \frac{dt}{t} \qquad (3)$$

For maximum error, adding the errors

$$\frac{d\dot{\varepsilon}}{\dot{\varepsilon}} = \frac{d(\Delta l)}{\Delta l} + \frac{dl_0}{l_0} + \frac{dt}{t} \qquad (4)$$

Typically, $\Delta l \approx 0.5$ mm and $l_0 \approx 25$ mm; error in the measurement of time is negligible.

$$\Rightarrow \frac{d\dot{\varepsilon}}{\dot{\varepsilon}} = \frac{0.09\,mm}{0.5\,mm} + \frac{0.04\,mm}{25.0\,mm}$$

$$= 16.2\% \tag{5}$$

Stress (σ) can be expressed as

$$\sigma(inMPa) = \frac{wt.(in\,g) * 10^{-3} * 9.8}{thickness(in\,mm) * width(in\,mm)} \tag{6}$$

Proceeding as above,

$$\frac{d\sigma}{\sigma} = \frac{d(wt)}{wt} + \frac{dt}{t} + \frac{dw}{w}$$

$$= \frac{0.1\,g}{20\,g} + \frac{0.005\,mm}{0.6\,mm} + \frac{0.01\,mm}{3.06\,mm}$$

$$= 1.7\,\% \tag{7}$$

APPENDIX 3

Calculation of threshold stress due to surface tension

Consider one grain-element of volume V containing one grain-boundary. On application of stress σ the work done by external force to extend the foil by length dl is given as

$$W_{force} = \sigma l_0 \delta dl \qquad (1)$$
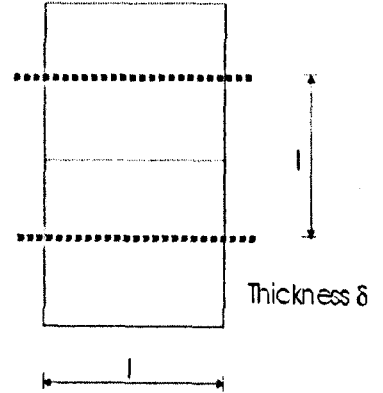
where l is the grain length, δ is the foil thickness and σ is the applied stress. If the surface free energy and grain boundary energies are γ_s and γ_g respectively, then the increase in the internal energy is given by

$$W_{internal} = \gamma_s dA_s + \gamma_g dA_g \qquad (2)$$

where A_s and A_g are free surface and grain boundary areas respectively.

$A_s = 2l^2$, $A_g = l\delta$ and $V = l^2\delta$

$$\Rightarrow A_g = \frac{V}{l} \qquad (3)$$

During plastic deformation, V remains constant.

$$\Rightarrow \frac{dA_s}{dl} = 4l; \qquad \frac{dA_g}{dl} = -\frac{V}{l^2} = -\delta \qquad (4)$$

Work done by the external force should be equal to increase in the internal energy of the system. Therefore, substituting (4) in (2) and equating to (1) we get,

$$\gamma_s(4l) - \gamma_g\delta = \sigma_0 l_0 \delta \qquad (5)$$

where σ_0 is the stress for zero creep.

$$\Rightarrow \sigma_0 = \frac{4\gamma_s}{\delta} - \frac{\gamma_g}{l} \qquad (6)$$

$\gamma_g \approx \gamma_s/3 = 0.46$ J/m^2 for copper and $\delta \approx 3*10^{-4}$ m gives

$\sigma_0 \approx 0.015$ MPa.

APPENDIX 4

Publications based on this and related work

1. Departures from model predictions for creep in pure metals at low stresses near their melting point
   McNee, K. R., V. Srivastava, Greenwood, G. W. and H. Jones. TMS annual meeting, Seeatle, United States, Feb 2002.

2. Effect of low stresses on creep and surface profiles of thin copper wires
   Srivastava, V., K. R. McNee, H. Jones and G. W. Greenwood. Acta Materialia, Vol. 51(2003), Issue 15, 2011-2019.

3. Creep behaviour of AZ61 Magnesium alloy at low stresses and intermediate temperatures
   Srivastava,V., K. R. McNee, G. W. Greenwood and H. Jones. (to be published in Materials Science and Technology, 2003)

4. Creep of copper foils under bending loads
   Srivastava, V., G. W. Greenwood and H. Jones. (to be submitted to Philosophical Magazine)

5. The creep performance of a sand-cast Mg-2.8Nd-0.8Zn-0.5Zr-0.3Gd alloy at 241 to 262°C
   Bell, A., V. Srivastava, G. W. Greenwood and H. Jones. (to be submitted to Zeitschrift fur Metallkunde)

6. Diffusional creep in a fine-grained 7075 aluminium alloy
   Srivastava,V., G. W. Greenwood and H. Jones. (under preparation)

7. Low stress creep of coarse-grained copper foils at high homologous temperatures
   Srivastava,V., K. R. McNee, G. W. Greenwood and H. Jones (under preparation)

8. Effect of grain aspect ratio on creep of bamboo structure wires
   Srivastava,V., K. R. McNee, G. W. Greenwood and H. Jones (under preparation)

Table 2.1 Value of proportionality constants in diffusional creep equations 2.1 and 2.2 for various grain geometries (from Burton [11]).

Grain Shape	Stress	A_{NH}	A_{CO}
Sphere, Diameter d	Shear	40	
	Tensile	13.3	$150/\pi$
Cylinder, length/diameter <2	Tensile	12.2	
Cube, Side d	Tensile	12	
Foil, width d, thickness t	Tensile	7.5	12

† See Greenwood [54] for diffusional creep equations developed for the case of multiaxial stresses applied to orthorhombic grains.

Table 2.2 Dislocation density as a function of applied stress for pure aluminium [66].

Applied Stress $(10^4$ Pa)	Dislocation Density $(10^7$ m$^{-2})$
0 (annealed)	1.32
1.45	3.88
2.12	4.88
5.72	5.10
6.00	9.69
6.60	8.20
8.07	4.08
9.80	4.28
11.8	5.72
14.0	5.99
14.0	8.40

Table 2.3 Major characteristics of Harper-Dorn creep at high temperature in pure metals (adapted from Yavari *et al.* [65] and Nabarro [63]).

S. No.	Characteristic
(i)	The stress exponent is equal to 1.
(ii)	The creep rate is independent of the specimen grain size and similar rates are reported for single crystals.
(iii)	The activation energy for the process is equal to that for lattice self diffusion.
(iv)	The strain is essentially uniform through out the material.
(v)	Short primary stage is observed preceding the steady state.
(vi)	The dislocation density is low and independent of the stress level, though many authors have questioned this observation.
(vii)	Sub-grain formation may or may not occur.
(viii)	The values of A_{HD} obtained by different authors agree closely.
(ix)	Creep strains as large as $\varepsilon=0.12$ are reported in the Harper-Dorn regime.
(x)	Harper-Dorn creep is suppressed by presence of precipitates.
(xi)	Similar values of A_{HD} are reported for pure Al and Al-Mg alloys.
(xii)	If initial dislocation density is high, the creep rate is much less than that corresponding to Harper-Dorn creep.
(xiii)	The dislocations in the Harper-Dorn regime are predominantly (>50%) close to edge orientation; only a small proportion of dislocations (~10%) are close to screw orientation.

Table 2.4 Experimental reports of Harper-Dorn creep in pure metals (adapted from Yavari et al. [65] and Fiala and Langdon [71]).

Material	T/T_m	A_{HD}	References
Al	0.99	$1.7*10^{-11}$	Harper and Dorn [3], Barrett *et al.* [66] and Mohamed *et al.* [67]
Al[a]	0.99	$1.6*10^{-11}$	Ardell and Lee [147]
Cu	0.97	$2.8*10^{-11}$	Pines and Sirenko [72]
Cu[a]	0.97	$3.7*10^{-11}$	Pines and Sirenko [72]
Pb	0.92-0.98	$2.9*10^{-11}$	Mohamed *et al.* [67]
Sn	0.98	$2.4*10^{-11}$	Mohamed *et al.* [67]
β-Co	0.61	$7.4*10^{-10}$	Malakondaiah and Rama Rao [70]
α-Ti	0.51-0.54	$1*10^{-9}$	Malakondaiah and Rama Rao [70] and [69]

[a] Single crystal samples

Table 2.5 Compilation of early results obtained on copper wires and foils at temperatures close to melting point at low applied stress (adapted from Jones [16]).

Reference	Sample Geometry	Grain length/ Size (μm)	Temperature (°C)	$\sqrt{\dfrac{D_l t}{al}} = P$	Applied Stress (kPa)	Threshold Stress (kPa)	$\dfrac{d\dot{\varepsilon}}{d\sigma}$ (Pa−s)$^{-1}$
Udin et al. [12]	72 μm wire	140	950	2.0	17-83	39	2.82 x 10^{-13}
			1000	2.1	0.72-81	39	9.04 x 10^{-13}
			1050	2.4	0.96-75	38	1.53 x 10^{-12}
	128 μm wire	125	950	1.6	0.76-45	23	3.44 x 10^{-13}
			999	1.4	0.69-46	23	1.18 x 10^{-12}
			1024	1.3	0.91-46	24	2.37 x 10^{-12}
			1049	1.4	0.91-45	22	2.73 x 10^{-12}
Hoage [13]	80 μm wire	105	900	2.7	29-50	38	2.30 x 10^{-13}
Inman [20]	51 μm wire	81	950	4.1	2.7-123	64	3.82 x 10^{-13}
		70		4.8	10-96	55	3.58 x 10^{-13}
	89 μm wire	99		4.2	12-109	37	1.03 x 10^{-13}
Pranatis and Pound [104]	38 μm thick foil	150	1051	2.2^a	0.44-20	----	2.00 x 10^{-13}
			1024				1.44 x 10^{-13}
			1002				1.07 x 10^{-13}
			975				9.01 x 10^{-14}
			960				5.38 x 10^{-14}
	51 μm thick foil	188	1051				1.07 x 10^{-13}
			1024				8.26 x 10^{-14}
			1002				6.21 x 10^{-14}
	76 μm thick foil	197	1051				8.93 x 10^{-14}
			1024				7.19 x 10^{-14}
			1002				4.27 x 10^{-14}
	102 μm thick foil	166	1051				8.93 x 10^{-14}
	127 μm thick foil	189	1051				4.90 x 10^{-14}
Pines and Sirenko [72]	840 μm wire	1000	1040	0.06	245	----	1.02 x 10^{-12}
	1400 μm wire	2000		0.01			4.49 x 10^{-13}
	350 μm strip^b	350		0.02			2.29 x 10^{-10}
	300 μm strip^c	1000		0.06			2.16 x 10^{-12}

^{a} A representative value from the test duration reported for one test
^{b} Prepared by powder metallurgy
^{c} Rolled strip

Table 3.1 Nominal composition of as-received copper wires and foils.

Element	Content[†]
Iron	3
Lead	2
Manganese	<1
Magnesium	<1
Nickel	3
Silver	10
Tin	1
Calcium	<1
Oxygen	<10
Copper	Balance

† All compositions in ppm.

Table 3.2 As-received wire diameters compared to nominal wire diameters.

Nominal wire diameter (μm)	Measured wire diameter (μm)
25	27.8 ± 1.17
50	59.8 ± 1.86
125	138.2 ± 2.37
250	268.6 ± 5.20
500	----

Table 3.3 Nominal composition of as-received aluminium alloy 7075 and magnesium alloy AZ61.

	7075	AZ61
Element	Amount (wt%)	Amount (wt%)
Aluminium	Bal.	6.4
Chromium	0.22 ± 0.02	---
Copper	1.51 ± 0.02	---
Iron	0.33 ± 0.02	---
Magnesium	2.34 ± 0.02	Bal.
Manganese	0.04 ± 0.02	0.2
Silicon	0.10 ± 0.02	---
Titanium	0.07 ± 0.02	---
Zinc	5.30 ± 0.04	0.90
Zirconium	<0.02 ± 0.02	---

Table 4.1 Summary of results obtained from low stress creep tests carried out at 990°C on high purity copper wires of different diameters. The applicable Harper-Dorn value of $d\dot{\varepsilon}/d\sigma$ is 6.25×10^{-14} m^2 N^{-1} s^{-1}.

Nominal wire diameter, a (μm)	Test Duration, (h)	$\sqrt{\dfrac{D_l t}{al}} = P$	Total Strain (%)	Grain length/size, l (μm)	$\dfrac{d\dot{\varepsilon}}{d\sigma}$ (experimental) (m^2 N^{-1}s^{-1})	$\dfrac{d\dot{\varepsilon}}{d\sigma}$ (NH creep) (m^2 N^{-1}s^{-1})	$\dfrac{(d\dot{\varepsilon}/d\sigma)_{exp}}{(d\dot{\varepsilon}/d\sigma)_{NH}}$
25	50-252	4-10	-3.7 to +10.9	54	$(2.2 \pm 0.2) \times 10^{-12}$	8.6×10^{-13}	2.6
50	122-408	4-7	-4.86 to +6.15	96	$(5.7 \pm 1.0) \times 10^{-13}$	2.4×10^{-13}	2.4
125	116-320	2-3	-0.98 to +3.42	131	$(1.4 \pm 0.3) \times 10^{-13}$	7.0×10^{-14}	2.0
250	356, 398	1.9	+0.56 to +1.13	250	$(3.4 \pm 0.6) \times 10^{-14}$	1.8×10^{-14}	1.8
500	360	1.2	+0.36 to +1.18	362	$(4.2 \pm 0.8) \times 10^{-14}$	8.9×10^{-15}	4.7
500	1061	2.0	+0.91 to +1.63	362	$(1.3 \pm 0.2) \times 10^{-14}$		1.5

Table 4. 2 Contribution to total creep strain from grain boundary sliding for low stress creep of 25-500 μm diameter copper wires at 990°C.

Wire diameter (μm)	Stress (kPa)	Time (h)	Total measured strain (%)	Total length examined (mm)	Elongation on length examined due to sliding (μm)	Strain on length examined due to sliding (%)	Proportion of total strain from sliding (%)
25	195	126	5.3	56	0	0	0
25	169	150	5.8	63	0	0	0
50	150	138	5.6	36	36	.10	1.80
50	104	408	3.2	64	59	0.09	2.88
125	187	232	3.39	45	149	0.33	9.77
125	276	320	3.42	52	142	0.27	7.98
250	46	356	0.56	34	31	0.09	16.28
250	155	356	1.05	27	42	0.16	14.14
500	161	360	0.96	38	84	0.22	22.90

Table 4.3 Summary of results of tensile creep tests on copper foils conducted as part of this work.

Serial No.	Specimen No.	Temperature (K)	Thickness (mm)	Stress (MPa)	Strain (%)	Strain rate (s^{-1})
1	1	1335	0.412	0.23	1.93	5.37×10^{-8}
	2	1335	0.37	0.08	-0.59	-1.65×10^{-8}
	3	1335	0.378	0.49	2.88	7.99×10^{-8}
	4	1335	0.416	0.60	8.93	2.48×10^{-7}
2	1	1338	0.614	0.16	0.71	2.47×10^{-8}
	2	1338	0.625	0.29	1.14	3.96×10^{-8}
	3	1338	0.631	0.39	1.49	5.19×10^{-8}
3	1	1347	0.634	0.51	2.46	6.83×10^{-8}
	2	1347	0.626	0.15	1.01	2.81×10^{-8}
	3	1347	0.621	0.29	0.78	2.18×10^{-8}
	4[a]	1347	0.607	0.52	1.25	3.47×10^{-8}
4	1	1336	0.614	0.10	0.06	1.69×10^{-9}
	2	1336	0.591	0.53	7.15	1.99×10^{-7}
	3	1336	0.593	0.41	1.86	5.17×10^{-8}
	4[b]	1336	0.64	0.41	0.67	1.87×10^{-8}
5[c]	1	1347	0.398	0.09	0.52	1.45×10^{-8}
	2	1347	0.408	0.15	1.91	5.29×10^{-8}
	3	1347	0.388	0.30	3.61	1.00×10^{-7}
	4	1347	0.404	0.42	9.24	2.57×10^{-7}
6[d]	1	1284	0.584	0.28	1.86	2.45×10^{-8}
	2	1284	0.588	0.52	1.33	1.76×10^{-8}

[a] Sample with only three grains in the gauge length, grain size ~10 mm.
[b] Sample coated with 20 nm layer of alumina.
[c] Initial grain size of the specimens in this test was 0.58 mm.
[d] Test conducted in argon atmosphere in which the sample oxidized during testing.

Table 4.4 Creep rates of copper foils tested in tension at 850°C.

S. No.	Foil thickness (mm)	Grain size (mm)	Stress (MPa)	Strain (%)	Expt. strain rate(s^{-1})	N-H strain rate (s^{-1})
1	0.40	0.42	0.12	1×10^{-2}	1.14×10^{-10}	7.10×10^{-11}
			0.22	8×10^{-2}	2.46×10^{-10}	1.30×10^{-10}
			0.36	1.1	4.58×10^{-10}	2.13×10^{-10}
			0.54	0.2	1.64×10^{-9}	3.37×10^{-10}
2	0.60	0.81	0.12	3×10^{-3}	1.51×10^{-10}	1.90×10^{-11}
			0.22	7×10^{-2}	4.57×10^{-10}	3.50×10^{-11}

Table 4.5 Mechanical data from bridge-type creep tests on copper foils at 1000°C. The maximum bending moment was at the midpoint of the foil length and was estimated to be 2.55 x 10⁻⁶ Nm (corresponding stress was 0.26 MPa).

S. No.	Coating	Test duration (h)	Grain size (μm)	Measured curvature (m^{-1})	Rate of change of curvature, $\dot{\kappa}$ (10^{-5} $m^{-1}s^{-1}$)	Theoretical rate of change of curvature, $\dot{\kappa}$ (10^{-3} $m^{-1}s^{-1}$)	$\dfrac{\dot{\kappa}_{expt}}{\dot{\kappa}_{predicted}}$ (10^{-2})
1		24	---	3.9×10^{-4}	9.0	2.4	3.8
2	No coating	98	330 ± 93	6.8×10^{-4} (1.59×10^{-3})[†]	3.9 (9.0)[†]	1.4	2.8 (6.4)[†]
3		198	280 ± 84	11×10^{-4} (1.51×10^{-3})[†]	3.1 (4.2)[†]	1.9	1.6 (2.2)[†]
4[*]	Coating on tensile surface	198	114 ± 68	8.7×10^{-4} (1.01×10^{-3})[†]	2.4 (2.8)[†]	11.3	0.2 (0.3)[†]
5		210	179 ± 12	6.0×10^{-4}	1.6	4.6	0.3

[†] The values in parenthesis were obtained from the local curvature in the central 10 mm of the crept foil.
[*] Thinner coating deposited at 0.9 kW for 12 min.

Table 4.6 Results for cantilever tests at 950°C on 100 and 250 μm thick copper foils[†].

Test No.	Time (h)	Foil Thickness (μm)	Foil Length (mm)	Coating	$M_{b,0}$ (10^{-6} Nm)	Measured K (10^5 m^{-3}) *	Predicted K (10^5 m^{-3})	$\dfrac{K_{NH}}{K_{exp}}$
2	16	100	15	None	5.8	3.22 (0.997)	24.2	8
3	16	250	17	None	18.5	1.16 (0.915)	1.1	1
8	32	100	9	None	2.1	22.6 (0.968)	48.4	2
9	32		9.5	None	2.3	4.02 (0.932)		12
11	64	100	11	Top	3.1	9.11 (0.979)	96.7	11
16	64		13.8	Top	4.9	8.72 (0.983)		11
14	64		10.9	Bottom	3.0	7.52 (0.997)		13
18	64		12.3	Bottom	3.9	7.36 (0.978)		13
10	64	250	18	None	20.7	0.46 (0.987)	4.4	10
13	64		22.3	None	31.8	0.34 (0.979)		13
15	64		18.5	Top	21.9	0.36 (0.965)		12
17	64		17	Bottom	18.5	0.67 (0.981)		7

[†] $M_{b,0}$ is the value of maximum bending moment applied on the foil and K is the proportionality constant in Eq. (5.18).
* The values in parantheses indicate the value of correlation coefficient (R^2) during curve fitting to obtain the value of K.

Table 4.7 Test conditions, total strain and steady state strain rates for creep of 7075 aluminium alloy.

Test No.	Temperature (°C)	Stress (MPa)	Time (h)	Strain (%)	Steady state strain rate (10^{-9} s^{-1})
1.1	350	3.6			7.0
1.2		5.3			50
1.3		1.8			0.4
1.4		5.3			34
2.1	350	1.9	139	0.18	2.15
2.2		2.9	25	0.18	7.44
2.3		3.9	22.5	0.12	8.02
2.4		4.8	23	0.30	8.83
2.5		5.8	4.7	0.20	35.5
2.6		6.3	3	0.07	51.7
2.7		5.3	18.7	0.02	8.31
2.8		4.4	31	0.02	3.41
2.9		3.4	78	0.21	2.40
3.1	369		82	0.09	7.0
3.2	390	2.9	80	0.16	11.3
3.3	410		122	1.0	42.8

Table 4.8 Test conditions and resulting incremental strains ε and associated secondary

creep rates $\dot{\varepsilon}$ for tensile creep of AZ61 magnesium alloy.

Test No.	Stress MPa	Duration h	Temperature ^{0}C		ε percent	$\dot{\varepsilon}$ 10^9 s^{-1}
1.1	4.00	5	250		0.20	138
1.2	2.67	16			0.25	41.6
1.3	1.78	30			0.13	12.0
1.4	0.89	67			0.03	1.7
1.5	0.89	16	300		0.40	72.7
1.6	2.20	5	330		2.10	1320
1.7	1.33	15			3.40	528
				Total	6.51	
2.1	1.80	21	303		2.30	368
2.2	2.70	30			7.10	624
2.3	0.90	113			1.70	41.8
2.4	1.10	72			1.9	71.9
				Total	13.0	
3.1	0.90	81	300		1.40	46.6
3.2	1.35	22	303		1.10	146
3.3	1.35	7	317		1.00	423
3.4	0.90	16			1.12	200
3.5	0.90	21	333		3.30	443
3.6	1.35	3			1.00	886
3.7	1.35	11	346		5.20	1490
3.8	0.90	2			0.40	931
3.9	1.80	3			2.60	2520
3.10	2.25	0.3			0.40	3550
3.11	0.90	24	320		2.20	263
3.12	1.35	4			1.20	529
3.13	1.80	16			4.30	729
3.14	2.25	5	317		1.80	1030
3.15	1.80	1	319		0.30	684
3.16	1.80	15	289		0.60	166
3.17	1.35	215			4.90	73.5
3.18	1.80	17			0.90	147
3.19	2.25	21			1.50	214
3.20	1.35	69			1.60	69.4
3.21	0.90	26			0.14	18.1
				Total	31.2	

Table 4.9 Threshold stress σ_o and steady state strain rate per unit stress $d\dot{\varepsilon}/d\sigma$ versus text temperature T for AZ61 from the data in Fig. 4.26. Values of $D_B\delta$ derived via Eq. (5.19) from the $d\dot{\varepsilon}/d\sigma$ results are also shown together with the Coble creep derived values of $D_B\delta$ obtained by Crossland [124] for pure Mg.

Test temperature $^\circ$C	Threshold stress, σ_o MPa	$d\dot{\varepsilon}/d\sigma$ 10^{-13} Pa^{-1} s^{-1}	Equivalent $D_B\delta$ m^3/s	$D_B\delta$ for Mg m^3/s [124]	$\dfrac{D_B\delta(AZ61)}{D_B\delta(Mg)}$
250	1.25 ± 0.60	0.45 ± 0.11	2.44×10^{-20}	2.61×10^{-20}	0.94
289	0.82 ± 0.11	1.53 ± 0.10	8.74×10^{-20}	1.39×10^{-20}	0.63
303	0.84 ± 0.16	3.09 ± 0.26	1.81×10^{-19}	2.41×10^{-19}	0.75
318	0.51 ± 0.11	5.71 ± 0.40	3.43×10^{-19}	4.20×10^{-19}	0.82
330	0.27 ± 0.40	6.74 ± 1.76	4.13×10^{-19}	6.42×10^{-19}	0.64
346	0.50 ± 0.15	19.7 ± 1.8	1.24×10^{-18}	1.10×10^{-18}	1.12

Table 4.10 Mean linear intercept grain size $\bar{L}$ of AZ61 for different conditions.

Orientation relative to rolling direction and axis of creep loading	Parallel $\bar{L}_P$, μm	Normal $\bar{L}_n$, μm	$\bar{L}_p / \bar{L}_n$
As received	21.4 ± 1.3	21.9 ± 1.1	0.98
After 5h at 325°C	25.5 ± 1.7	25.0 ± 1.3	1.02
Sample 2 at end of test:			
in grip area	28.9 ± 2.4	29.3 ± 2.3	0.99
in gauge length (at 13% strain)	22.6 ± 1.8	20.6 ± 2.2	1.10
Sample 3 at end of test:			
in grip area	25.9 ± 1.5	26.2 ± 1.6	0.99
in gauge length (at 8% strain)	26.2 ± 1.3	23.4 ± 1.8	1.12
in gauge length (at 31% strain)	32.7 ± 2.5	28.6 ± 2.2	1.15

Table 5.1 Surface energy measurements by the zero creep method for copper close to its melting point. Specimens were wires except in ref [104] which used foils.

Purity	Wire diameter or foil thickness (μm)	Test temperature (°C)	Surface energy (J/m²)	Ref.
>99.9% pure	72 and 128	950-1050	1.64-1.05	[12]
99.99% pure	38-128 (foils)	960-1050	1.78-1.66	[104,129]
>99.999% pure	80	900	1.68-1.83	[13]
OFHC	51-88	950	1.58-1.83	[20]
99.999% pure	10-250	800-1018	2.35	[128]
>99.99% pure	25		1.49 ± 0.33	
	50	990	1.60 ± 0.47	This study
	125		1.58 ± 0.68	
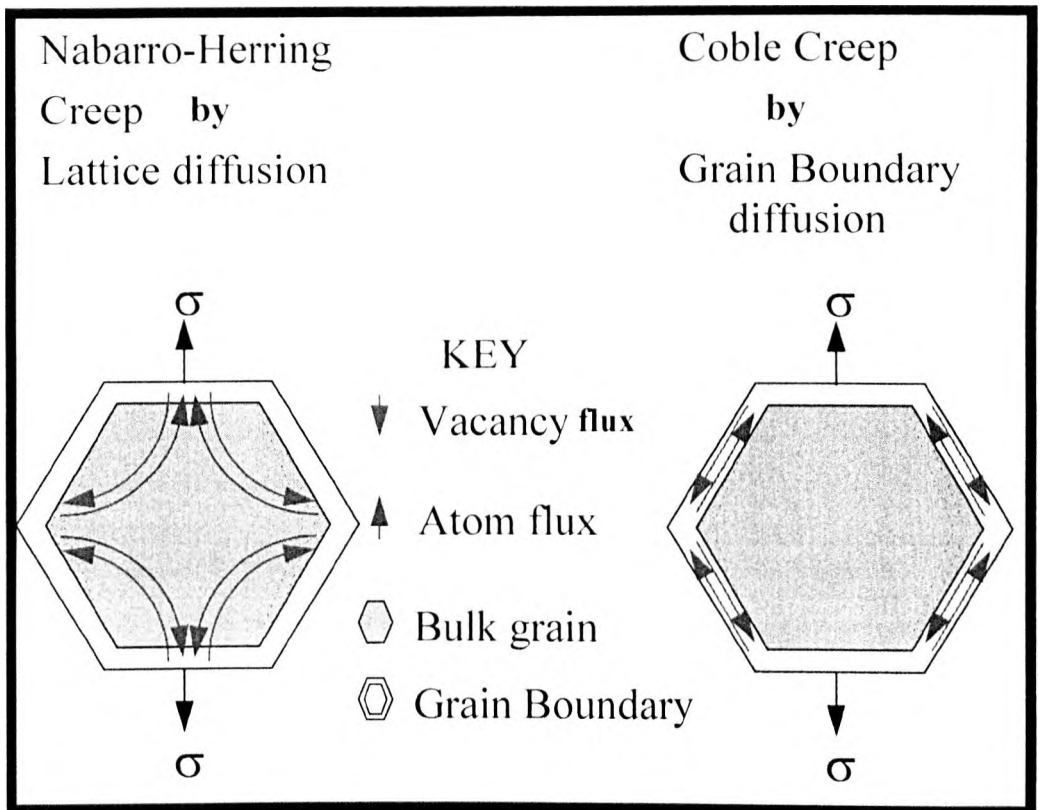
Figure 2.1 Schematic illustration of mechanism of diffusional creep (from [7]).
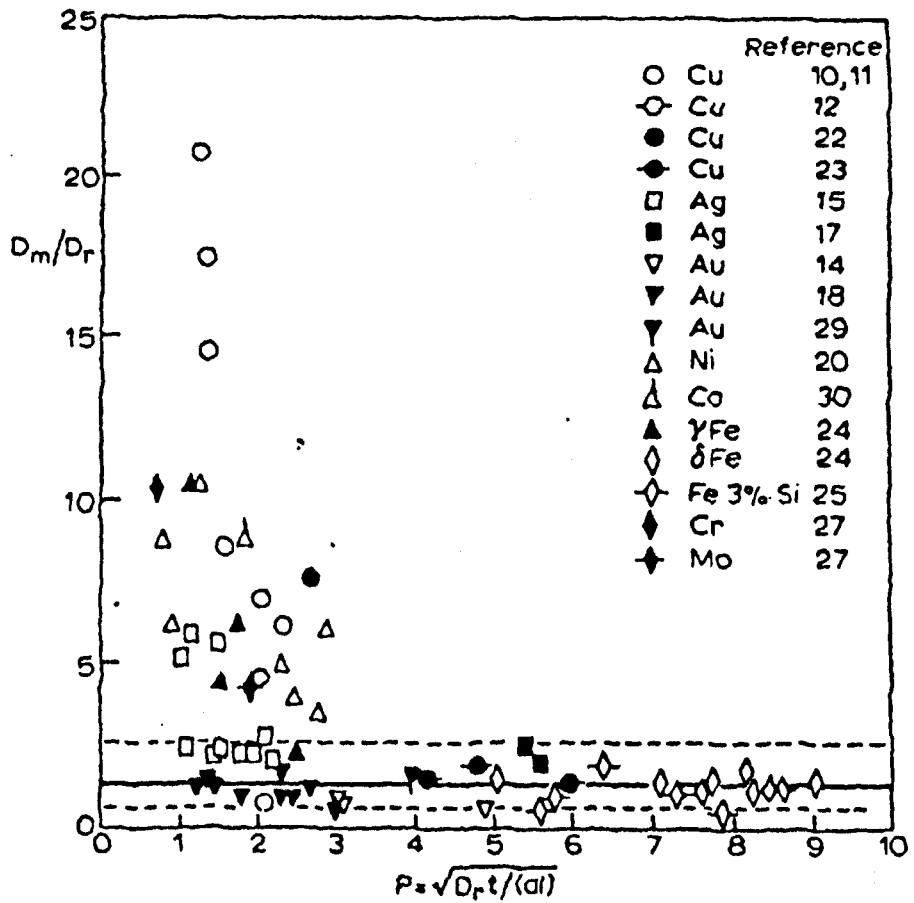
Figure 2.2 The ratio of diffusivity estimated from creep D_m to radiotracer diffusivity D_r plotted as a function of dimensionless test duration parameter P, indicating enhanced creep rates for low values of P (from Jones [11]).
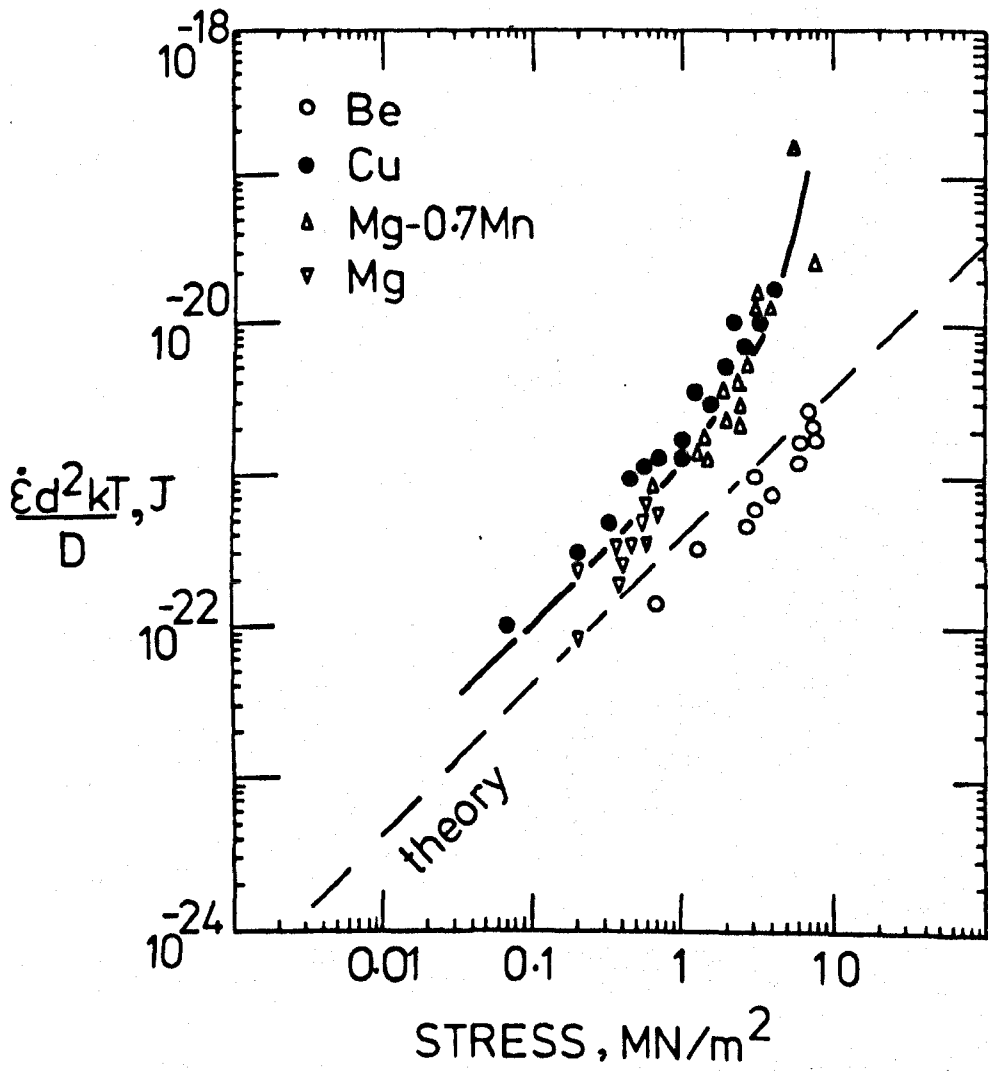
Figure 2.3 Grain size and temperature compensated creep rates plotted against stress for different metals providing evidence for diffusional creep. A transition to power law creep is shown at higher stresses (from Burton [11]).
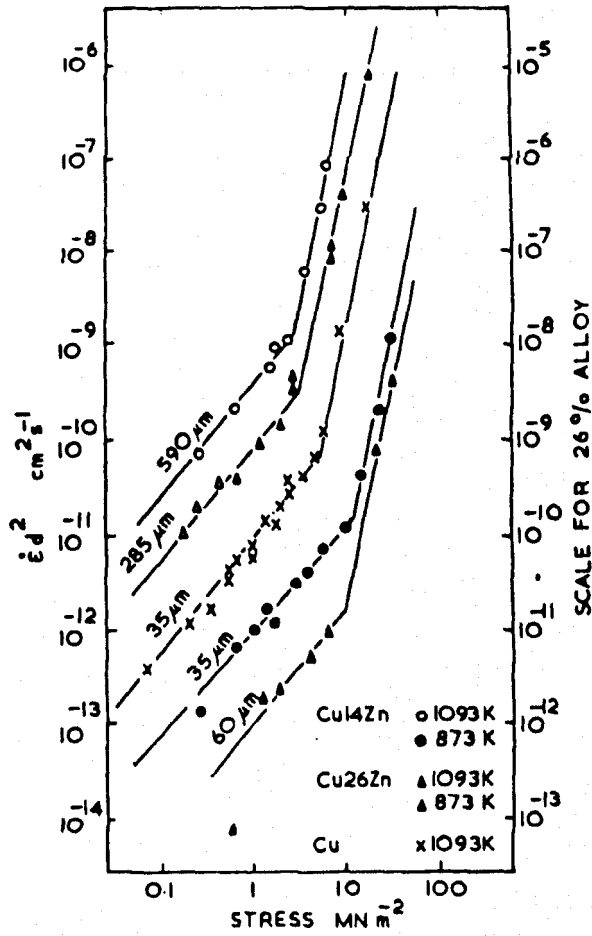
Figure 2.4 Evidence for diffusional creep at low stresses in Cu-Zn solid solution alloys showing transition to power law creep at higher stresses (from Burton [11]).
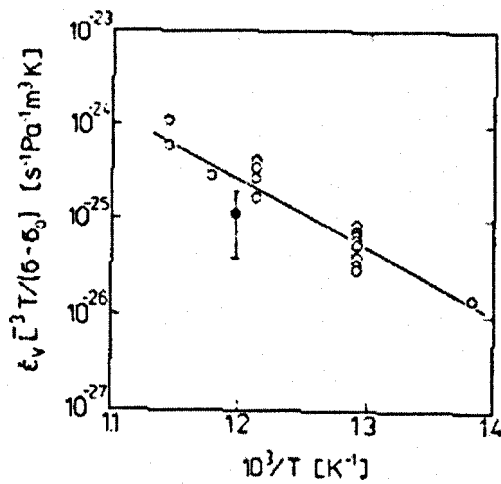
Figure 2.5 Coble creep observed in Cu-14%Al at intermediate temperatures and low stresses for mean grain intercept length less than 270 μm. The activation energy was found to be 136 kJ/mol and the creep rates were within a factor of 3 times faster than those predicted by Coble creep equation (from Kloc *et al.* [23]).
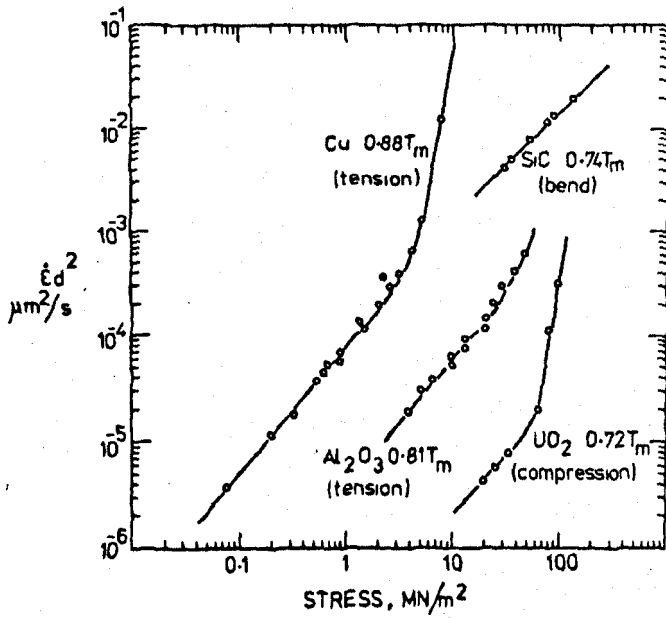
Figure 2.6 Linear stress dependence of grain size compensated creep rates for ceramics over three orders of magnitude in stress (from Burton [11]).
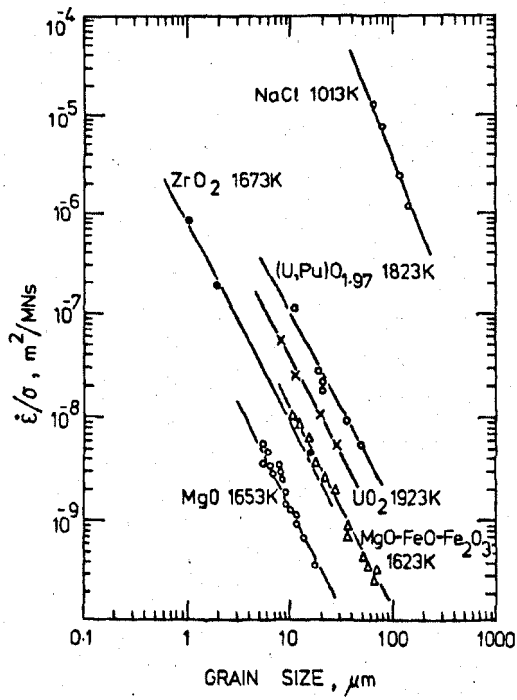
Figure 2.7 Inverse square grain size dependence of creep rate in accordance with Nabarro-Herring theory for a number of materials (from Burton [11]).
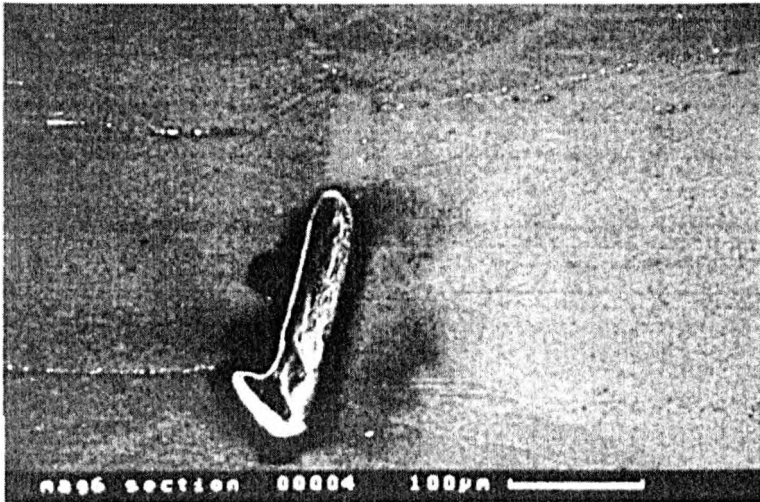
Figure 2.8 Micrographs from within the gauge length taken from longitudinal sections of Mg-Zr-H alloy ZR55 specimen. Cavitation and a precipitate-denuded zone are evident on the grain boundary transverse to the tensile stress. Tensile axis is horizontal (from McNee et al. [32]).

(a)   (b)   (c)

stress axis
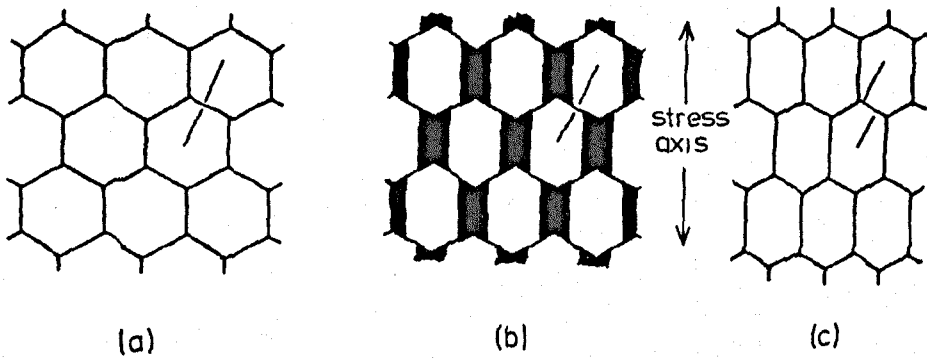
Figure 2.9 Schematic illustration of Lifshitz sliding during diffusional creep. If sliding did not occur, cavities would open up as shown in (b) (from Burton [11]).
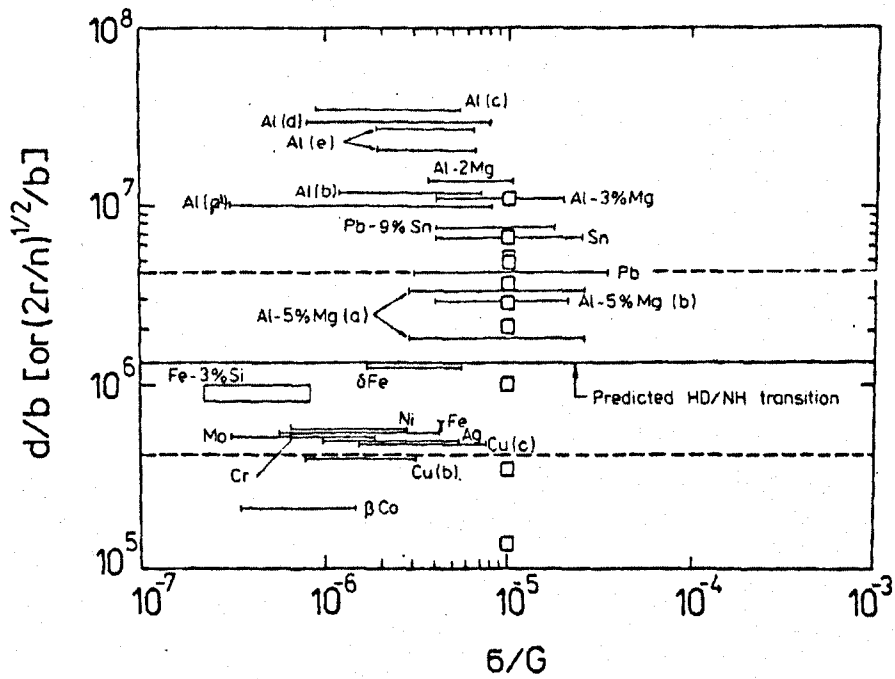
Figure 2.10 Evidence for Harper-Dorn creep in various metals and alloys (from Fiala and Langdon [71]).
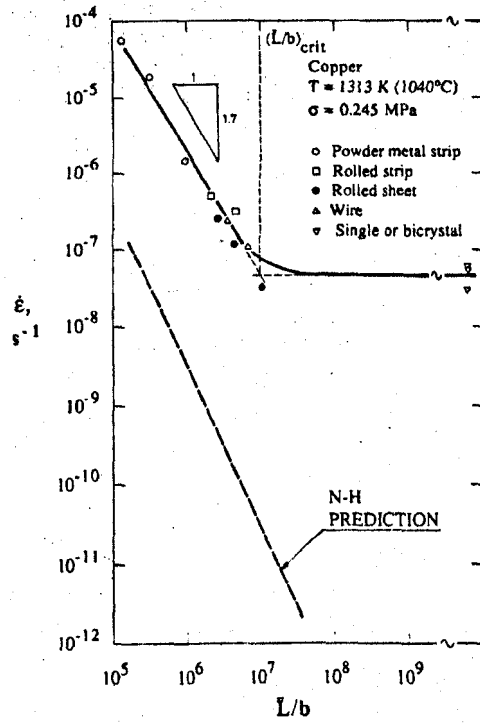
Figure 2.11 Data from Pines and Sirenko [72] for creep of copper at 1060"C and 0.25 MPa (from Ruano *et al* [73,106]).
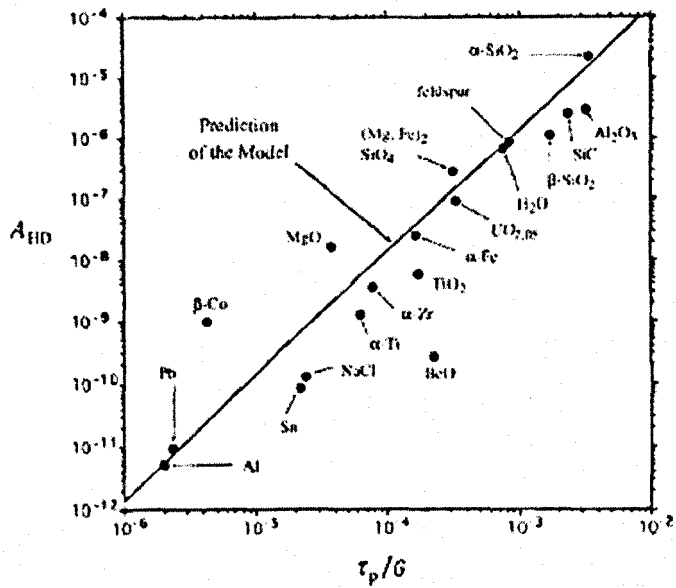
Figure 2.12 Variation of the Harper-Dorn constant, A_{HD}, with the shear modulus compensated Peierls stress for metals, ceramics and minerals. The line represents the prediction of the model proposed by Wang [74] (from Wang [74]).
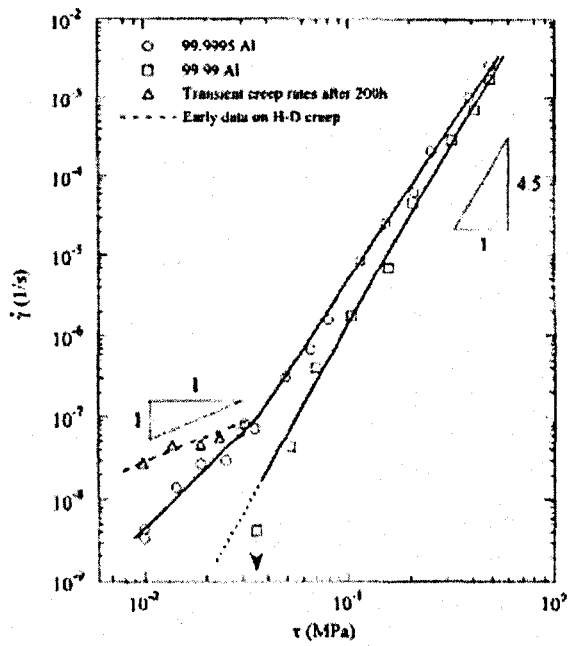
Figure 2.13 Shear strain rate vs applied shear stress on a logarithmic scale for 99.99 Al and
99.995 Al tested at 923 K (from Ginter *et al.* [78,79]).

initial state   intermediate   final state
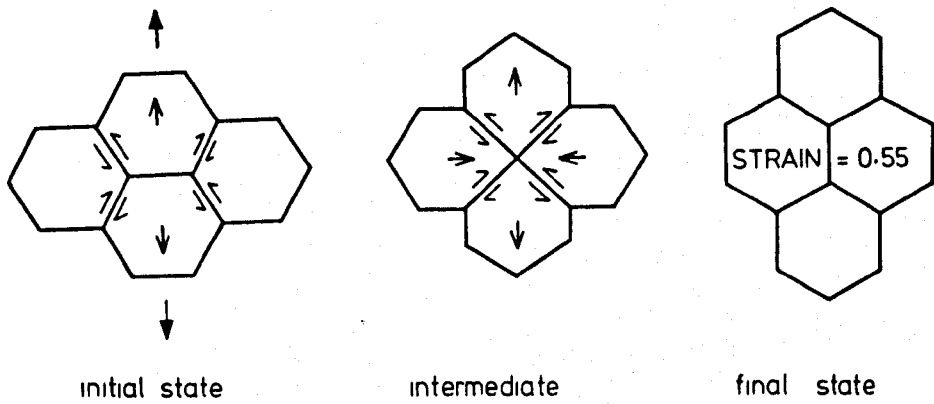
Figure 2.14 Schematic illustration of the mechanism for superplasticity based on diffusional accommodation model suggested by Ashby and Verrall [89].
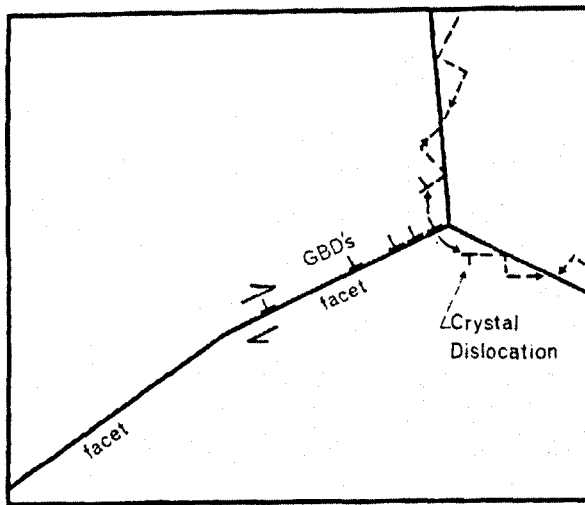
Figure 2.15 Grain boundary sliding and its accommodation to give deformation in Regime 11 of superplasticity. The grain boundary dislocations (GBDs) move to give grain boundary sliding and pile up at triple points. Under the stress concentration, these GBDs dissociate into crystal dislocations and then glide and clime in the grain along adjacent grain boundaries giving grain rotation. (from [5]).
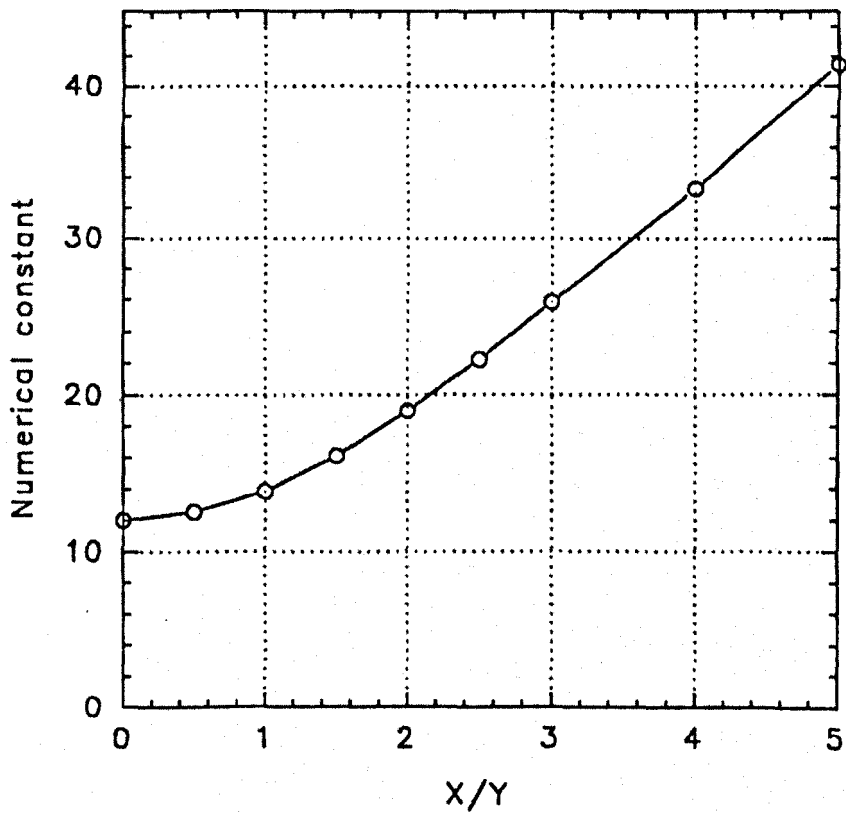
Figure 2.16 Value of numerical constant B in Eq. 2.5 calculated for various grain aspect ratios X/Y for creep of bamboo structured wires (from Burton [95]).
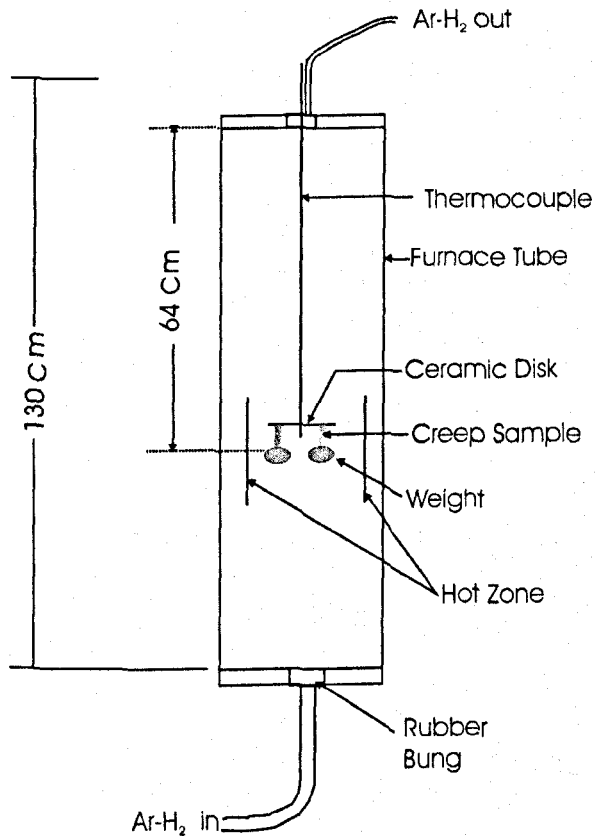
Figure 3.1 Schematic diagram of the equipment used for creep testing of wires.
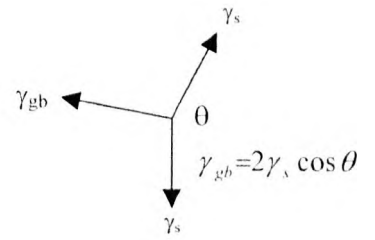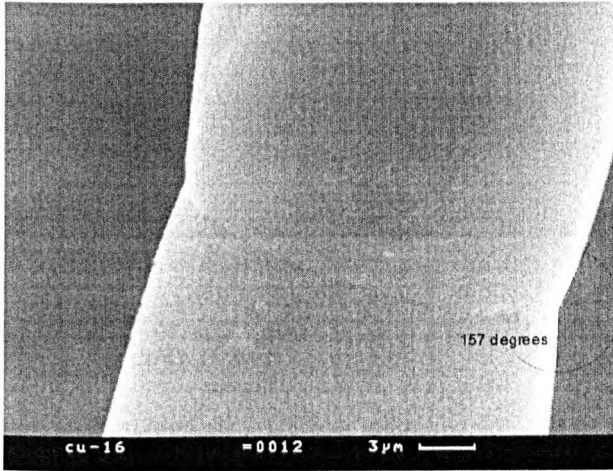
Figure 3.2 Determination of the ratio of γ_{gb}/γ_s from the root angle of grain boundary grooves.
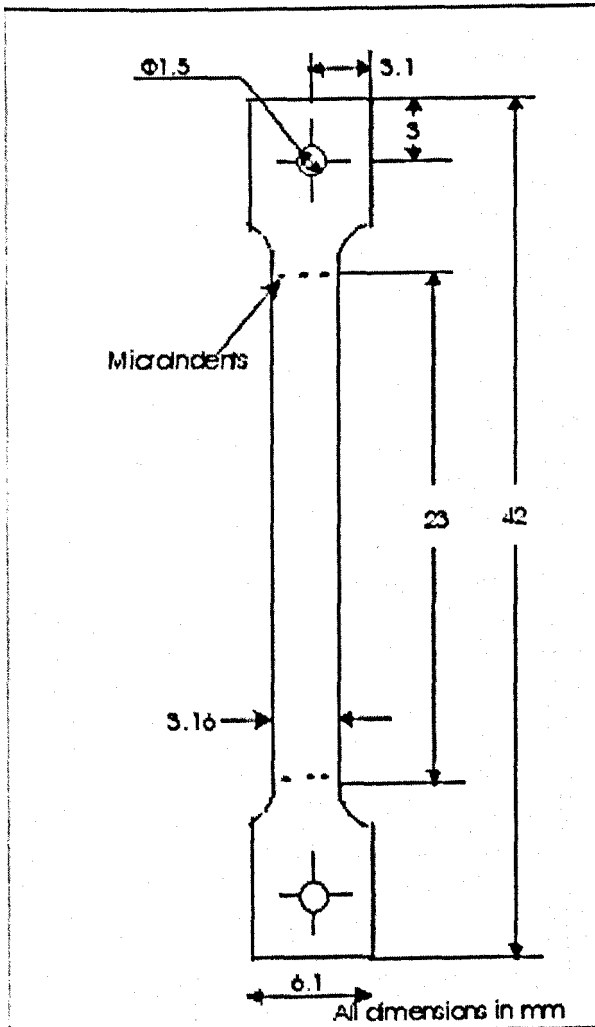
Figure 3.3 Dimensions of copper foil samples for creep testing in tension.
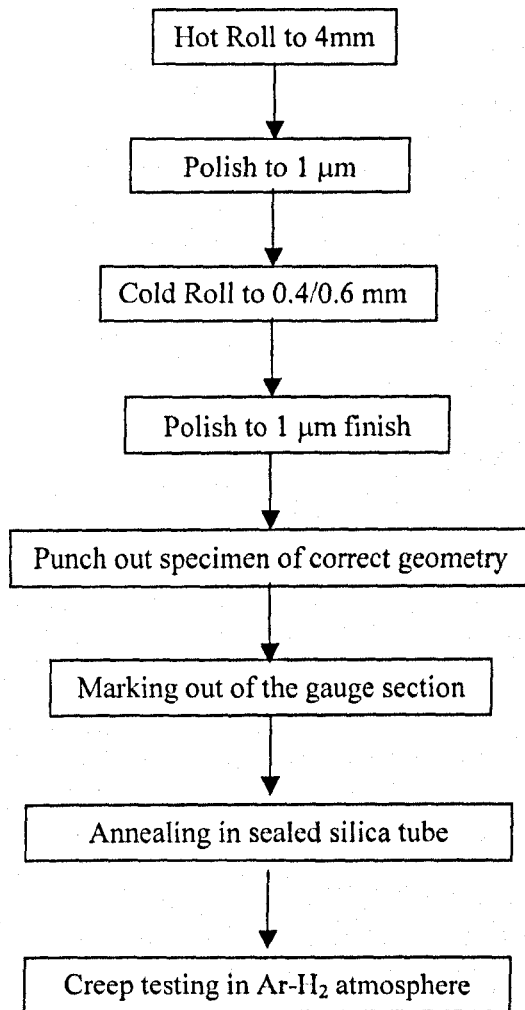
Figure 3.4 Sample preparation route for creep testing of copper foils in tension. The final sample thickness after polishing was 0.6 mm or 0.4 mm.
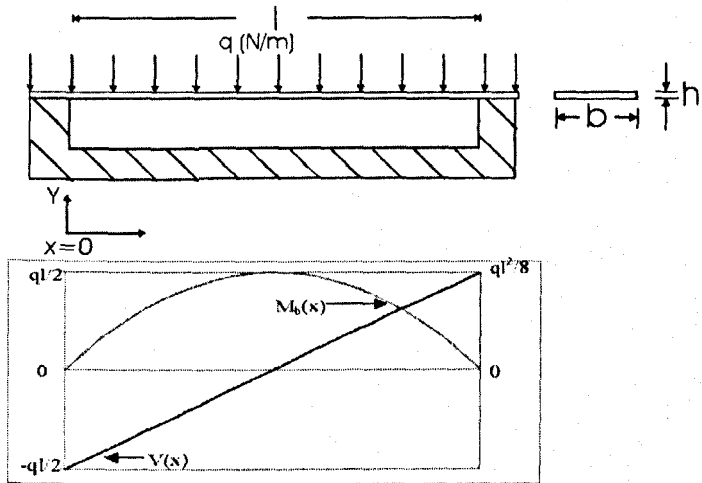
(a)
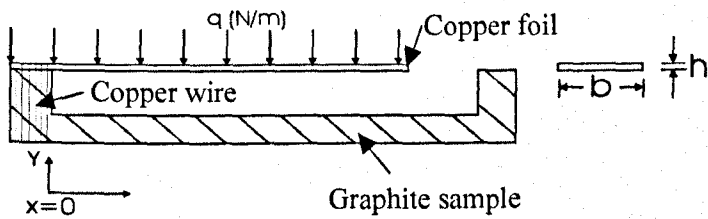
(b)

Figure 3.5 (a) Schematic of the bridge-type creep test arrangement. The variation of unrelaxed bending moment, M_b, and associated shear force, V, along the span of the foil is also shown. (b) Schematic assembly diagram for the cantilever type tests. In both cases, the assembled creep sample were sealed in a silica tube and placed in a tubular furnace.
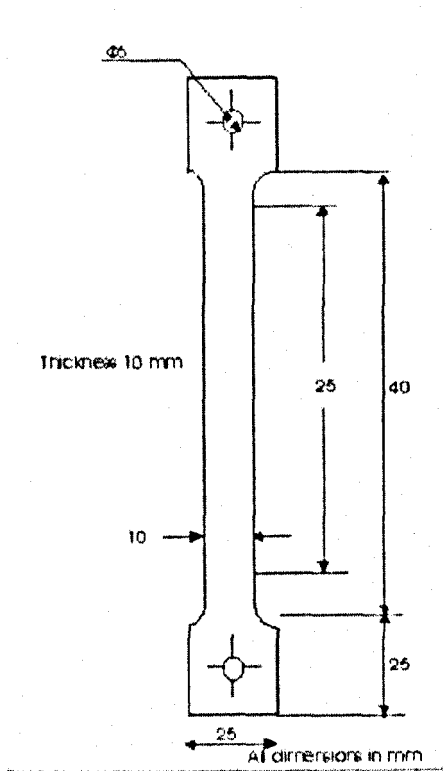
Figure 3.6 Dimensions of the creep test specimens used for superplastic 7075 and AZ61.
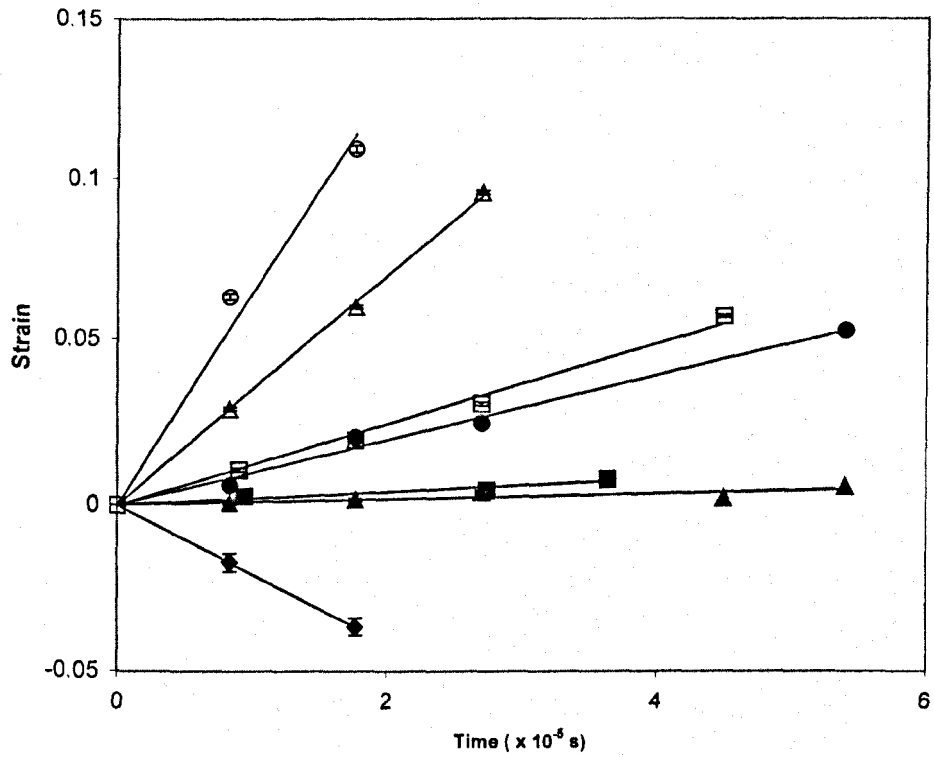
Figure 4.1 Fractional strain versus time curves for 25 micron diameter copper wires at 990°C. Complete testing conditions are given in Table 4.1. Stresses in kPa: ♦1.4 ▲87.2 ■96.4 ●169 □195 Δ259 ○335.
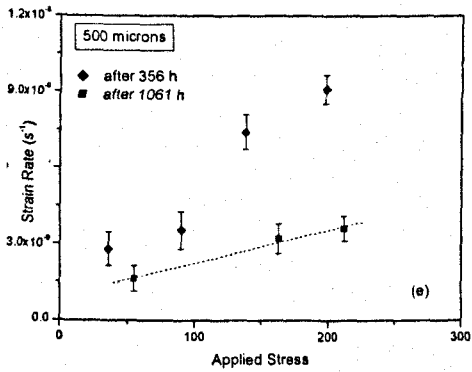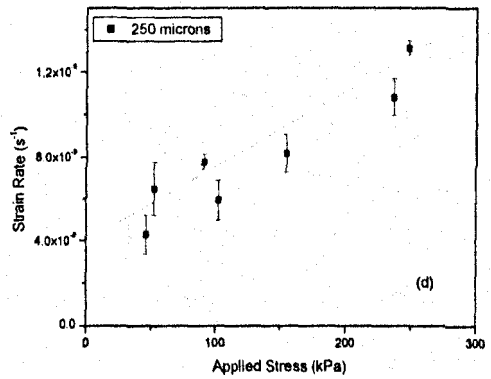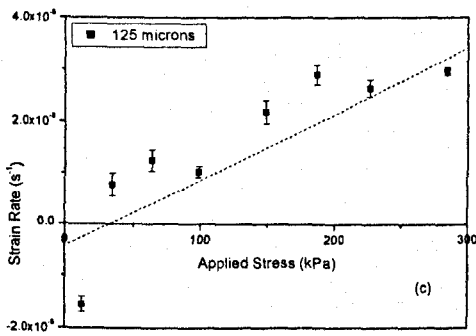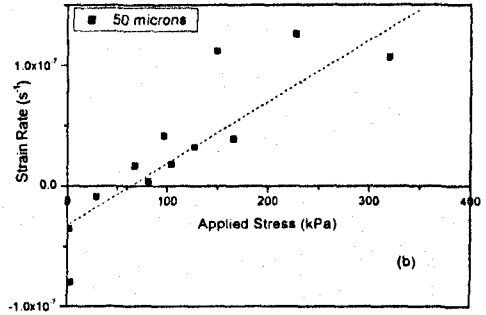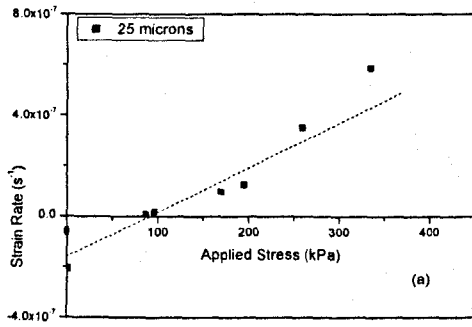
Figure 4.2 Strain rate plotted against applied stress for copper wires tested at 990°C in this study. Wire diameters (a) 25 μm (b) 50 μm (c) 125 μm and (d) 250 μm and (e) 500 μm.
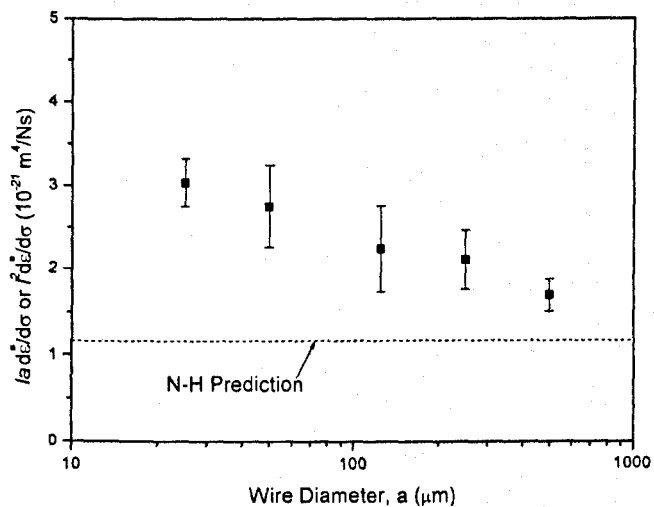
Figure 4.3 Steady state strain rate per unit stress, $d\dot{\varepsilon}/d\sigma$ compensated for specimen diameter, a, and grain size/length, l, for 25-500 μm diameter copper wires at 990°C plotted against wire diameter. For 500 μm diameter wires, when the grain size is less than the wire diameter, square of grain size (l^2) was used to normalise the ordinate. The expected value for Nabarro-Herring creep is also indicated.

$$\frac{T}{D_l}\frac{d\dot{\varepsilon}}{d\sigma}$$

K-N⁻¹
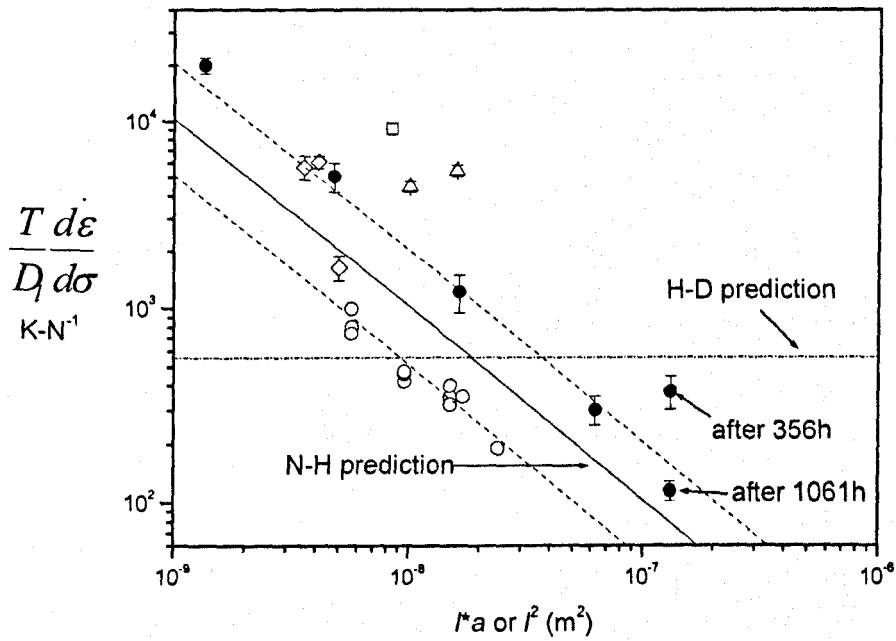
Figure 4.4 Temperature compensated strain rate per unit stress versus product of grain dimensions for copper near to its melting point. Δ[12] □[13] ◊[20] ○ [104] ● present work. All results are for wires except from ref. [104] which are for foils. Predictions from Nabarro-Herring and Harper-Dorn creep are indicated. Dashed lines indicate creep rates a factor of 2 above and below Nabarro-Herring predicted rates.
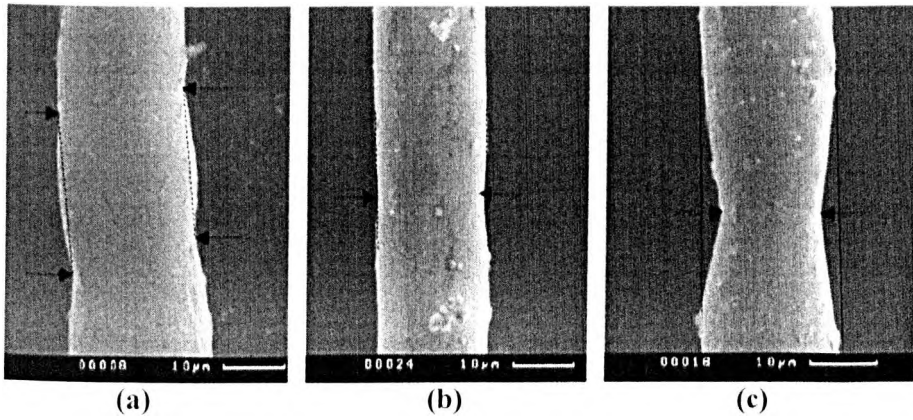
Figure 4.5 Profile of 25 μm diameter wires after testing at (a) 1.4 kPa, (b) 87.2 kPa and (c) 270 kPa and 990°C corresponding to effective stress being less than, equal to and greater than zero. Locations of grain boundaries are indicated by arrows. Note the considerable local necking in (c) associated with the grain boundary. Dashed lines indicate the notional position of wire surface before creep.
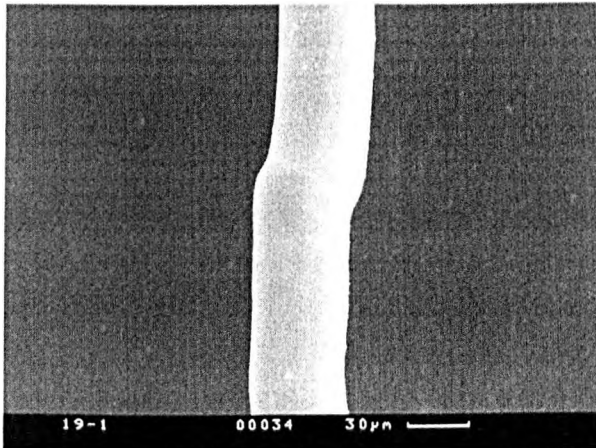
(a)
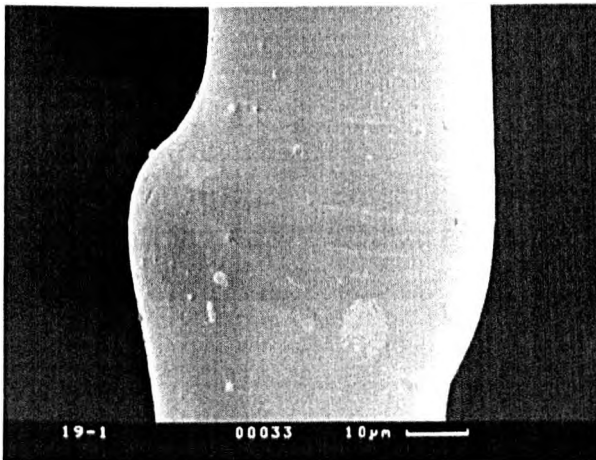
(b)

Figure 4.6 Deformation of an individual grain with large aspect ratio was confined to the vicinity of the grain boundary. Micrographs (a) and (b) obtained after creep in a 50 μm diameter wire at 990°C. Applied stress (4 kPa) was less than the zero creep stress. Total strain in the sample was -4.86% and the strain rate was measured to be -8.0 x 10^{-8} s^{-1}.
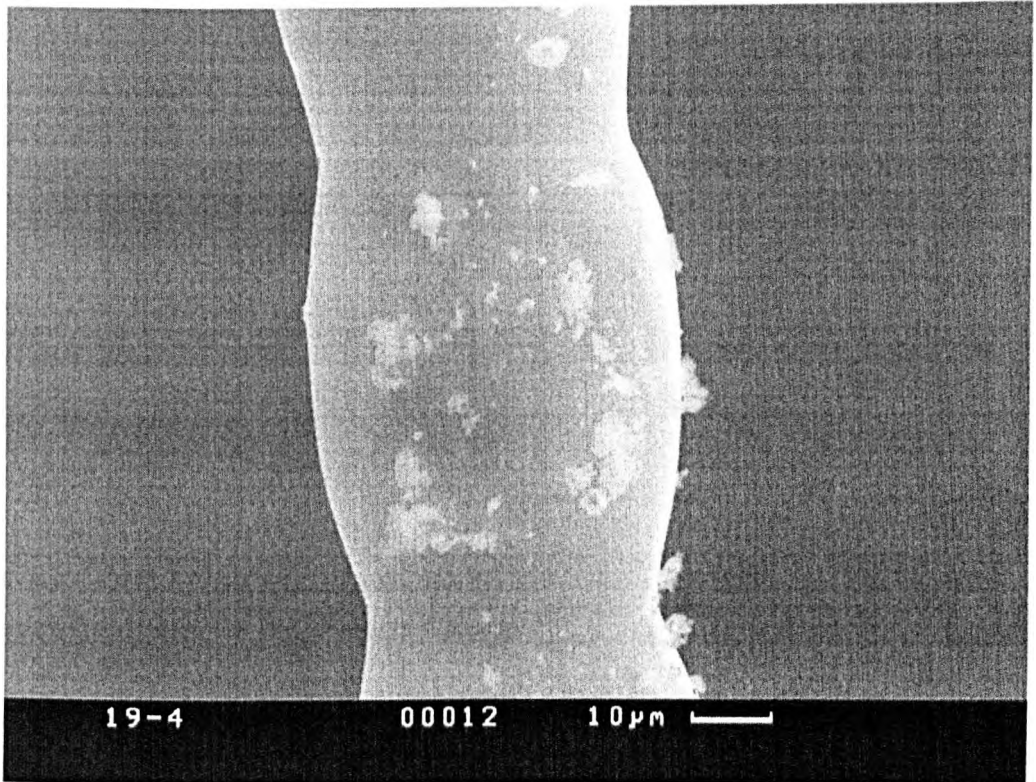
Fig 4.7 For smaller grain aspect ratio (close to unity) the deformation was observed to be more uniform. The micrograph was obtained after creep in a 50 μm diameter wire at 990°C. Applied stress (150 kPa) was greater than the zero creep stress. Total strain in the sample was 5.56% and the strain rate was measured to be $1.12 \times 10^{-7} s^{-1}$.
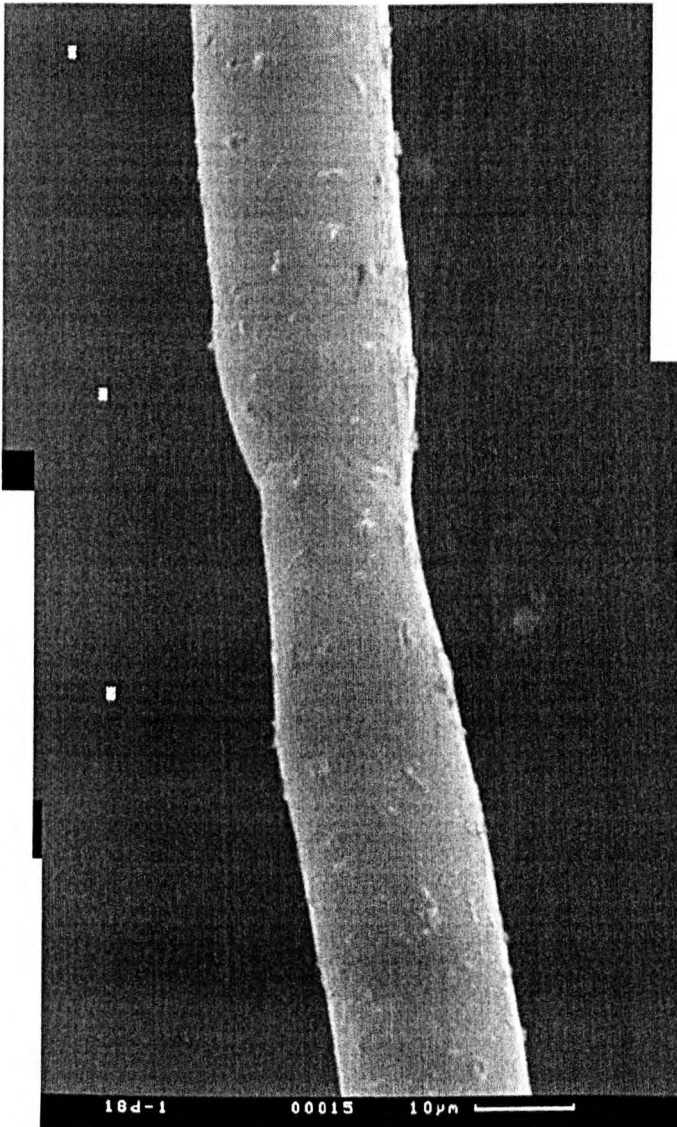
Fig 4.8 Localised deformation was also observed in grains having a large aspect ratio creeping under a large applied stress. The micrograph obtained after creep in a 25 μm diameter wire at 990°C. Applied stress (169 kPa) was greater than the zero creep stress. Total strain in the sample was 5.30% and the strain rate was measured to be $9.81 \times 10^{-8} \text{ s}^{-1}$.
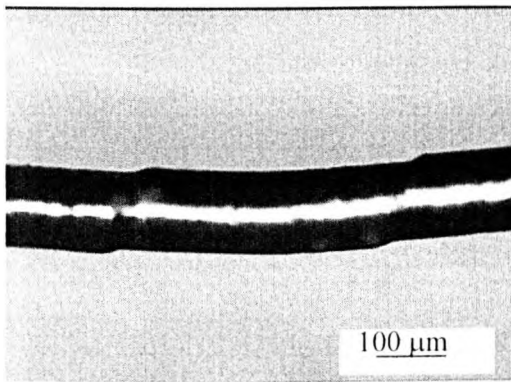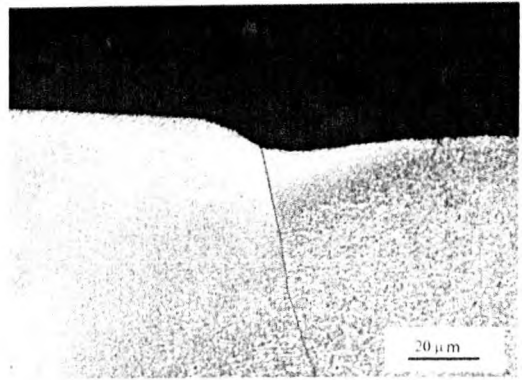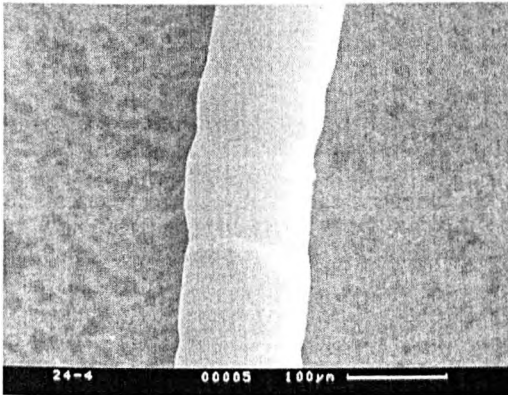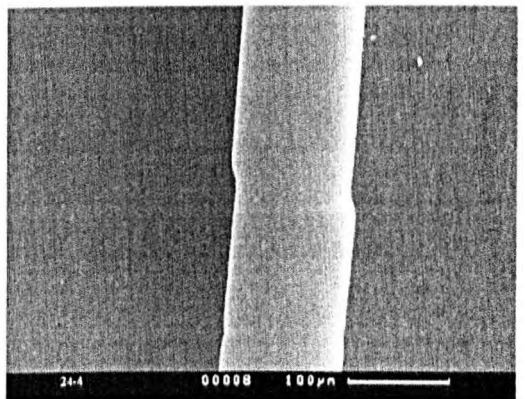
Figure 4.9 Microstructural features after creep at 990°C for 125 μm diameter copper wire at applied stress 221 kPa, total strain 1.87% and measured strain rate 2.64 x 10⁻⁸ s⁻¹. (a) Grain boundary sliding observed in 125 micron diameter wire. (b) Inclination of the grain boundary is believed to lead to sliding. (c) and (d) Diffusion creep is seen to be operative in parallel with grain boundary sliding in the same sample.
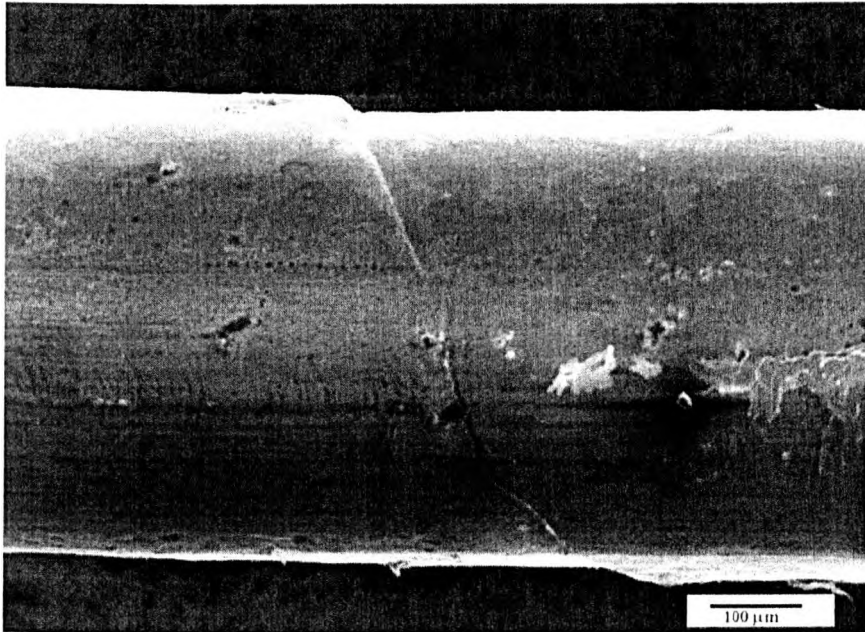
Figure 4.10 Grain boundary sliding was observed to be increasing prominent at larger wire diameters. Such images were used to estimate the contribution of grain boundary sliding to the total creep strain.

(a)

(b)
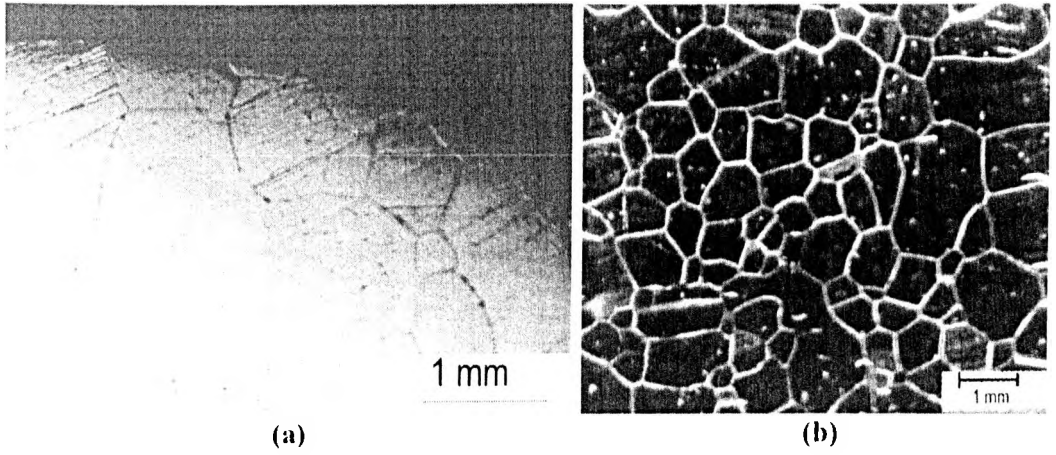
Figure 4.11 Microstructure of surface of copper sheet after annealing at 1075°C for (a) 1 h and (b) 40 h.

Strain Rate (s⁻¹)

3.0x10⁻⁷

○   1335K; d= 1.16mm; 0.4 mm thick
□   1338K; d=1.07 mm; 0.6 mm thick
△   1347K; d=1.48 mm; 0.6 mm thick
◇   1336K; d=0.97 mm; 0.6 mm thick
▽   1347K; d=0.58 mm; 0.4 mm thick
★   1284K; d=1.36 mm; 0.6 mm thick (oxidised)

2.5x10⁻⁷

2.0x10⁻⁷

1.5x10⁻⁷

1.0x10⁻⁷

5.0x10⁻⁸

grain size≈10 mm

0.0

coated

-5.0x10⁻⁸

0.0   0.1   0.2   0.3   0.4   0.5   0.6   0.7

Stress (MPa)
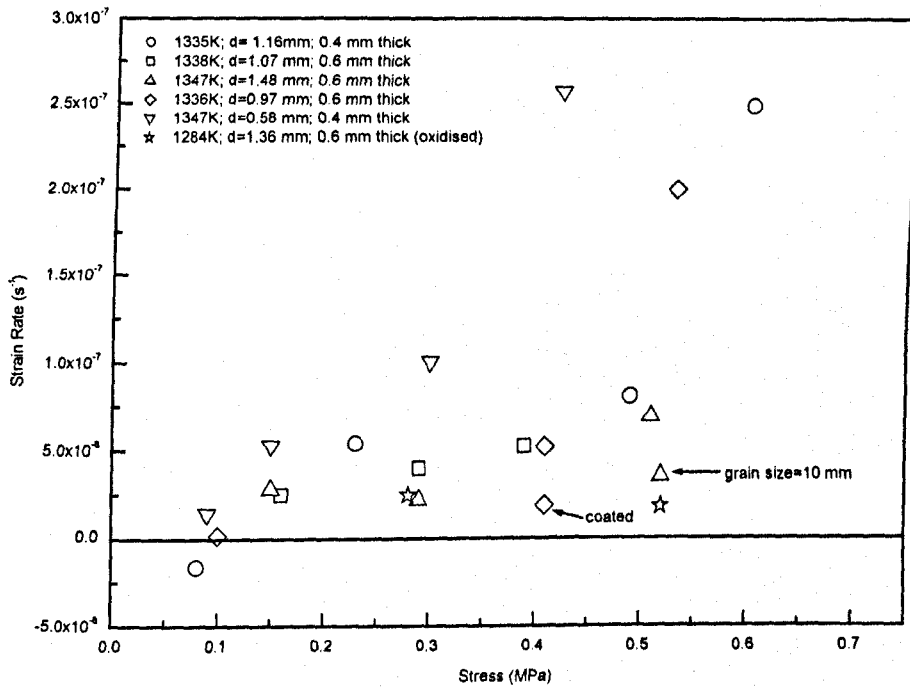
Figure 4.12 Complete summary of results for strain rate vs. tensile creep stress from tests carried out on copper foils at 1065°C in this study.
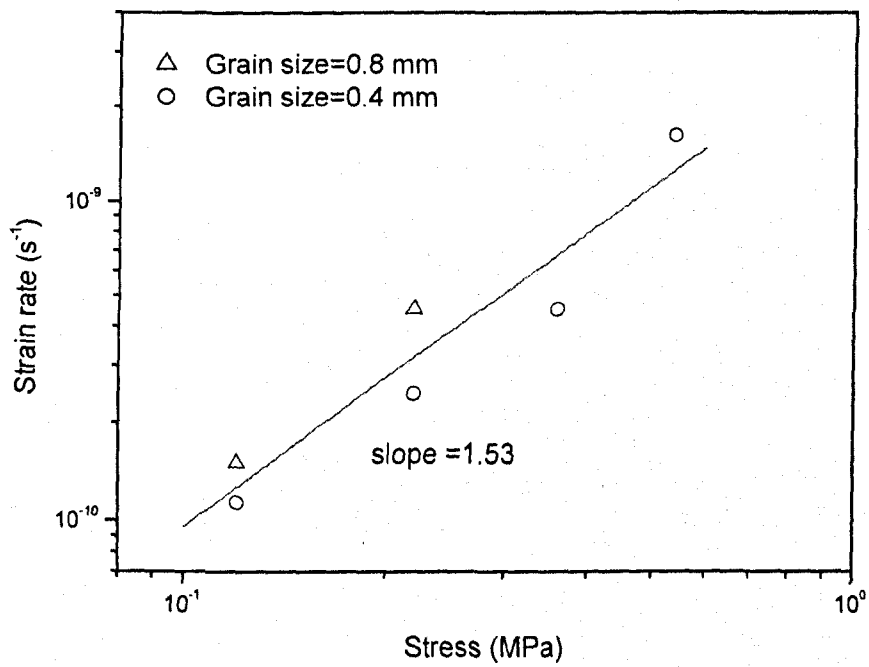
Figure 4.13 Double logarithmic plot of experimental strain rates against stress for 0.4 and 0.6 mm thick copper foils at 850°C. The tensile creep rates were measured from stress change experiments. The stress exponent was found to be 1.5 ± 0.2.
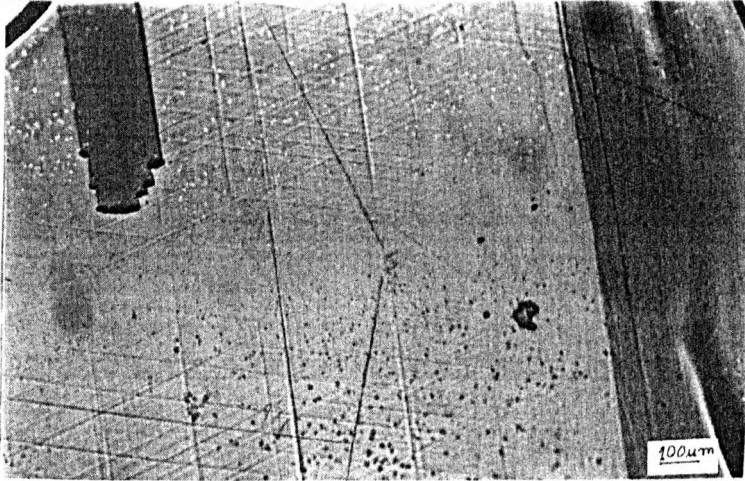
Figure 4.14 Slip lines seen on the surface of a copper foil of thickness 0.6 mm after tensile creep testing at 1065°C and 0.16 MPa. The strain measured was 0.57%.
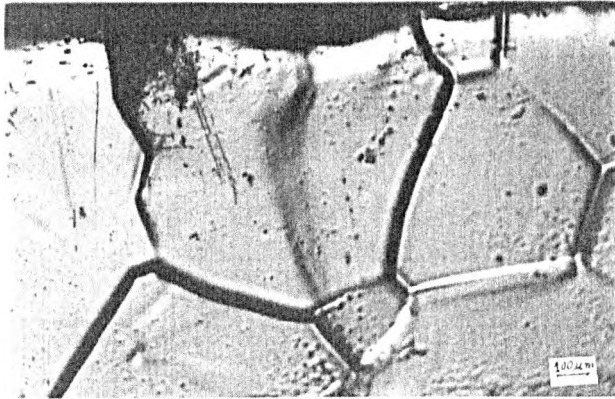
(a)
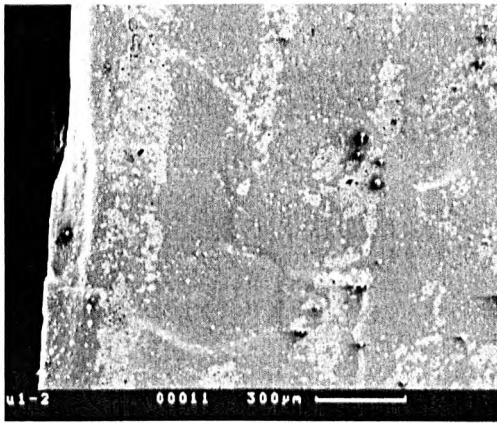
(b)

Figure 4.15 Localised surface slip bands observed at the edge of copper foil after tensile creep testing at 1074°C and (a) thickness 0.6 mm,; 0.51 MPa; total strain = 2.46% and (b) thickness 0.4 mm, 0.42 MPa; total strain =9.24 %.
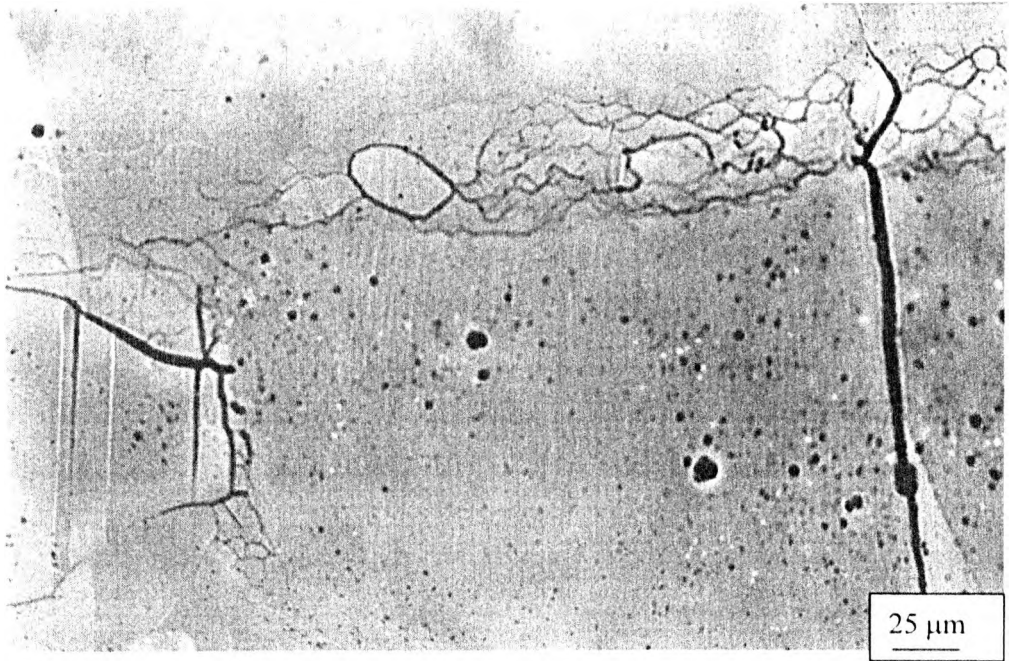
Figure 4.16 Surface substructure observed after tensile creep testing of a copper foil of thickness 0.6 mm at 995"C and 0.30 MPa even after a very low strain of 0.35%.
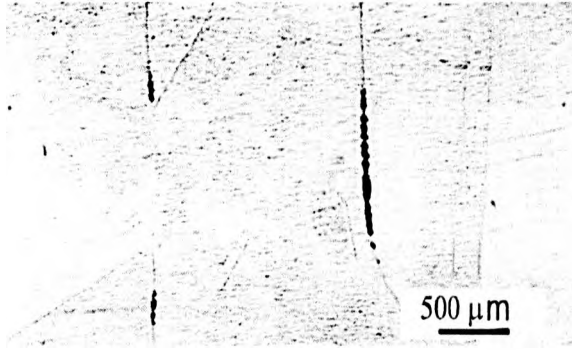
Figure 4.17 Cavities observed at grain boundaries on the polished surface of copper foil of thickness 0.6 mm after tensile creep at 1011°C and 0.52 MPa. The total strain measured was 1.4%. The stress axis is horizontal.
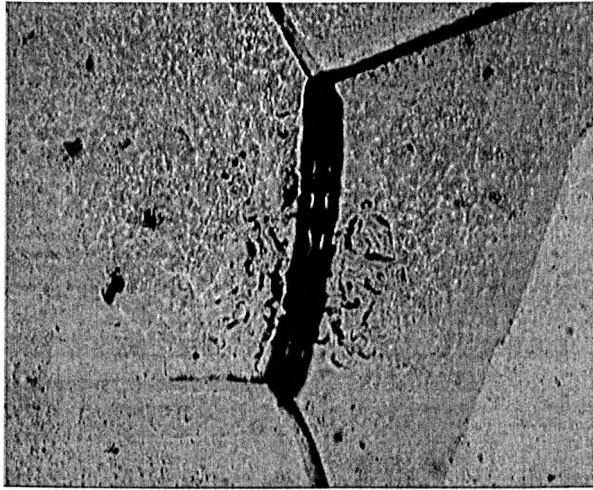
Figure 4.18 Deposition of material at a grain boundary transverse to the applied stress observed on the surface of a copper foil of thickness 0.6 mm after tensile creep at 948°C and 0.43 MPa. The stress axis is horizontal.
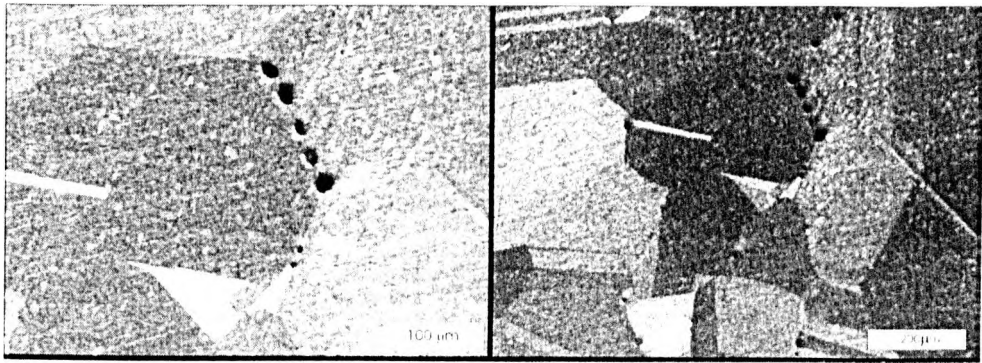
(a)   (b)

Figure 4.19 Micrographs from the surface of copper foils tensile creep tested at 850°C and low stresses. The creep rates were found to be an order of magnitude faster than N-H predictions. (a) 0.40 mm copper foil (b) 0.60 mm foil. See Table 4.4 for the creep stresses and associated strain rates. The tensile stress axis is horizontal.
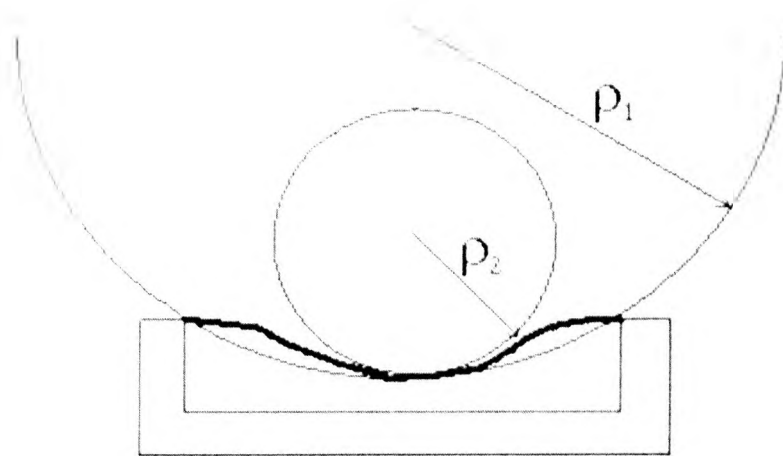
Fig. 4.20 Sintering of copper foils to end supports during bridge type creep tests was believed to restrict creep. Therefore, local curvature was estimated from the central span of the foil as shown schematically.
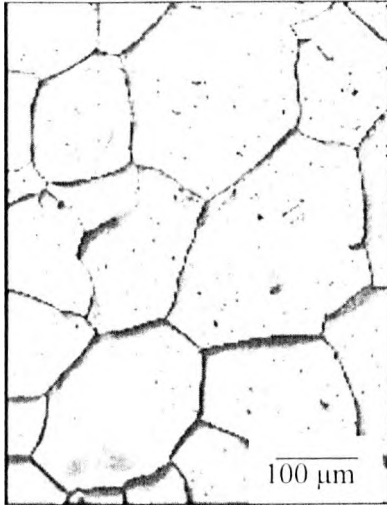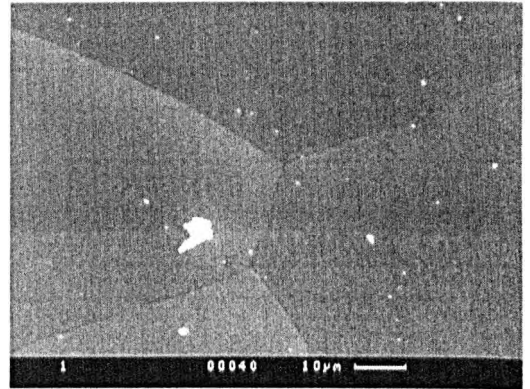
(a)   (b)

Figure 4.21 (a) The top surface of sample 3 (Table 4.5) after creep testing in bridge type configuration at 1000°C for 198h. The creep rate was measured to be 1.5×10^{-9} s^{-1}. (b) The top uncoated surface of a coated specimen (sample 5, Table 4.5) after creep. The test duration was 210h and measured strain rate was 7.9×10^{-10} s^{-1}. The compressive axis is vertical in both (a) and (b).
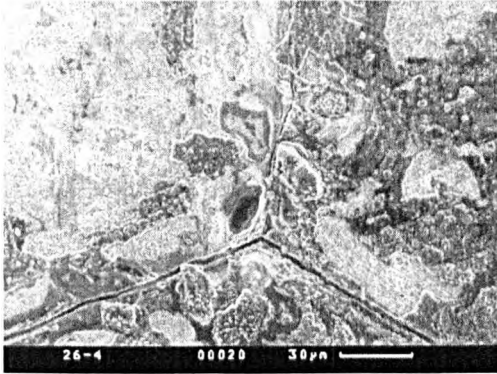
(a)
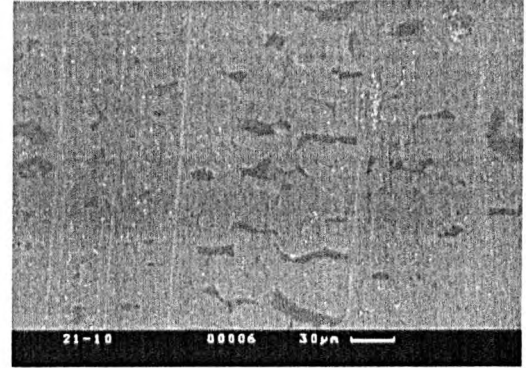
(b)
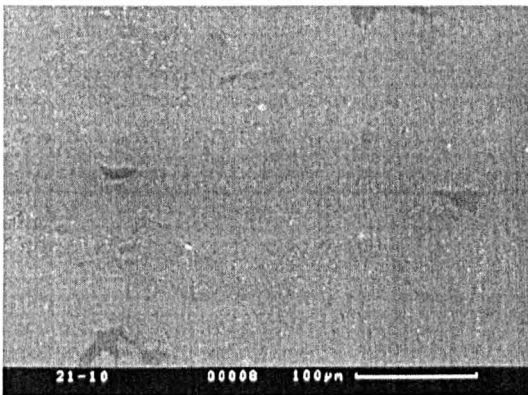
(c)

Figure 4.22 Microstructural observations on fracture of an alumina coating a few tens of nanometer thick after creep in 100 micron thick copper foils in bridge-type tests at 1000°C. The coatings were applied to the lower surface of the foil which was under tension. Tensile axis is vertical. (a) Crack width was dependent on the angle the boundary makes with the tensile axis. The major part of the coating was lost in this creep test so revealing the underlying structure (sample 4, Table 4.5). (b) The majority of the cracks were found to be perpendicular to the tensile axis (sample 5, Table 4.5). (c) Very few cracks were observed near the end of the foil where the bending moments were small and these cracks did not have any significant directionality (sample 5, Table 4.5).
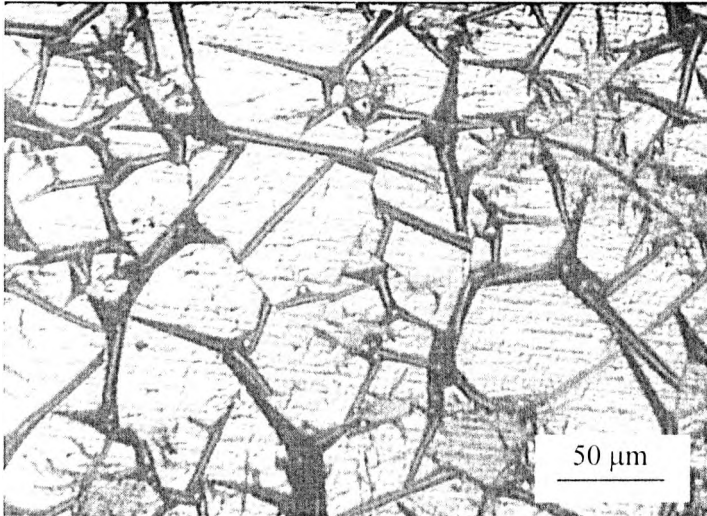
(a)
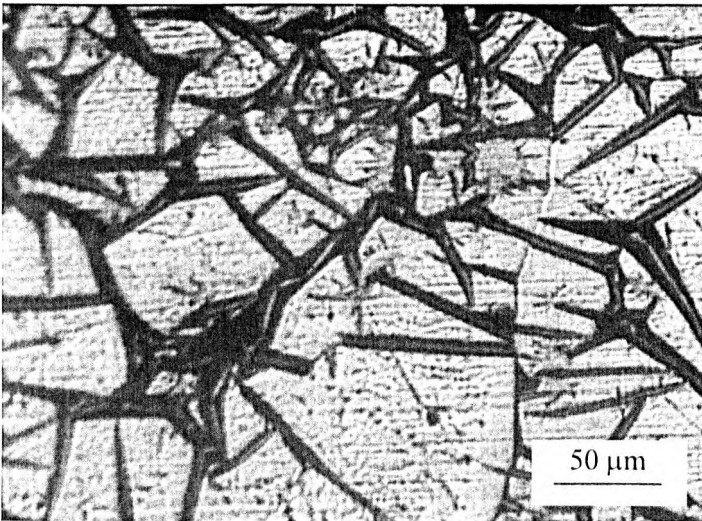
(b)

Figure 4.23 Micrographs from bottom surface of a cantilever sample of copper foil (Sample14; Table 4.6) (a) from an area close to the maximum compressive stress (b) from an area close to the zero stress region.
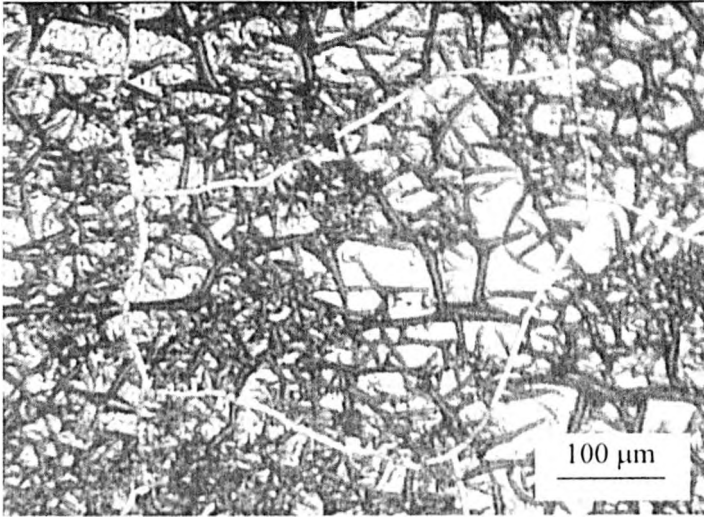
(a)
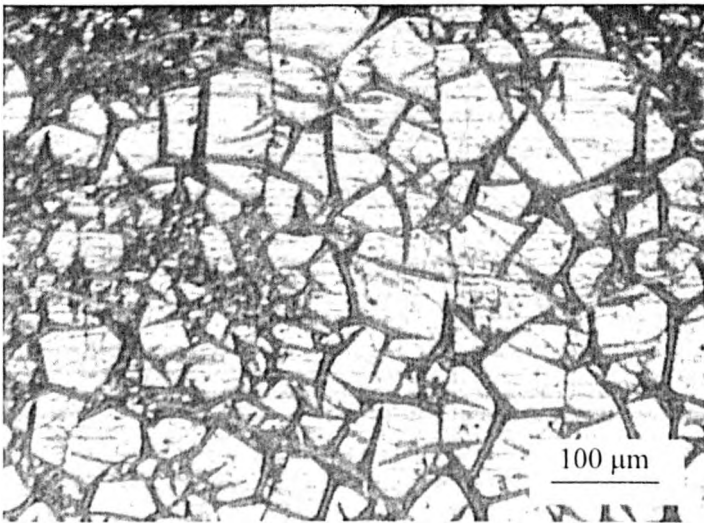
(b)

Figure 4.24 Micrographs from top surface of a cantilever sample of copper foil (Sample11; Table 4.6) (a) from an area close to the maximum tensile stress (b) from an area close to the zero stress region.
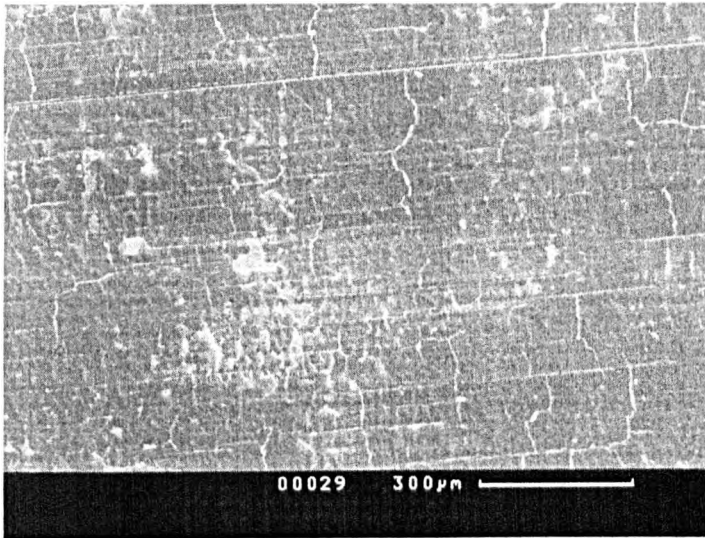
(a)
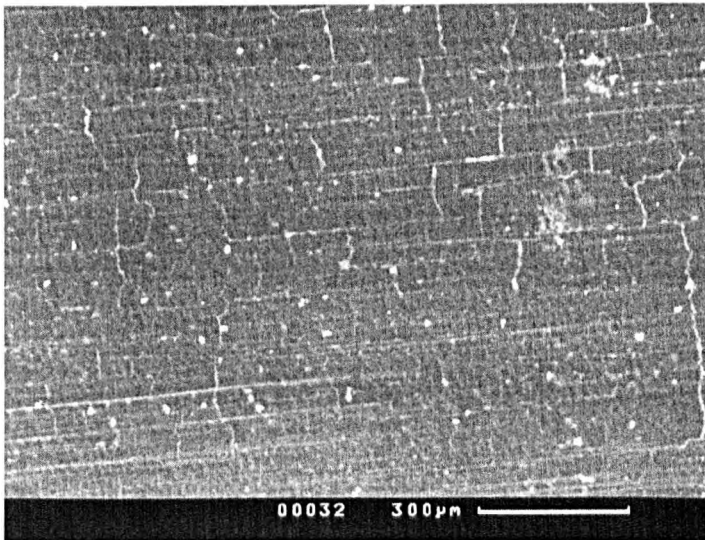
(b)

Figure 4.25 Micrographs from top surface of a cantilever sample of copper foil (Sample15; Table 4.6) (a) from an area close to the maximum tensile stress (b) from an area close to the zero stressed region. Note that the grain boundaries have more contrast and are therefore more easily visible in (a) compared to (b)
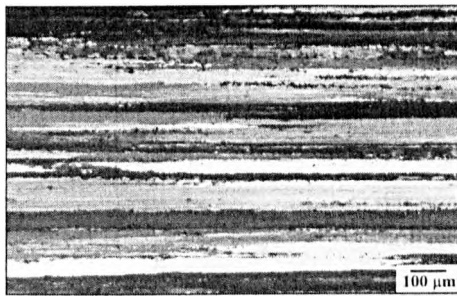
(a)
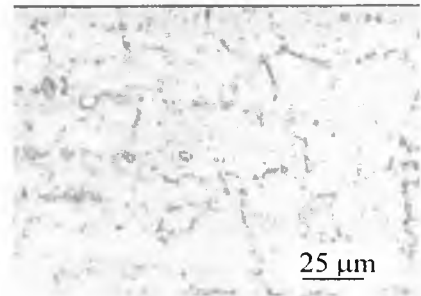
(b)
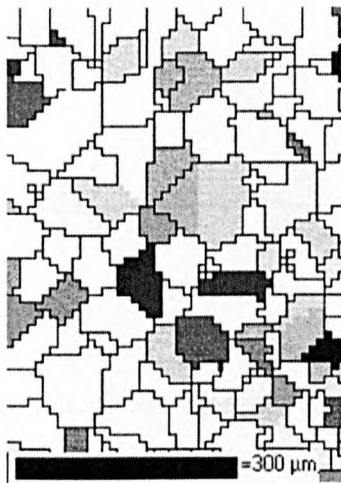
(c)
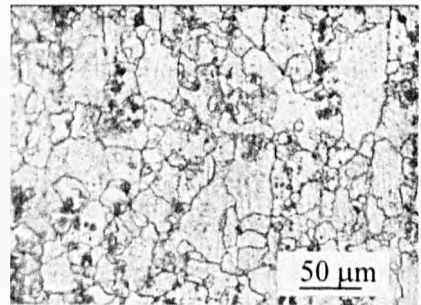
(d)

Figure 4.26 Microstructures of 7075 aluminium after various stages of processing (a) as-recieved (b) after TMT treatment(c) EBSD after TMT (d) after TMT treatment and annealing for 50 h at 350°C.
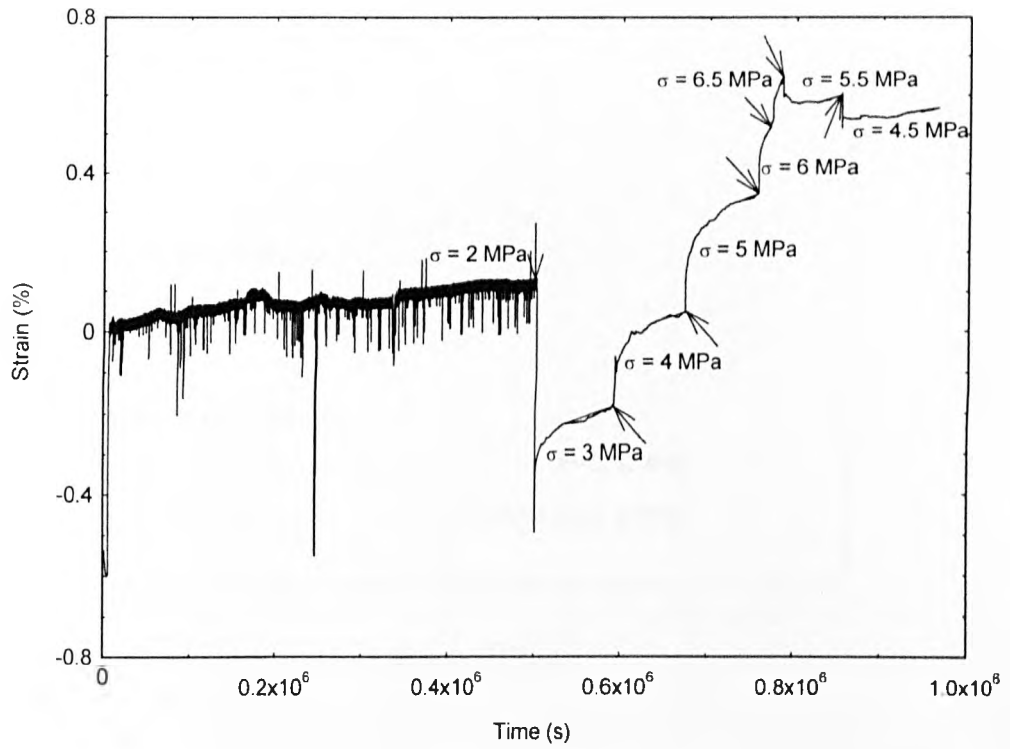
Figure 4.27 The creep curves of thermo-mechanically treated 7075 aluminium at low stresses as tabulated in Table 4.7.
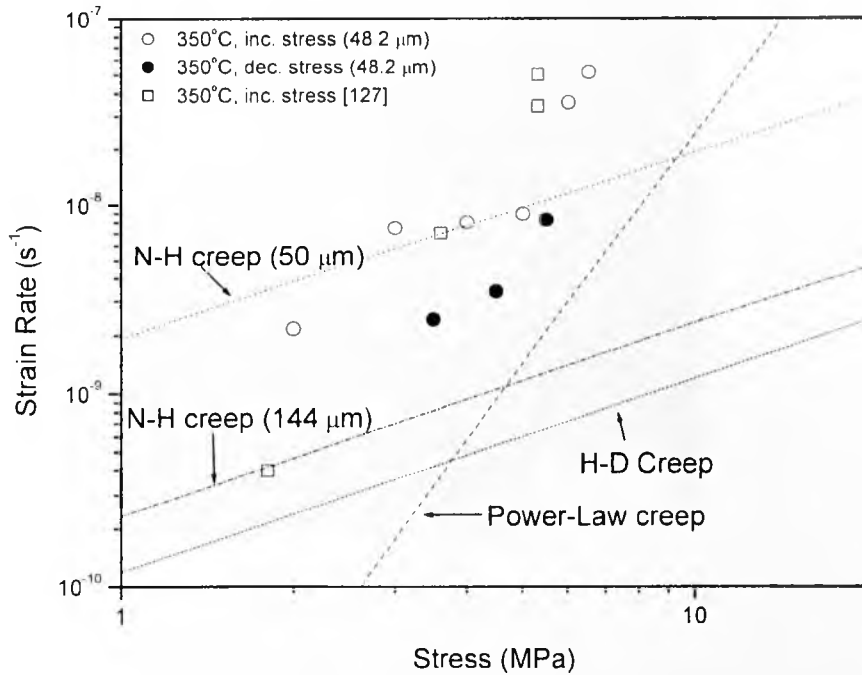
Figure 4.28 Steady state creep rates obtained in this work plotted against applied stress on a double logarithmic plot. The rates predicted by N-H creep theory and empirical H-D and power law creep rates are also shown for comparison. The data points shown by open squares (□) were obtained from McNee [127] for thixo-forged samples. Initial grain sizes for thermomechanically treated samples are indicated in parentheses.
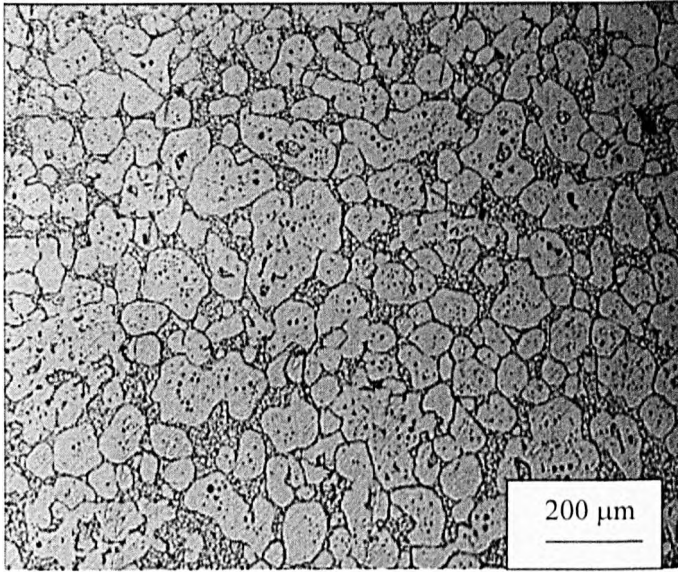
Figure 4.29 Microstructure of a cross-section of the thixo-formed 7075 aluminium sample used for tensile creep testing by McNee [127] at 350°C.
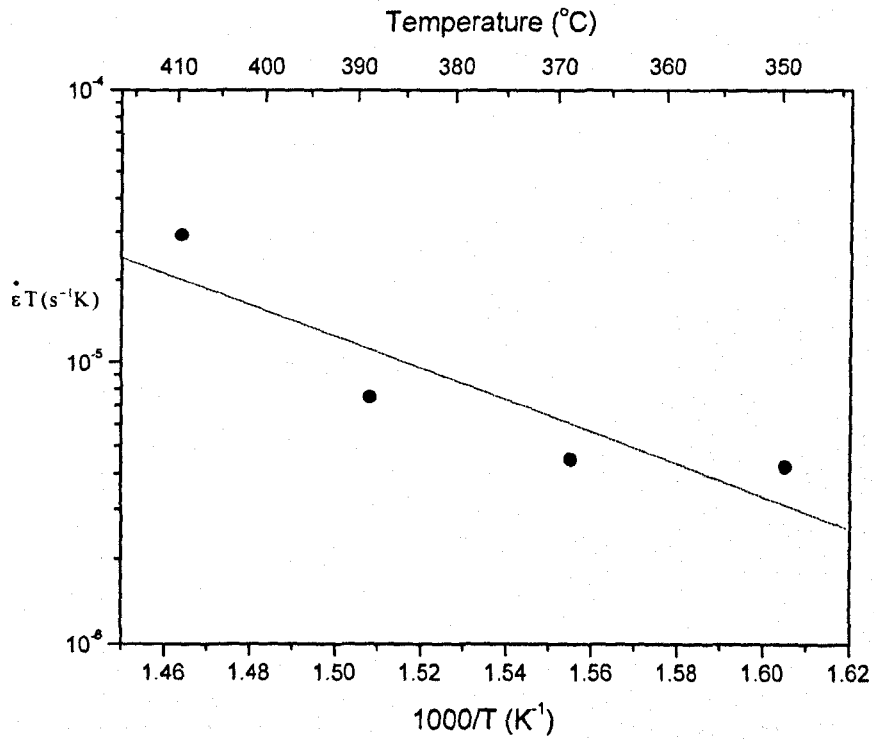
Figure 4.30 Logarithm of temperature compensated creep rate against the reciprocal of temperature at applied stress 2.9 MPa for 7075 aluminium alloy.
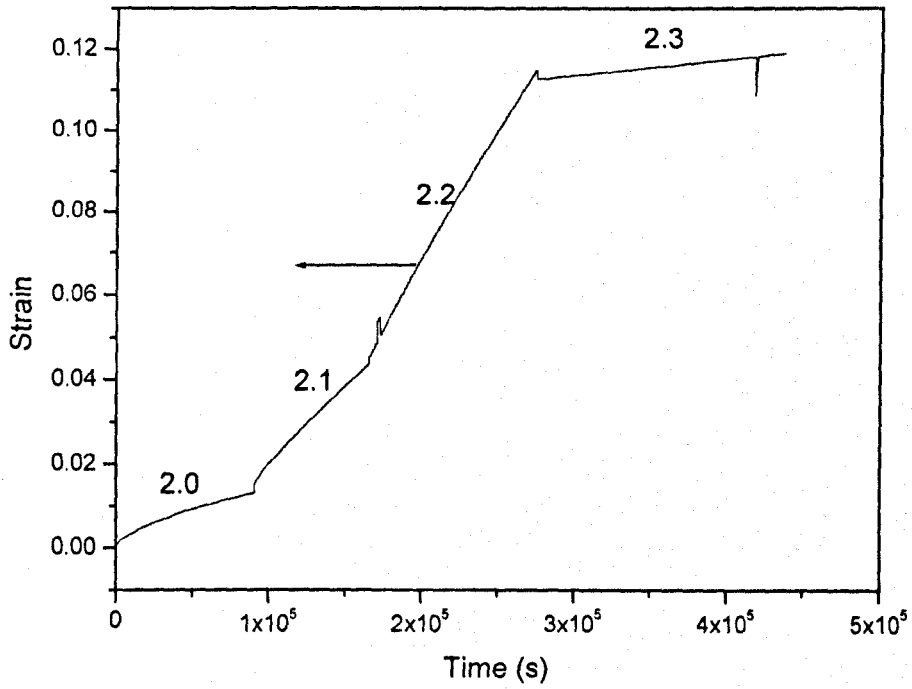
Figure 4.32 Fractional strain versus time curves for creep of AZ61 (test number 2, Table 4.8) at 303°C for stresses 0.9, 1.8, 2.7 and 0.9 MPa (2.0, 2.1, 2.2, 2.3).
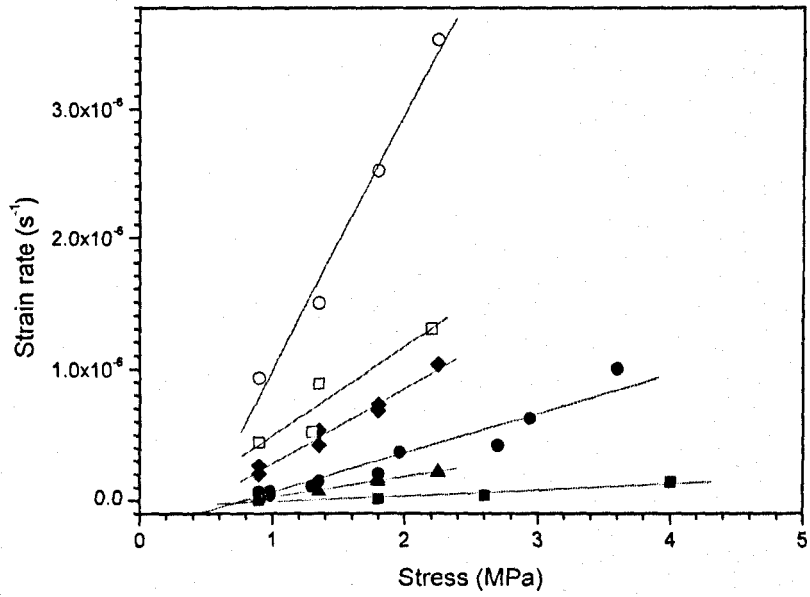
Figure 4.33 Steady state strain rate $\dot{\varepsilon}$ versus stress for AZ61 at temperatures ■250 °C, ▲ 289 °C, ● 302 °C, ♦ 318 °C, □ 330 °C, ○ 346 °C.
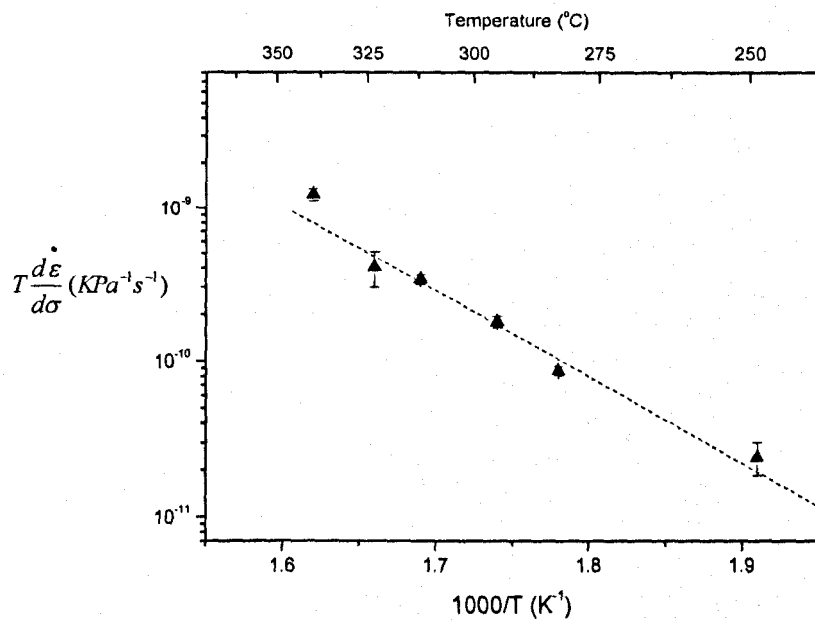
Figure 4.34 Logarithm of temperature-compensated steady state strain rate $Td\dot{\varepsilon}/d\sigma$ of AZ61 versus inverse test temperature T from the data in Table 4.9.
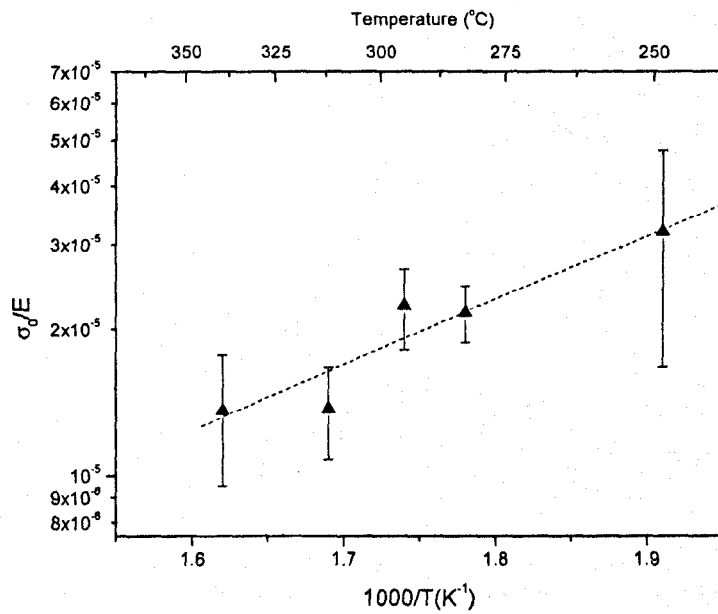
Figure 4.35 Logarithm of E-normalised threshold stress σ_0 of AZ61 versus reciprocal of test temperature T from the data in Table 4.9.
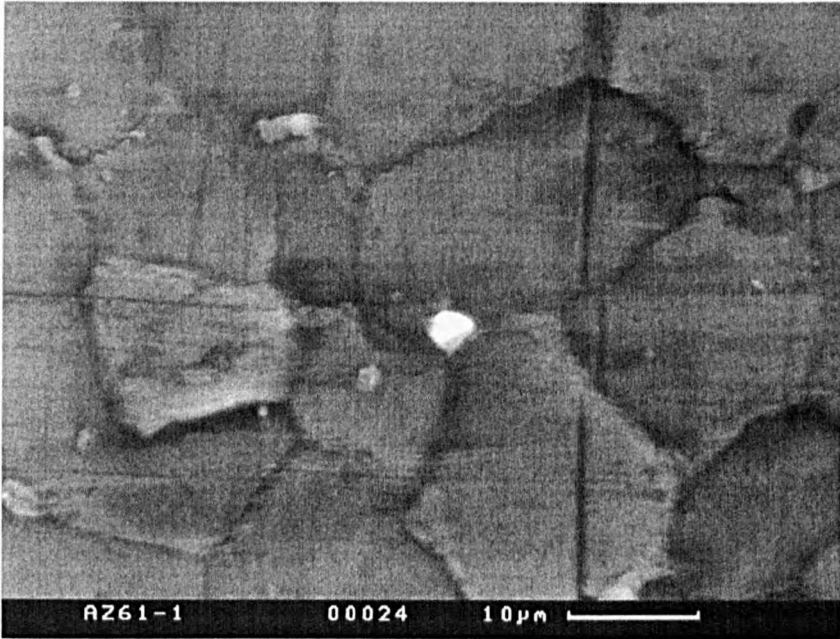
Figure 4.36 A micrograph from the surface of creep tested AZ61 alloy showing evidence of grain rotation during test number 2 (Table 4.9). Tensile axis is horizontal.
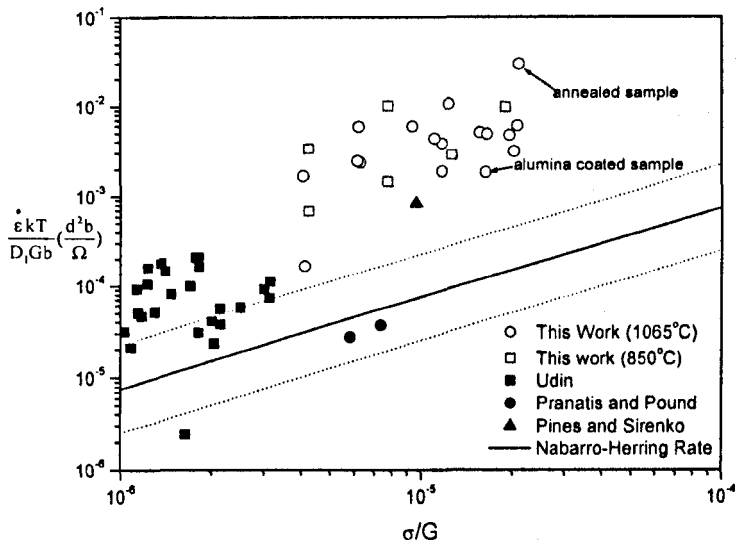
(a)
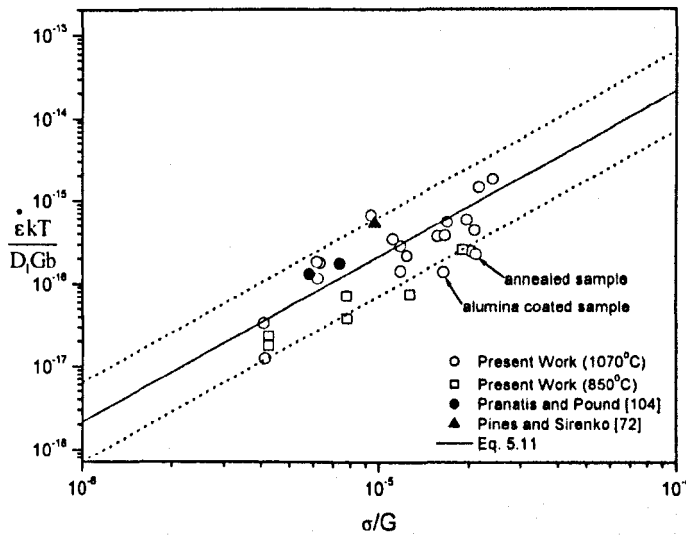
(b)

Figure 5.1 (a) Dimensionless strain rate of copper compensated for grain size according to Nabarro-Herring theory versus non-dimensional stress on a double logarithmic plot. Three data points including the annealed and coated sample from the total set were ignored from analysis as discussed in the text. (b) Same as (a) but assuming that the creep rate is independent of grain size. Predictions from Eq. (5.11) are shown for comparison. Dotted lines represent a factor 3 above and below the predictions.
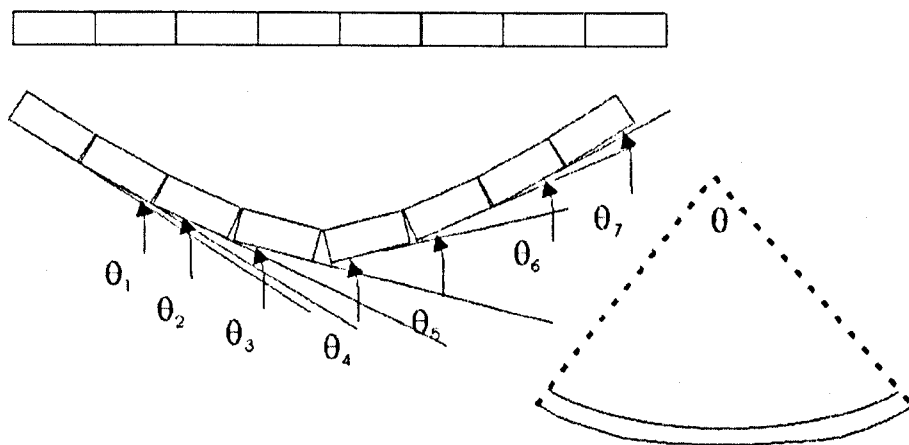
Figure 5.2 The expected curvature of the foil in bending was estimated by summing

individual grain rotations, $\Delta\theta$, at each grain boundary to estimate the total angle,

θ, subtended at the centre. This was then used to estimate the rate of change of curvature of

the foil.
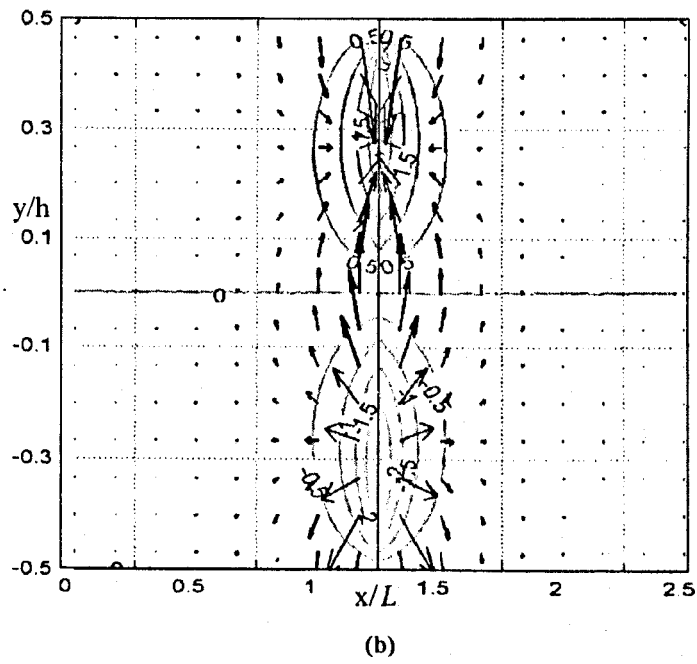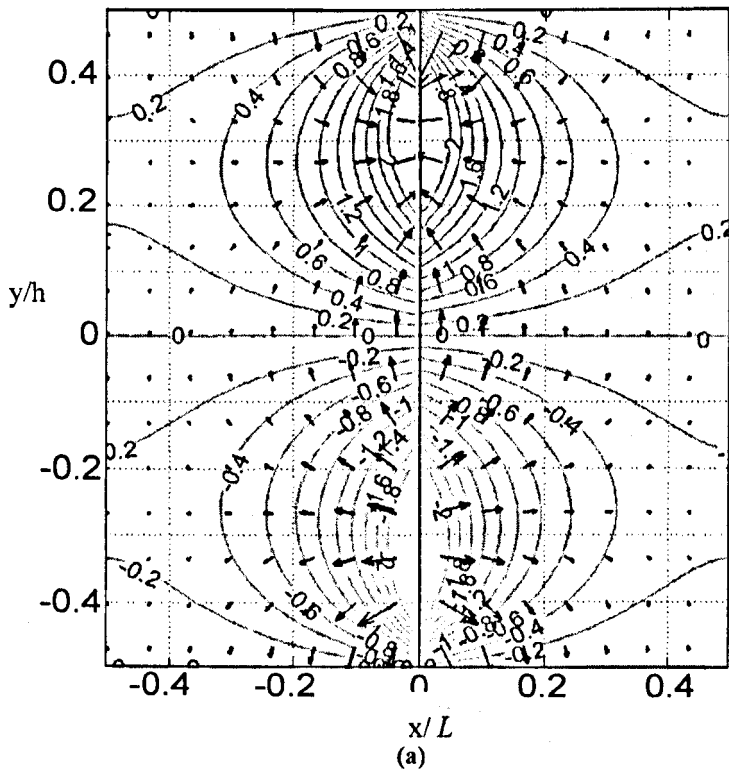
Fig 5.3 Schematic equipotential plots for a grain subjected to bending moment undergoing diffusional creep. The value and direction of atomic fluxes is indicated by arrows. The grain aspect ratios are (a) 1 and (b) 2.5.
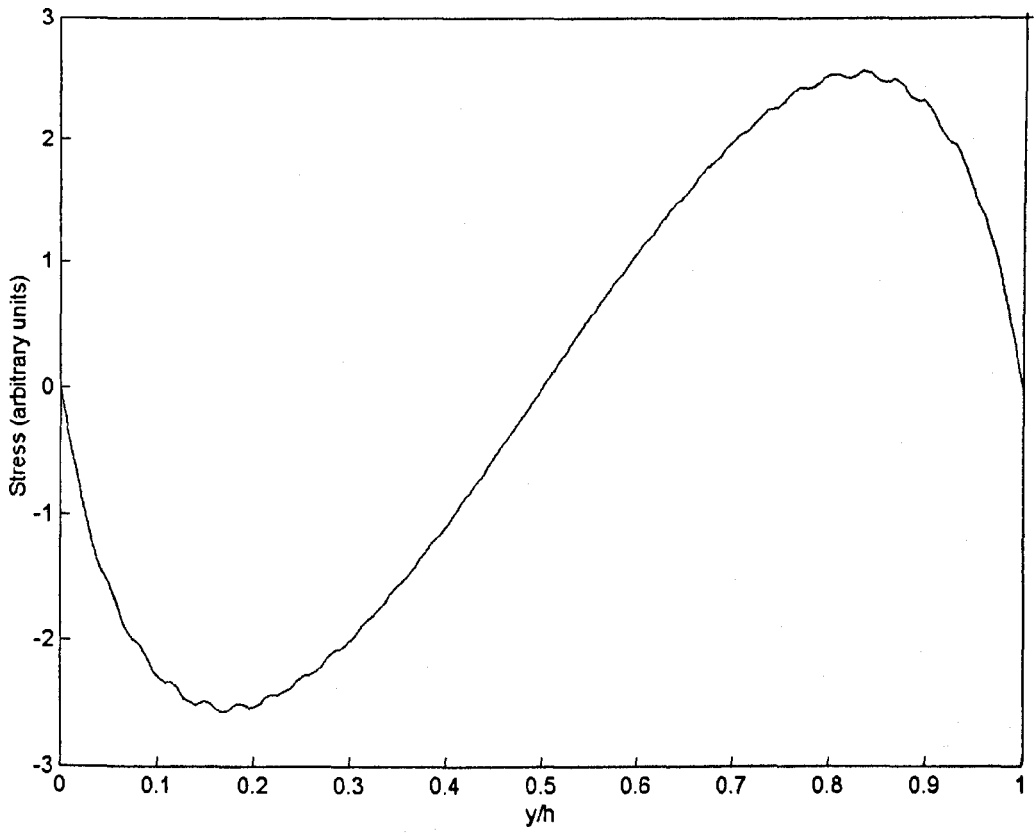
Figure 5.4. Schematic plot showing variation of relaxed stress across the thickness of the foil under bending stress at a particular grain boundary.
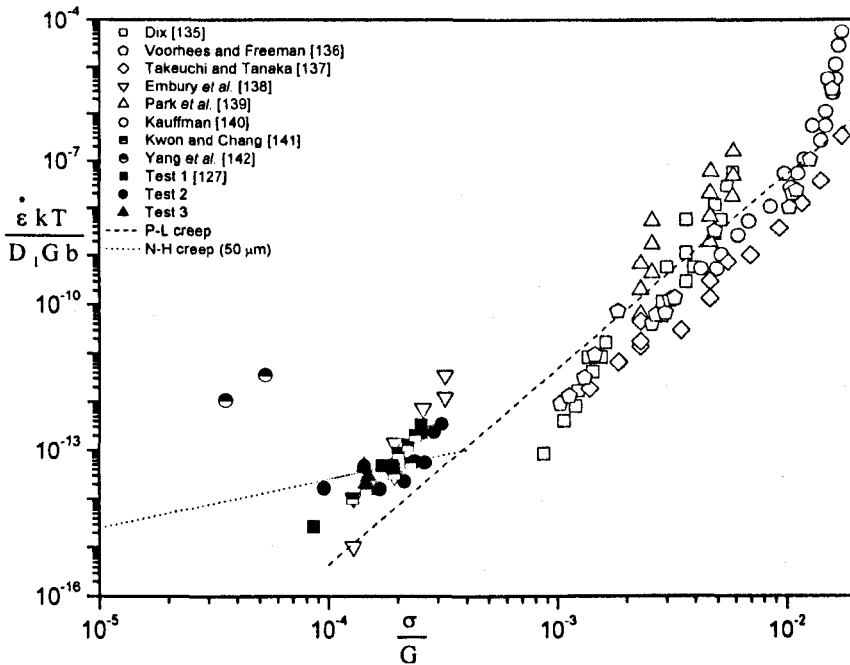
Fig. 5.5 Normalised creep data for 7075 Al alloy compared with previously reported creep data for higher stresses. The closed symbols represent data obtained in this work (Table 4.7) and open symbols are data from previous work. Top-filled symbols are recent superplasticity data for fine grained and cold-rolled material reported by [141] and [142] respectively. Dashed line is the best fit of the data from previous works. Dotted line represents Nabarro-Herring creep rates for 50 μm grain size.
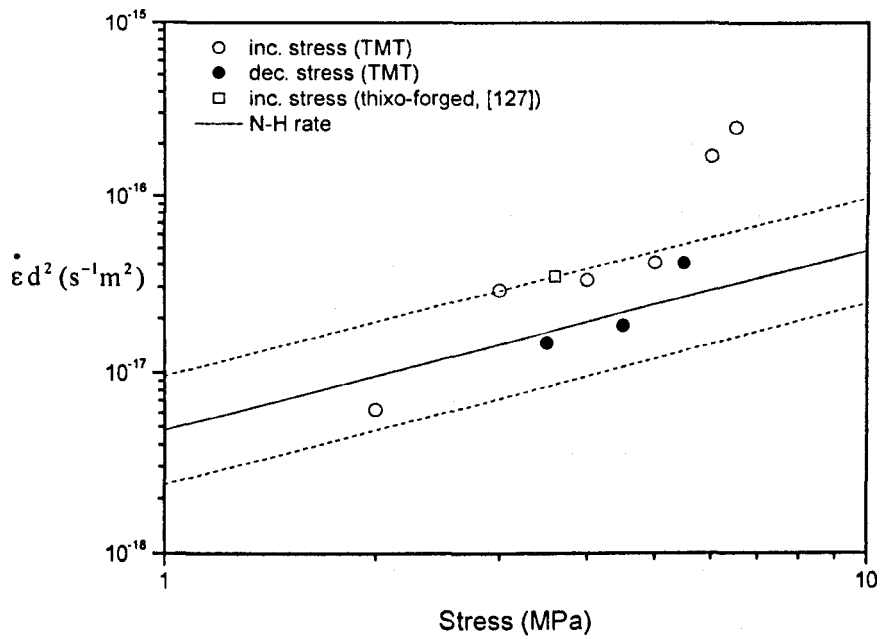
Figure 5.6 Steady state creep rates obtained in 7075 aluminium alloy at 350°C at low stresses compensated for grain size plotted on a log-log scale. The rates predicted by the N-H equation are shown for comparison. It is seen that the creep rates are within a factor of 2 for all the data obtained at lower stresses (<5 MPa).
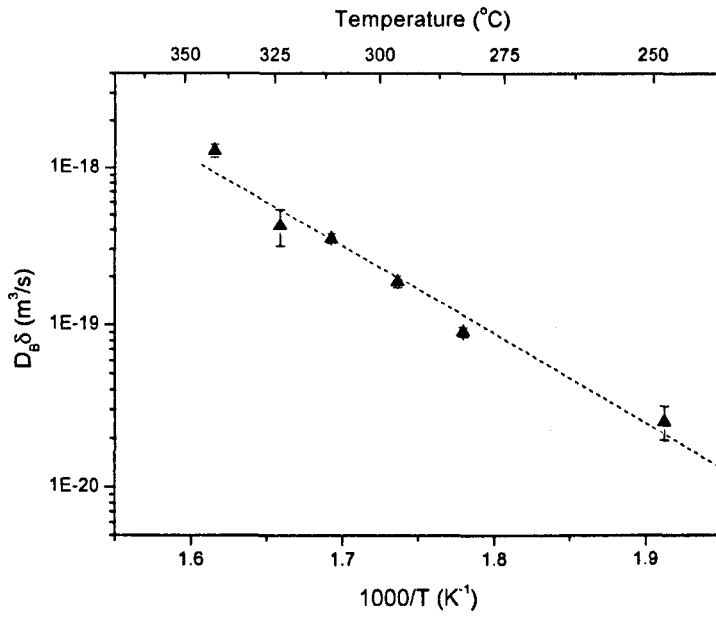
Figure 5.7 Dependence on reciprocal test temperature of logarithm of $D_B\delta$ given by Eq. (5.24) from measured $d\overset{\bullet}{\varepsilon}/d\sigma$ for AZ61 from Table 4.9.
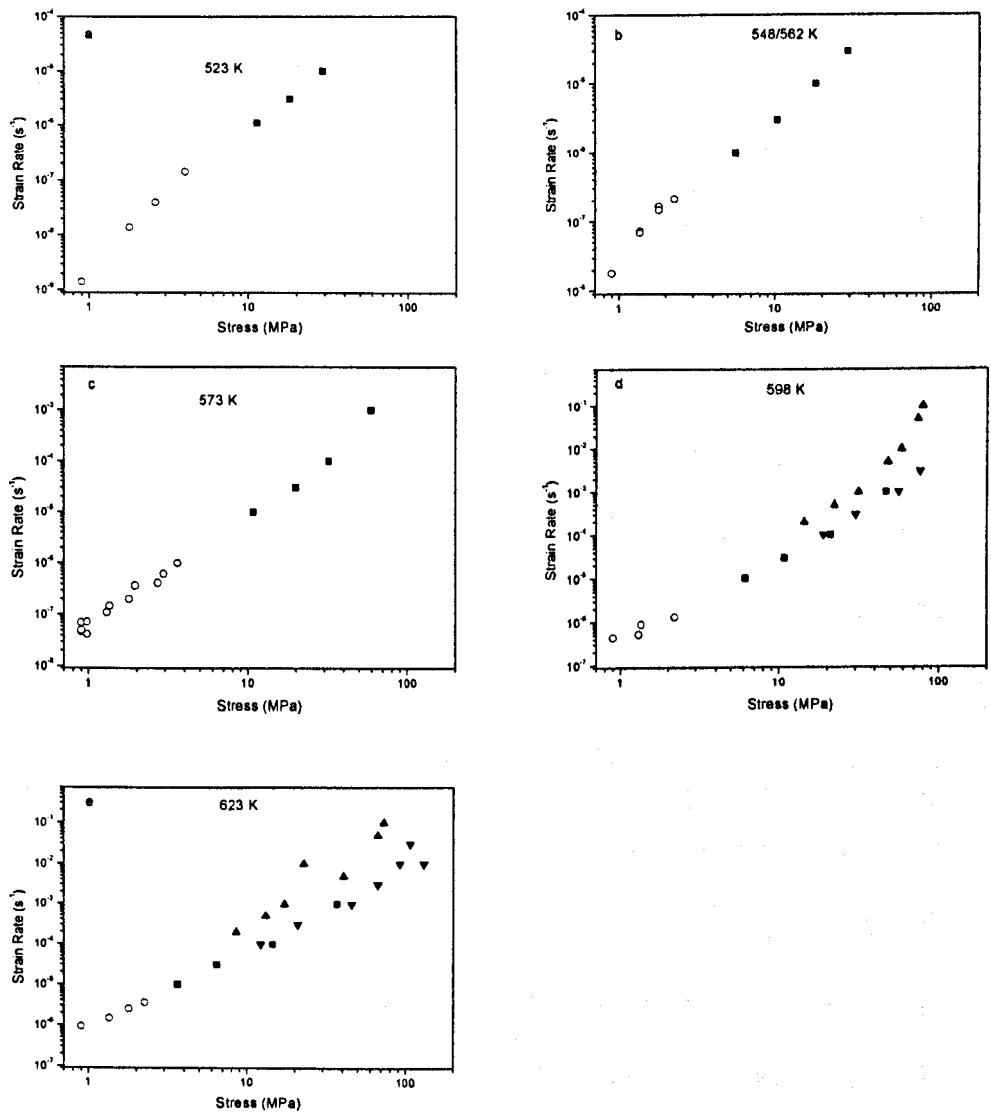
Figure 5.8 Strain rate versus stress for the five lowest temperatures used by Watanabe *et al.* [118] and Kim *et al.* [122] for their superplasticity work on AZ61, for comparison with our creep data at lower stresses and similar temperatures (a) 250 (b) 275/289 (c) 300/303 (d) 325/330 (e) 350/346°C. Key: ■ Watanabe *et al.* (ε = 0.1) ▲ Kim *et al.* ($\bar{L}$ = 5μm) ▼ Kim *et al.* ($\bar{L}$ = 6.7 μm) O present work.

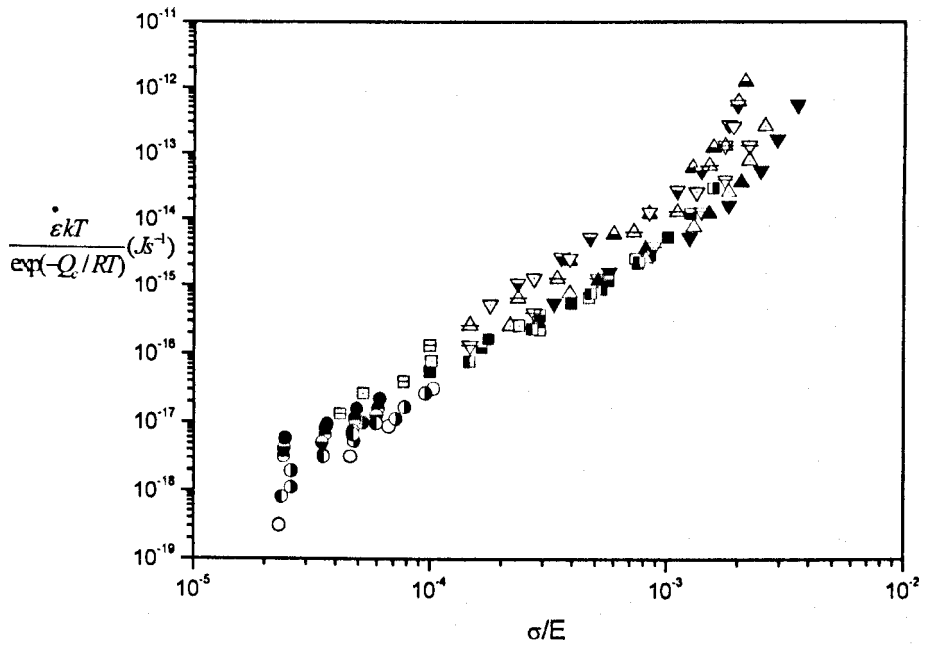$$\frac{\dot{\varepsilon}kT}{\exp(-Q_c/RT)}(Js^{-1})$$

σ/E

Figure 5.9 Temperature-compensated strain rate versus σ/E for superplasticity data [118, 122] compared with present creep data for AZ61 using the activation energy for creep 106 ± 9 kJ/mol from the present work.

Key: Watanabe *et al.* (ε=0.1): □ 250 ▥ 275 ▣ 300 ▨ 325 ■ 350 ⊡ 375 ⊟ 400°C

Kim *et al.* ($\overline{L}$ = 5 μm) : △ 325 ▲ 350 △ 375 △ 400

Kim *et al.* ($\overline{L}$ = 6.7 μm) : ▽ 325 ▼ 350 ▽ 375 ▽ 400

Present work: ○ 250 ◐ 289 ◑ 303 ◒ 318 ◒ 330 ● 346°C